ADDIS ABABA UNIVERSITY

ADDIS ABABA INSTITUTE OF TECHNOLOGY

SCHOOL OF CIVIL AND ENVIRONMENTAL ENGINEERING

FATIGUE BEHAVIOUR OF SHEAR-CRITICAL REINFORCED CONCRETE BEAMS

A Thesis in Structural Engineering

By Tsigereda Getachew

21/03/2018

Addis Ababa

A Thesis

Submitted in Partial Fulfillment of the Requirements for the Degree of Master of Science

ADDIS ABABA UNIVERSITY

ADDIS ABABA INSTITUE OF TECHNOLOGY

SCHOOL OF CIVIL AND ENVIRONMENTAL ENGINEERING

"Fatigue behavior of shear-critical Reinforced Concrete beams"

By

Tsigereda Getachew

Approved by the Board of Examiners:

Dr.-Ing. Adil Zekaria		
Advisor	Signature	Date
Dr.-Ing. Girma Zerayohannes		
Internal Examiner	Signature	Date
Dr. Abrham Gebre		
External Examiner	Signature	Date
Dr. Agizew Nigussie		
Chair person	Signature	Date

ACKNOWLEDGEMENT

While working on this research for over a year, I have had the support and guidance of several individuals who deserve my deepest gratitude. This accomplishment would not have been possible without any of you.

First and foremost, I would like to thank God for giving me the strength, perseverance and provision to undertake this thesis. I must also express my profound gratitude to my parents for their unfailing support and continuous encouragement throughout my years of study and during this research.

I would like to sincerely thank my advisor Dr. Ing. Adil Zekaria for his relentless belief in me and support. His door was always open whenever I ran into roadblocks, to steer me in the right direction. I would like to state my deepest gratitude to Dr. Esayas Gebreyouhannes who provided insight and expertise that greatly assisted this research through numerous consultations. I am truly inspired by your dedication and research abilities.

I would like to thank my colleagues Yonas Solomon, Mohammed Sirage, and friends Alazar Woldeyohannes and Selam Getahun as their well-rounded support was instrumental to bring this thesis into fruition. I would also like to thank Bezawit Fekade, Leamlak Minwuyelet, Dr. Mesele Haile, Firesenay Zerabruk and Yisshak Tadesse for their assistance in obtaining necessary resources for this research.

Furthermore, I would like to forward my esteemed appreciation to the laboratory technicians and staff of Construction Materials Laboratory of AAiT – Demise, Fikru, Biniyam, Tizazu and Wubet. Not only did you give me access to all required equipment and material to complete this thesis, but your individual support during the experimental program was vital. Thank you for going out of your way to make this experimental research possible.

Lastly, I would like to expand my gratitude to all those who have directly and indirectly helped me throughout my research. Thank you. ☺

TABLE OF CONTENTS

ACKNOWLEDGEMENT I
TABLE OF CONTENTS II
LIST OF FIGURES V
LIST OF TABLES VII
ABSTRACT 1
1 INTRODUCTION 2
1.1 Background 2
1.2 Significance 2
1.3 Objectives 3
1.4 Scope and limitations 3
2 LITERATURE REVIEW 4
2.1 Theoretical Background 4
2.1.1 Fundamentals of Shear 4
2.1.1.1 Fixed Angle theory 5
2.1.1.2 Rotating Angle theory 8
2.1.1.3 Summary of angle theories 9
2.1.2 Shear cracking in reinforced concrete members 10
2.2 Shear behavior of RC elements under cyclic Loading 11
2.2.1 Fenwick and Fong (1979) 11
2.2.2 Ang et al. (1989) 12
2.2.3 Stevens et al. (1991) 13
2.2.4 Priestley et al. (1994) 14
2.2.5 Biskins et al.(2004) 14
2.2.6 Mihaylov et al. (2010) 15
2.2.7 Arslan and polat (2013) 16
2.2.8 Ruggiero et al. (2016) 17
2.2.9 Research gap 18
3 EXPERIMENTAL PROGRAM 20
3.1 Specimen Summary 20
3.2 Material properties 22
3.2.1 Concrete 22
3.2.2 Steel 25
3.3 Specimen Fabrication 26

3.3.1 Preparation of the rebar 26
3.3.2 Installation of the rebar cages into the formwork 27
3.3.3 Casting of the concrete 28
3.4 Test Setup 29
3.5 Instrumentation and data acquisition 29
3.6 Loading Pattern 31
4 FEM ANALYSIS USING DUCOM-COM3 32
4.1 About the software 32
4.2 Specimens 32
4.3 Materials 36
4.4 Modeling 37
4.5 Support condition and loading 38
5 RESULT AND DISCUSSION 39
5.1 Results 39
5.1.1 Test summaries 39
5.1.1.1 B1M 39
5.1.1.2 B1C90 41
5.1.1.3 B2M 42
5.1.1.4 B2C90 43
5.1.1.5 B2C85 45
5.1.1.6 B2C80 47
5.1.2 Experimental results 48
5.1.2.1 Load deflection curves 48
5.1.2.2 Strain measurements 53
5.1.3 Analytical results 63
5.1.3.1 Load deflection curves 64
5.2 Discussion 67
5.2.1 Shear behavior of experimental beams 67
5.2.1.1 Capacity prediction 67
5.2.1.2 Comparison in response of Type one beams 69
5.2.1.3 Comparison in response of Type two beams 70
5.2.1.4 Comparison between type 1 and type 2 beams 73
5.2.1.5 Diagonal crack path 74
5.2.2 Comparison between experimental and analytical results 77

5.2.3 S-N Curve 80
6 CONCLUSION AND RECCOMENDATION 83
6.1 Conclusion 83
6.2 Recommendation 85
REFERENCE 86
ANNEX A 89
ANNEX B 92

LIST OF FIGURES

Figure 2.1 : Flexural and shear stress acting on elements in the shear span [4] 4
Figure 2.2 : Reinforced Concrete membrane element subjected to biaxial and shear stress [5] 5
Figure 2.3 : Principal coordinate 1-2 for applied stress [5] 6
Figure 2.4 : Assumed crack direction in fixed angle model [5] 6
Figure 2.5 : Principal coordinate r-d for internal concrete stress [5] 8
Figure 2.6 : Assumed crack direction in Rotating angle model [5] 8
Figure 2.7 : shear cracking in Reinforced Concrete beams [6] 11
Figure 3.1 : Typical beam (Type 1 and Type 2) layout and strain gauge arrangement 21
Figure 3.2 : Beam Layout and strain gauge arrangement for B2C80 22
Figure 3.3 : Slump tests 22
Figure 3.4: Compressive Strength testing machine 23
Figure 3.5 : Split Cylinder testing machine 23
Figure 3.6 : Tension test performed on Rebar 26
Figure 3.7 : Rebar preparation 27
Figure 3.8 : Reinforcement cage for Type 2 Beams 27
Figure 3.9 : Strain gauge installation for B2C80 27
Figure 3.10 : Reinforcement cage placement in formwork 28
Figure 3.11 : Concrete Mixer 28
Figure 3.12 : Casting Concrete in Metal formwork 28
Figure 3.13 : Test Setup 29
Figure 3.14: Hydraulic Jack 30
Figure 3.15 : Load Cell 30
Figure 3.16 : Data logger 30
Figure 3.17 : Linear variable displacement transducer (LVDT) 31
Figure 3.18 : Strain Gauge 31
Figure 3.19 : Loading Pattern 31
Figure 4.1: Type one beam Finite Element mesh 33
Figure 4.2 : Reinforcement cage of Type one beam 34
Figure 4.3: Reinforcement cage of Type 1 beam on DUCOM-COM3 34
Figure 4.4: Type two beam finite element mesh 35
Figure 4.5 : Reinforcement cage for Type two beam on DUCOM-COM3 35
Figure 5.1 : Damage on B1M 40
Figure 5.2 :B1M after failure 41
Figure 5.3 : B1C90 after failure 42
Figure 5.4 : B2M after failure 43
Figure 5.5 : B2C90 after failure 44
Figure 5.6 : B2C90 after failure (half view) 44
Figure 5.7 : B2C90 after failure (half view) 45
Figure 5.8 : B2C85 after failure 46
Figure 5.9 : B2C85 after failure (bottom) 46
Figure 5.10 : B2C80 after failure (half view) 48
Figure 5.11 : B2C80 after failure 48
Figure 5.12 : Load deflection diagram for specimen B1M 49

Figure 5.13 : Load deflection diagram for specimen B1C90 49
Figure 5.14 : Load deflection diagram for specimen B2M 50
Figure 5.15 : Load deflection diagram for specimen B2C90 50
Figure 5.16 : Load deflection diagram for specimen B2C85 51
Figure 5.17 : Load deflection diagram for specimen B2C80 51
Figure 5.18 : Mid-span deflection history for specimen B2C85 53
Figure 5.19 : Load Vs Strain from strain gauge S1 on B2M 54
Figure 5.20 : Load Vs Strain from strain gauge S2 on B2M 54
Figure 5.21 : Load Vs Strain from strain gauge S1 on B2C90 55
Figure 5.22 : Load Vs Strain from strain gauge S2 on B2C90 55
Figure 5.23 : Load Vs Strain from strain gauge S1 on B2C85 56
Figure 5.24 : Load Vs Strain from strain gauge S1 on B2C80 57
Figure 5.25 : Load Vs Strain from strain gauge S2 on B2C80 57
Figure 5.26 : Load Vs Strain from strain gauge S3 on B2C80 58
Figure 5.27 : Load Vs strain from strain gauge S4 on B2C80 58
Figure 5.28 : Load Vs strain from strain gauge S5 on B2C80 58
Figure 5.29 : Load Vs strain from strain gauge S6 on B2C80 59
Figure 5.30 : Load Vs strain from strain gauge S7 on B2C80 59
Figure 5.31 : Strain Readings from specimen B2C90, B2C85 and B2C80 62
Figure 5.32 : Strain contour and displacement output of A-B2M in load-step 43 63
Figure 5.33: Strain contour and displacement output of A-B2C90 in load-step 10 63
Figure 5.34 : Load deflection diagram for specimen A-B1M 64
Figure 5.35 : Load deflection diagram of A-B1C90 65
Figure 5.36 : Load deflection diagram of A-B2M 65
Figure 5.37 : Load deflection diagram of A-B2C90 66
Figure 5.38 : Load deflection diagram of A-B2C85 66
Figure 5.39 : Load deflection diagram of A-B2C80 67
Figure 5.40 : Comparison between B1M and B1C90 69
Figure 5.41 : comparison between B2M and B2C90 70
Figure 5.42 : Comparison between B2M and B2C85 71
Figure 5.43 : Comparison between B2M and B2C80 72
Figure 5.44 : Comparison between B1M and B2M 73
Figure 5.45 : Comparison between B1C90 and B2C90 74
Figure 5.46 : Diagonal crack path of Type two beams 75
Figure 5.47 : Diagonal crack path of B2C85 76
Figure 5.48 : Diagonal crack path of B2M 76
Figure 5.49 : Diagonal crack path of B2M and B2C85 76
Figure 5.50 : Analytical and experimental load deflection diagram of specimen B1M 77
Figure 5.51 : Analytical and experimental load deflection diagram of specimen B1C90 78
Figure 5.52 : Analytical and experimental load deflection diagram of specimen B2M 78
Figure 5.53 : Analytical and experimental load deflection diagram of specimen B2C90 79
Figure 5.54 : Analytical and experimental load deflection diagram of specimen B2C85 79
Figure 5.55 : Analytical and experimental load deflection diagram of specimen B2C80 80
Figure 5.56 : relationship between Mid-span deflection and number of cycles 81
Figure 5.57 : S-N diagram for Type-two beam 82

LIST OF TABLES

Table 3-1 : Summary of experimental specimens, as built 21
Table 3-2 : Average Concrete Strengths (Test day) 24
Table 3-3 : Average Cylindrical Compressive Strength of core samples 24
Table 3-4 : Mix proportion of Concrete 25
Table 3-5 : Mechanical properties of Reinforcement 26
Table 4-1 : Specimen Description 33
Table 4-2 : Mechanical Property of Concrete 36
Table 4-3: Mechanical property of Reinforcement bars 37
Table 5-1 : summary of experimental results 39
Table 5-2 : Summary of analytical results 64
Table 5-3 : Predicted capacity of experimental beams 68

ABSTRACT

The shear strength of Reinforced Concrete structures degrades under cyclic loading; leading to unforeseen, brittle shear failures. This thesis presents both experimental and analytical investigation to the fatigue behavior of Reinforced concrete beams failing in shear. The fatigue life of shear-critical beams is also discussed in light of the experimental and analytical output.

An experimental research on six shear-critical Reinforced Concrete slender beams was conducted to investigate shear behavior under low-cycle fatigue loading. The variables were shear reinforcement ratio (0.00% and 0.13%) and type of loading (monotonic and one-side cyclic loading). All members fail in shear before yielding of longitudinal reinforcement as intended. The provision of only 0.13% of shear reinforcement significantly increased the capacity of the beam under monotonic loading by 51.93%. For beams with shear reinforcement, the load deflection response measured under monotonic loading provided an excellent envelope for cyclic response and shear strength degradation was significant with much reduced fatigue life in low-cycle fatigue ranges. Moreover, Strain measurements on shear reinforcements exhibited progressive increase in strain with each cycle confirming cyclic material softening of both the concrete and the stirrups. Surprisingly, a single beam with shear reinforcement under cyclic loading exhibited a higher capacity than its expected monotonic capacity. This has been attributed to alteration of diagonal crack path and possible favorable effects of fatigue loading are discussed.

Key words: shear-critical, low-cycle fatigue, diagonal crack path, slender beams

1 INTRODUCTION

1.1 Background

Due to lack of a unifying rational theory explaining the internal mechanism of shear in members, the problem of shear remains an elusive subject in the research community by large. Despite the many unknowns related to shear, various researches clearly show the degradation in the shear strength of Reinforced Concrete members under cyclic loading. However international codes, such as American Concrete Institute's Building code (ACI 318)[1] and the Eurocode 2 (EN1992-1-1: 2004)[2] use semi-empirical equations based on experiments performed under monotonic loading conditions with general and allegedly conservative provisions to account for shear degradation under cyclic loading.

There is a general consensus that a significant amount of shear is transferred in the web of the beam, most of this across inclined cracks due to aggregate interlock. Hence Shear strength of Reinforced Concrete members deteriorates under cyclic loading because the widening of flexure-shear cracks reducing the capacity for shear transfer by aggregate interlock. Most researches show pronounced shear degradation in plastic hinge zones where flexural yielding occurs. Hence the research community has long been focused in investigating degradation of shear resistance mainly in these zones and its implications on ductility. Therefore there's a sparse data on the response of members failing in shear under cyclic loading. Hence this thesis sets out to discover fatigue behavior of shear-critical Reinforced Concrete slender beams. Moreover an analytical simulation using nonlinear finite element analysis software: DuCOM-COM3 will be utilized for further investigation and careful observation.

1.2 Significance

Ethiopia has recently adopted the Eurocode as the national building code in ES: EN 2015 which is a commendable move towards joining the international world of Engineering and construction. Furthermore, the seismic hazard map of the country has been changed in line with different seismological findings; doubling the expected lateral force in some areas such as Addis Ababa. [3] Along with the capacity design principles that are recently to be implemented in the Engineering practice of the country, many structures could be found shear-critical if evaluated according to the latest code. Opportunely, this thesis gives insight to the performance of beams failing due to shear under cyclic loading. Since shear capacity degradation has implications on ductility and shear to flexure over strength factors, observations and findings in the research can have extensive impact on internal shear stress models and earthquake resistant design.

1.3 Objectives

- To investigate the performance of beams failing due to shear (shear-critical beams) under one-side cyclic loading
- To investigate the performance of beams without web reinforcement under low-cycle fatigue loading
- To quantify shear strength degradation of RC beams with number of cycles for low-cycle fatigue analysis

1.4 Scope and limitations

The six experimental beams are all slender and similar in cross-section, size and shape. They will be designed to fail in shear; hence longitudinal reinforcements are not expected to yield as in flexural hinge zones. (Shear-critical members)

Due to limitations in capacity of the current laboratory, monotonic and one-side cyclic loading will be performed using force based approach; yet displacement shall be measured throughout the experiments. This research will not be directly correlated to structures designed according to capacity design philosophy and won't have any implications on ductility of RC members.

2 LITERATURE REVIEW

2.1 Theoretical Background

In the structural design of reinforced concrete members flexure and shear are primary considerations for the determination of the size of the section and provision of flexural and shear reinforcement. Because shear failure is frequently sudden and brittle, the design for shear must ensure that the shear strength equals or exceeds the flexural strength at all points in the beam. Moreover for seismic design of members according to capacity design principles, there needs to be a definitive shear to flexure over-strength to ensure ductile failure under seismic event.

The manner in which shear failures can occur varies widely with section geometry and size, loading condition, material and other properties of the members. For this reason, there is no unique way to design for shear. In this section, we shall briefly discuss the internal shear force, V, in slender beams and current theories being utilized for analytical modeling of shear capacity.[4]

2.1.1 Fundamentals of Shear

Fundamentally, the intensity of a force acting tangent to an area, A is called the shear stress, $\tau = \frac{F}{A}$. In any typical beam shear stress and shear force will exist in those parts of a beam where the moment changes from section to section since V = dM/dx. For homogeneous, elastic beam, we can calculate the shear stress at any section by using the common shear formula derived from basic calculus and equilibrium condition as follows: $\upsilon = \frac{VQ}{It}$. [4]

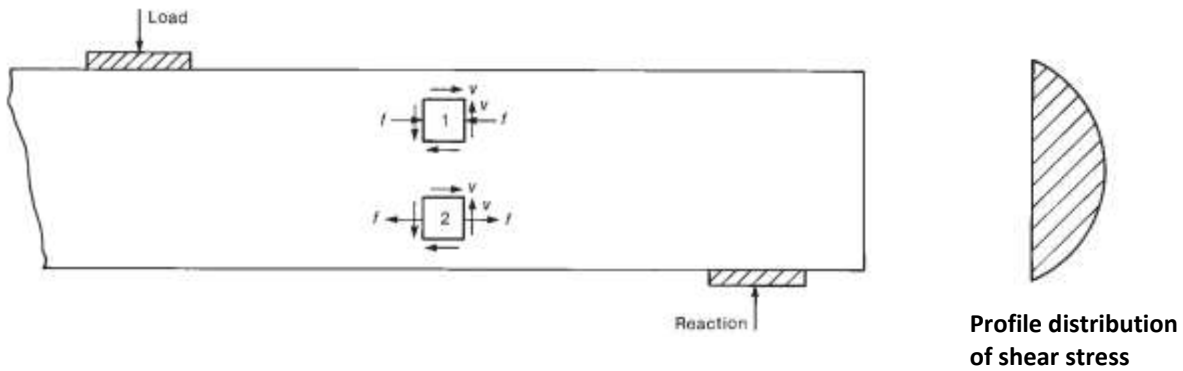

Figure 2.1 : Flexural and shear stress acting on elements in the shear span [4]

Equal shearing stress exists on both the horizontal and vertical planes through an element, as shown in Figure 2.1. To satisfy equilibrium conditions for a 2D element under pure shear, all

four shear stresses must have equal magnitude and be directed either toward or away from each other at opposite edges of the element. The same principle can be extrapolated to 3D elements to determine $\tau_{zx} = \tau_{xz,}$ $\tau_{zy} = \tau_{yz}$ and $\tau_{xy} = \tau_{yx.}$ For the general state of the stress, this principle derived from mechanics reduces the number of shear stresses from six to three.

The elements in Figure 2.1 are subjected to combined normal stresses due to flexure, f, and shearing stresses, v. The largest and smallest normal stresses acting on such an element when seen from a specific plane are referred to as principal stresses. The principal stresses and planes are found by using mathematical formulations for stress transformation. [4] The general equation for principal stresses in the form of a Mohr circle is displayed on equation (2.1).

$$\sigma_{1,2} - \frac{\sigma_l + \sigma_t}{2} = \pm\sqrt{\left(\frac{\sigma_l - \sigma_t}{2}\right)^2 + \tau_{lt}{}^2} = \pm r \qquad (2.1)$$

2.1.1.1 Fixed Angle theory

Before we begin to discuss the different theories currently under research to estimate shear capacity, let's consider a reinforced concrete 2D element as shown in the figure below.

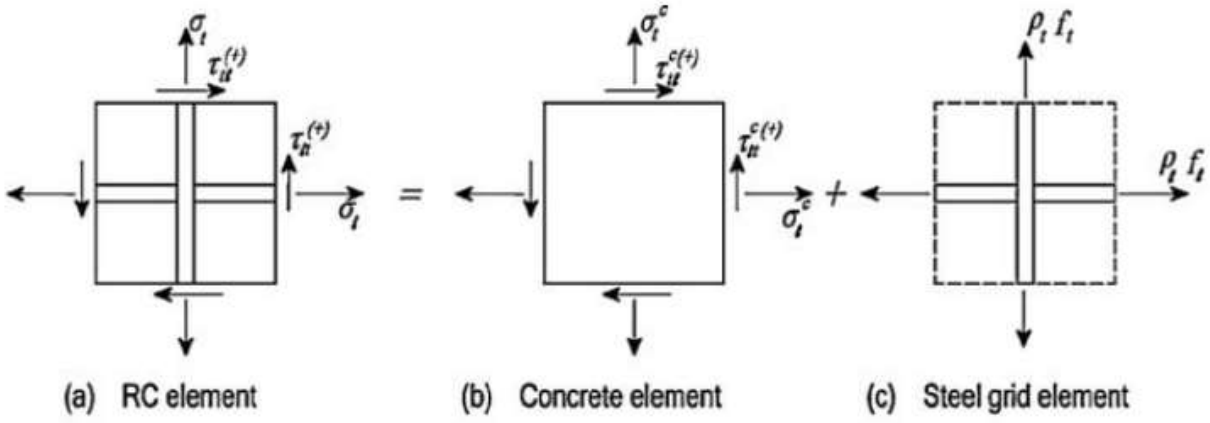

Figure 2.2 : Reinforced Concrete membrane element subjected to biaxial and shear stress [5]

Figure 2.2 clearly displays RC element subjected to in plane shear stress and normal stresses. The longitudinal and transverse steel bars coincide with the ℓ and t axis of the ℓ-t coordinate system. Hence the normal and shear stress applied on the element can be designated as σ_ℓ, σ_t and $\tau_{\ell t}$.

The RC element shown in Figure 2.2 can be separated into a concrete element (Figure 2.2 (b)) and a steel grid element (Figure 2.2 (c)). The normal and shear stresses on the concrete element are designated as σ^c_ℓ, σ^c_t and $\tau^c_{\ell t}$.in the $\ell - t$ coordinate system. The smeared steel stresses on the

steel grid element are designated as $\rho_\ell f_\ell$ and $\rho_t f_t$ in the $\ell - t$ coordinate system. The symbols f_ℓ and f_t are the stresses in the steel bars. The steel bars are assumed to take only axial stresses, neglecting any possible dowel action. [5]

Summing the concrete stresses (σ^c_ℓ, σ^c_t and $\tau^c_{\ell t}$) and the steel stresses ($\rho_\ell f_\ell$ and $\rho_t f_t$), respectively, in the l- and t -directions and equating them to the externally applied stresses gives:

$$\sigma_l = \sigma^c_l + \rho_l f_l \qquad (2.2)$$

$$\sigma_t = \sigma^c_t + \rho_t f_t \qquad (2.3)$$

$$\tau_{lt} = \tau^c_{lt} \qquad (2.4)$$

The applied principal stresses for the RC element are referred to as σ_1 and σ_2 based on 1-2 coordinate system as shown in the figure below.

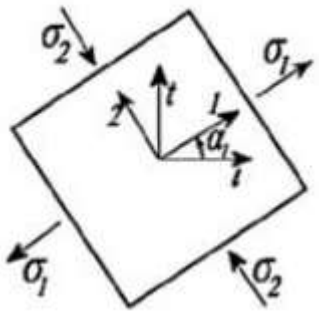

Figure 2.3 : Principal coordinate 1-2 for applied stress [5]

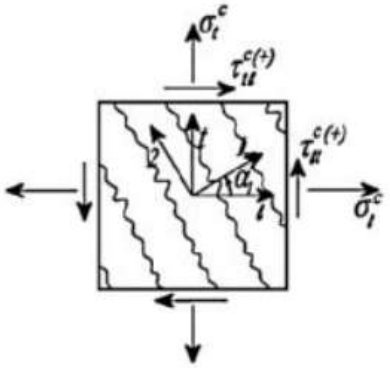

Figure 2.4 : Assumed crack direction in fixed angle model [5]

The angle from the $\ell - t$ coordinate to the $1 - 2$ coordinate is defined as the fixed angle α_1, because this angle does not change when the three in-plane stresses increase proportionally. The fixed angle theories are based on the assumption that the direction of subsequent cracks is perpendicular to the applied principal tensile stress, as shown in Figure 2.4. However in reality, after cracking the principal tensile stress in the concrete will rotate from the 1-2 axes; which means crack direction shall rotate as well. Yet since fixed angle theory is only based on the principal applied stress, α_1 shall remain constant. [5]

Now reversing the stress transformation process that yield equation (2.1), to transform the stresses in the 1-2 coordinate system (σ_1, σ_2 and τ_{12}) into the stresses in the ℓ-t coordinate system (σ_ℓ, σ_t and $\tau_{\ell t}$), we have

$$\sigma^c_{\ l} = \sigma^c_{\ 1}\cos^2\alpha_1 + \sigma^c_{\ 2}\sin^2\alpha_1 - \tau^c_{\ 12}2\sin\alpha_1\cos\alpha_1 \quad (2.5)$$

$$\sigma^c_{\ t} = \sigma^c_{\ 1}\sin^2\alpha_1 + \sigma^c_{\ 2}\cos^2\alpha_1 + \tau^c_{\ 12}2\sin\alpha_1\cos\alpha_1 \quad (2.6)$$

$$\tau^c_{\ lt} = (\sigma^c_{\ 1} - \sigma^c_{\ 2})\sin\alpha_1\cos\alpha_1 + \tau^c_{\ 12}(\cos^2\alpha_1 - \sin^2\alpha_1) \quad (2.7)$$

Inserting equations (2.5), (2.6) and (2.7) to equations (2.2), (2.3) and (2.4) respectively gives the three equilibrium equations for Fixed angle theories as:

$$\sigma_l = \sigma^c_{\ 1}\cos^2\alpha_1 + \sigma^c_{\ 2}\sin^2\alpha_1 - \tau^c_{\ 12}2\sin\alpha_1\cos\alpha_1 + \rho_l f_l \quad (2.8)$$

$$\sigma_t = \sigma^c_{\ 1}\sin^2\alpha_1 + \sigma^c_{\ 2}\cos^2\alpha_1 + \tau^c_{\ 12}2\sin\alpha_1\cos\alpha_1 + \rho_t f_t \quad (2.9)$$

$$\tau_{lt} = (\sigma^c_{\ 1} - \sigma^c_{\ 2})\sin\alpha_1\cos\alpha_1 + \tau^c_{\ 12}(\cos^2\alpha_1 - \sin^2\alpha_1) \quad (2.10)$$

Similarly we can use the reverse transformation matrix $[T]^{-1}$ to transform a set of strains in the 1–2 coordinate (ε_1, ε_2 and γ_{12}) into their respective set of strains in the $\ell - t$ coordinate (ε_ℓ, ε_t and $\gamma_{\ell t}$). Consequently, the three compatibility equations for fixed angle theories are:

$$\varepsilon_l = \varepsilon_1\cos^2\alpha_1 + \varepsilon_2\sin^2\alpha_1 - \frac{\gamma_{12}}{2}2\sin\alpha_1\cos\alpha_1 \quad (2.11)$$

$$\varepsilon_t = \varepsilon_1\sin^2\alpha_1 + \varepsilon_2\cos^2\alpha_1 + \frac{\gamma_{12}}{2}2\sin\alpha_1\cos\alpha_1 \quad (2.12)$$

$$\frac{\gamma_{lt}}{2} = (\varepsilon_1 - \varepsilon_2)\sin\alpha_1\cos\alpha_1 + \frac{\gamma_{12}}{2}(\cos^2\alpha_1 - \sin^2\alpha_1) \quad (2.13)$$

For the solution of these three stress equilibrium equations and the three strain compatibility equations, stress–strain relationships for concrete and for mild steel bars are required. In Fixed Angle theory, this concrete constitutive relationship is as follows:

$$\begin{bmatrix} \sigma^c_{\ 1} \\ \sigma^c_{\ 2} \\ \tau^c_{\ 12} \end{bmatrix} = \begin{bmatrix} E_1 & 0 & 0 \\ 0 & E_2 & 0 \\ 0 & 0 & G_{12} \end{bmatrix} \begin{bmatrix} \varepsilon_1 \\ \varepsilon_2 \\ \frac{\gamma_{12}}{2} \end{bmatrix} \quad (2.14)$$

2.1.1.2 Rotating Angle theory

In the rotating angle theory the direction of cracks is defined by the rotating angle α_r in the principal r − d coordinate of concrete, as shown in Figure 2.5. The rotating angle theories are based on the assumption that the direction of cracks is perpendicular to the principal tensile stress in the concrete element; not to the applied principal stresses like Fixed Angle theory. [5]

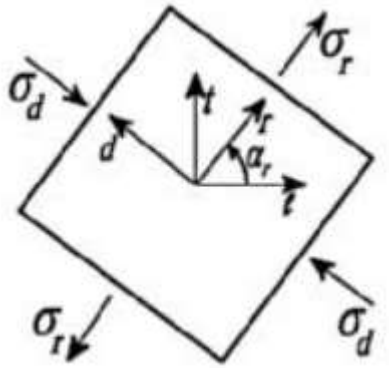

Figure 2.5 : Principal coordinate r-d for internal concrete stress [5]

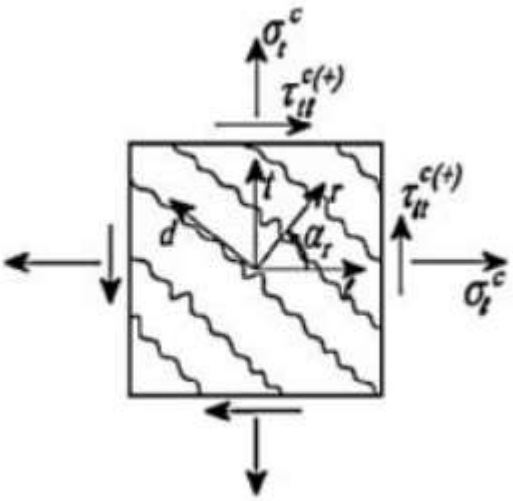

Figure 2.6 : Assumed crack direction in Rotating angle model [5]

Similar to the derivation of equilibrium equations for fixed angle theories, we can reverse the stress transformation process to transform the stresses in the r-d coordinate system (σ_r, σ_d and τ_{rd}) into the stresses in the l-t coordinate system (σ_l, σ_t and τ_{lt}). Yet in this case, the shear stress in the concrete τ_{rd} must vanish ($\tau_{rd} = 0$), because the r-d coordinate is a principal coordinate for the internal stresses in the concrete.

$$\sigma^c{}_l = \sigma_r \cos^2 \alpha_r + \sigma_d \sin^2 \alpha_r \qquad (2.15)$$

$$\sigma^c{}_t = \sigma_r \sin^2 \alpha_r + \sigma_d \cos^2 \alpha_r \qquad (2.16)$$

$$\tau^c{}_{lt} = (\sigma_r - \sigma_d) \sin \alpha_r \cos \alpha_r \qquad (2.17)$$

Inserting equations (2.15), (2.16) and (2.17) to equations (2.2), (2.3) and (2.4) respectively gives the three equilibrium equations for Rotating angle theories as:

$$\sigma_l = \sigma_r \cos^2 \alpha_r + \sigma_d \sin^2 \alpha_r + \rho_l f_l \qquad (2.18)$$

$$\sigma_t = \sigma_r \sin^2 \alpha_r + \sigma_d \cos^2 \alpha_r + \rho_t f_t \qquad (2.19)$$

$$\tau_{lt} = (\sigma_r - \sigma_d)\sin\alpha_r \cos\alpha_r \qquad (2.20)$$

Similarly the three compatibility equations for Rotating angle theories are:

$$\varepsilon_l = \varepsilon_r \cos^2\alpha_r + \varepsilon_d \sin^2\alpha_r \qquad (2.21)$$

$$\varepsilon_t = \varepsilon_r \sin^2\alpha_r + \varepsilon_d \cos^2\alpha_r \qquad (2.22)$$

$$\frac{\gamma_{lt}}{2} = (\varepsilon_r - \varepsilon_d)\sin\alpha_r \cos\alpha_r \qquad (2.23)$$

For the solution of these three stress equilibrium equations and the three strain compatibility equations, stress–strain relationships for concrete and for mild steel bars are required. In Rotating angle theory, the shear modulus G_{rd} is usually taken as a small value to provide stability in calculation. The concrete constitutive relationship can be expressed in matrix form as follows:

$$\begin{bmatrix} \sigma^c{}_r \\ \sigma^c{}_d \\ \tau^c{}_{rd} \end{bmatrix} = \begin{bmatrix} E_r & 0 & 0 \\ 0 & E_d & 0 \\ 0 & 0 & G_{rd} \end{bmatrix} \begin{bmatrix} \varepsilon_r \\ \varepsilon_d \\ \frac{\gamma_{rd}}{2} \end{bmatrix} \qquad (2.24)$$

2.1.1.3 Summary of angle theories

Generally if a similar reinforcement ratio is not provided in the two orthogonal directions ($\rho_\ell f_\ell \neq \rho_t f_t$), when the principal tensile stress σ_1 reaches the tensile strength of concrete, cracks will form and the r-d coordinate after cracking will deviate from the 1-2 coordinate. The deviation angle is defined as $\beta = \alpha_r - \alpha_1$. However experimentally recorded deviation angle will be less than the theoretical deviation; where at ultimate load it might be about one-half of the theoretically calculated β –angle. This can be one indication that the reality lies between the two reviewed theories for shear

Moreover, the contribution of concrete is represented differently in the two theories. In fixed angle theories a concrete strut, under axial compression $\sigma^c{}_2$, is also subject to a concrete shear stress $\tau^c{}_{12}$ in the direction of cracks. Thus concrete contribution, Vc is extant and a function of this shear stress $\tau^c{}_{12}$ on the concrete element. However rotating angle theory assumes at the principal r-d coordinate, a concrete strut is subjected only to an axial compressive stress σ_d; and

hence concrete shear stress τ^c_{12} vanishes. Therefore the concrete contribution, which is a function of τ^c_{12} in fixed angle theories, is zero in rotating angle theory.

The fixed angle theory is more accurate because it can predict the Vc term observed in tests. (Hsu and Mo, 2010, P. 144) However the additional τ^c_{12} to its equilibrium equations makes the calculation complicated and cumbersome. Moreover, rotating angle theory is suitable to study the effect of steel reinforcement through the Vs term, without the complication induced by the concrete shear stress. [5]

2.1.2 Shear cracking in reinforced concrete members

For a plain concrete beam without reinforcements, as the load is increased a tension crack will occur where the tensile stresses are the largest (at the point of maximum bending moment) and will immediately cause failure. This is why horizontal reinforcements are required to restrain the opening of a vertical flexural crack. Similarly web reinforcements are provided to avoid diagonal tension failure or shear failure immediately after inclined cracking. Web reinforcements carry the additional shear force after inclined cracking and allow stress redistribution. Ideally inclined stirrups would be efficient to carry the principal tensile stress due to the shear; however they are not effective in beams resisting shear reversals such as seismic loads. [4], [6]

Inclined cracks must always precede shear failure. Inclined cracks form in two different ways depending on the relative values of M and V. At locations of large shear stress and lower flexural stresses such as: sections near support, pre-stressed beams etc., there will be little or no flexural cracking prior to the development of diagonal tension cracks in the web. For this case, according to the parabolic shear stress distribution cracks will first form near the neutral axis and propagate. These cracks appear when the internal principal tensile stress equals the tensile strength of the concrete at the centroid.

In most reinforced concrete beams however, flexural cracks form first and then extend into the beam. This is to be generally expected when both the shear and the moment are large values. When cracks occur the stress at the cracks will drop down to zero, being relieved due to energy dissipation, causing stress concentration at the head (or tip) of the cracks. For shear critical members, diagonal cracks will branch out of the initial flexural cracks creating flexural shear cracks. Due to the redistribution of stress during formations of flexural cracks, the onset of

inclined cracking in a beam cannot be predicted from the principal stresses unless shear cracking precedes flexural cracking. [4]

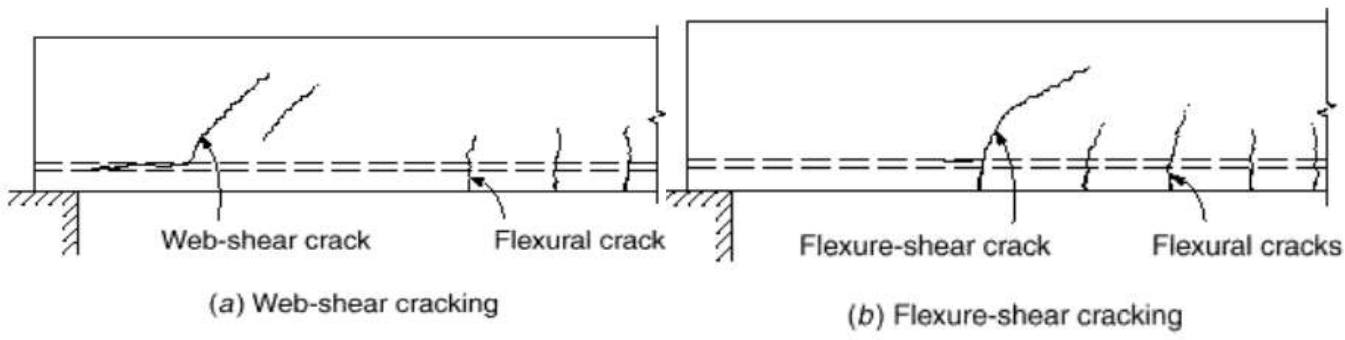

Figure 2.7 : shear cracking in Reinforced Concrete beams [6]

2.2 Shear behavior of RC elements under cyclic Loading

The importance of the cyclic behavior of Reinforced Concrete structures, particularly pertaining to seismic events, has long been appreciated. Hence there is no shortage of experimental research concerning the reversed cyclic loading of Reinforced Concrete beams, columns, walls etc. Since this research mainly focus on cyclic shear response of Reinforced Concrete slender beams failing in shear, the review will mainly focus on analogous or relevant experiments and models. Therefore, researches not in direct consequence to this thesis may not be extensively discussed; however their underlying concepts might be reviewed in reference to other papers that reiterated the concepts. However it should be noted that consequential papers such as Paulay[7], Hsu[8], Okamura et al.[9], Okamura and Ueda[10], Martin Pèrez and Pantazopoulou[11], Vecchio[12] and Park et al.[13] have also been reviewed and used as a basis for this thesis's experimental work.

2.2.1 Fenwick and Fong (1979)

The behavior of beams failing in flexure, in which plastic hinges are formed under cyclic loading, is examined in this early research. The research bases most of its general concepts on current papers and codes of the time. The general consensus of the time reflected in Paulay's paper such as: a) shear resisted by the concrete in the region of the beam where flexural steel yields, should be taken as zero, b) To prevent sliding shear failure, shear stress should not exceed $0.5\sqrt{f_c'}$ etc. are discussed and affirmed.

The paper is based on five beam tests carried out at the University of Auckland, in 1977. These beam tests were carried out to investigate the influence of shear stress levels on plastic hinge

zone performance. For this intent, shear stress was varied in the beams by changing the span to depth ratio. According to the test results, higher shear stress level resulted in more pinched load deflection characteristics and reduced the number of cycles sustained by the beam. Serious stiffness degradation at low loads and appreciable strength degradation at maximum displacements were also observed on such beams.

The paper concludes as shear stress level increases plastic hinge zone performance is adversely affected. Yet to find a rational cutoff point for design further investigation is recommended. Nevertheless a view held by previous researches that cyclic shear stress in excess of $0.29\sqrt{f_c^{'}}$ in the plastic hinge zone could lead to a significant reduction in energy dissipation of the hinge was partially concurred. [14]

2.2.2 Ang et al. (1989)

This paper discusses capacity design principles by reviewing two codes of the time: ACI 318 and NZS 3101, in an attempt to establish a realistic level for the design shear force for circular columns. The paper also improves on suggested design equations based on results from an experimental program designed to investigate the influence of transverse reinforcement, axial load, and flexural ductility on the shear strength of circular columns.

According to current design codes of the time, in plastic hinge regions of axial load level $p \le 0.1 f_c^{'} A_g$, Vc (concrete contribution) is taken as zero. Because concrete contribution, which is majorly dependent on aggregate interlock and intact concrete in the compression zone, is likely to be undependable when wide flexural cracks occur under reversed cyclic loading.

25 circular columns of 400 mm diameter were constructed and tested under cyclic reversals of lateral loading as part of a major investigation into the strength and ductility of bridge columns. Variables in the test program included axial load level, flexural reinforcement ratio, shear reinforcement ratio and aspect ratio or MV/d (also known as a/d). The columns were divided into four categories based on ductility levels they can achieve before exhibiting shear failure: ductile flexural ($\mu \ge 6$), moderately ductile with shear failure ($4 < \mu \le 6$), limited ductile with shear failure ($2 < \mu \le 4$) and Brittle shear failure ($\mu \le 2$).

The following observations were made based on the test results. Columns under brittle shear failure category exhibited severe strength and stiffness degradation. Commonly for all the columns with different ductility levels, the concrete contribution gradually decreases until

maximum load is achieved, with much more rapid strength degradation in the post ultimate stage of testing. Shear capacity of concrete increases with axial load because of reduced crack width and hence enhanced aggregate interlock and improved compression shear transfer. Shear at diagonal loading also increased with axial load and with decreasing aspect ratio. Most codes take the concrete contribution to shear at the onset of diagonal cracking and shear carried by web reinforcement using 45^0 truss analogy to be the shear capacity of a section ($V_n = V_c + V_s$). However the test results showed the concrete contribution to shear at maximum lateral load is approximately 30 percent higher than at the onset of diagonal cracking.

The paper concludes that the current U.S. and New Zealand design equations for the concrete contribution were found to be very conservative in light of the test results and makes recommendation for further study to form the shear strength versus flexural ductility relationships. Although such relationships will soon come into existence, the exact value of the concrete contribution for shear still remains unanswered. [15]

2.2.3 Stevens et al. (1991)

This paper is based on reversed cyclic pure shear tests done on three reinforced concrete panels, 1600 x 1600 x 285 mm in the University of Toronto's shell element tester. The research was intended to discover the exact deterioration of the concrete compressive strength due to transverse tensile strains in a pure shear element. The post cracking tensile stresses in the concrete and the direction of the principal stresses and principal strains in the concrete were also of particular interest. Testing was done by applying principal compression and tension stress on a panel with reinforcement steel (x-y axes) oriented at 45^0 to the horizontal (or principal axes).

Test results clearly showed dramatic reduction of the concrete compressive strength due to co-existing principal tensile strain as quantified by Vecchio and Collins[16] in an earlier work. Enough cycles of shear stress above flexural yield will eventually cause failure of a Reinforced Concrete element. Hence it follows that the shear reinforcement of beam-column joints which will be subjected to seismic effects should be designed to remain elastic while resisting maximum shear. It should also be noted that biaxial compression on one of the panels produced large strength gain and delay in cracking.

A constitutive model similar to modified compression field theory was also proposed by the paper to reproduce the behavior of reinforced concrete panels subjected to monotonic and reversed cyclic membrane loading. Although the assumption that principal stress and principal

strain are coincident had disparities, the model was still able to reproduce well with the experimental results. [17]

2.2.4 Priestley et al. (1994)

This paper builds on the design codes of the time such as: ACI 318, ATC-6 model and experimental researches by Ang et al.[15] and Wong et al.[18]. A review of existing design equations showed wide differences in predicted response. Moreover the effect of flexural ductility on the shear strength of the concrete mechanism was not distinctly incorporated in design code equations. A rudimentary recommendation of abandoning Vc, concrete contribution, based on axial load level was mainly listed in design codes.

Existing models and experiments of the time displayed direct proportionality between shear strength and axial load; and inverse relationship between shear strength and aspect ratio or a/d. The paper examines a number of methods to predict shear strength of columns based on already established relationships. By refining different experimental and analytical models, a novel approach of predicting the shear strength of reinforced concrete rectangular and circular columns subjected to cyclic lateral shear force was formulated. The shear strength of the column is considered to consist of three independent components: concrete contribution, V_c, whose quantity depends on ductility level, an axial load component, V_p, depending on column aspect ratio and truss mechanism, V_s, depending on the amount of shear reinforcement.

Degradation of concrete shear strength with displacement ductility, V_p as a function of span to depth ratio and the contribution of transverse reinforcement to shear strength as a 30^0 truss mechanism were individually formulated and cumulatively taken as a predictive equation ($V_n = V_c + V_p + V_s$). The proposed approach provided improved prediction of shear strength than alternative methods. The influence of flexural ductility, axial load and aspect ratio are closely simulated in the equations. [19]

2.2.5 Biskins et al.(2004)

The main aim of this paper was to evaluate two alternative models for degradation of shear resistance correlated with cyclic displacement ductility demand; based on a database of 239 tests on Reinforced concrete specimens of Beams, columns, walls and hollow rectangular piers. All specimens failed in shear after their longitudinal reinforcement yielded in flexure. Such specimens are selected because cyclic degradation of shear is expected to be prominent within flexural plastic hinge regions. This is because degradation occurs due to the breakdown of

internal shear transfer mechanism due to extensive cracking and inelastic strains in longitudinal and transverse reinforcements.

The two models were based on prior models developed in previous researches. In the first model, only V_c (concrete contribution) is taken to degrade with inelastic cyclic displacement. However on the second model, both V_c and V_s degrade with inelastic cyclic displacement. The effect of axial compression on shear strength is incorporated in both models; while the contribution of web reinforcement to shear strength (V_s) is based on the classical 45-degree truss analogy. Between the two models, the second model, where both V_c and V_s are assumed to degrade, gave a slightly better fit to the data. The model also suggests shear resistance doesn't degrade below a displacement ductility demand of 6. This conforms to previous observations and models developed in researches referred by the paper.

An attempt was made to cast this research work within the framework of shear design advocated by present European codes. The variable strut inclination approach that allows the strut angle θ to be as low as 22^0 (Cot θ =2.5) is employed in these codes, with the concrete contribution (V_c) entirely neglected if shear reinforcement is provided. According to this paper, this approach was criticized for not being suitable for design against seismic loads. A Ritter-Mörsch 45-degree truss model supplemented with Vc that degrades with displacement ductility demand is recommended as a better means for shear design of RC members under seismic loads. [20]

2.2.6 Mihaylov et al. (2010)

An experimental study on eight reinforced Concrete deep beams was carried out to observe their behavior under reversed cyclic loading. The variables were shear span-depth ratio (a/d = 1.55 or 2.9), quantity of stirrups (0.0 or 0.1%) and type of loading (monotonic or fully reversed cyclic loading). Since there's a gap in the database for members failing in shear where flexural hinging is not expected to occur, all members were designed to fail in shear before yielding of the longitudinal reinforcement. Naturally the shorter specimens (a/d = 1.55), where load is internally transferred in arch action, were found to be stiffer and stronger than the longer specimens (a/d = 2.9). The overall transition from beam action to arch action, mainly after extensive diagonal cracking; was evident from the changing pattern of the strains in the longitudinal reinforcement, which became nearly constant from support to support prior to failure.

Minimum stirrups provided for the beams, though it's actually lower than code recommendation for minimum shear reinforcement, significantly contributed in improving crack width and crack propagation. Moreover providing shear reinforcement enables the diagonal compressive stresses in the concrete to follow a more efficient path in carrying the shear, hence the failure load for members with stirrups was 62% higher than members without stirrups in the longer specimens.

According to this study, shear strength under reversed cyclic loading was not significantly reduced; yet ductility was evidently lowered. For members with shear reinforcement, the load-deformation response measured under monotonic loading was observed to be an excellent envelope to the cyclic response. Surprisingly for the members without shear reinforcement, members under cyclic loading achieved higher failure load and showed higher shear strength than those under monotonic loading. However this was accounted for random variation in the path of diagonal crack and possible local variations of material properties. The paper explicitly concludes: "*deep beams subjected to reversed cyclic loading where direct struts can form between the applied load and the reaction location can be designed for shear using the same provisions as those for monotonically loaded members, provided that the longitudinal reinforcement remains in the elastic range".* (Mihaylov et al., 2010, P. 9) [21]

2.2.7 Arslan and polat (2013)

The aim of this experimental study was to investigate the contribution of concrete to shear strength of Reinforced Concrete beams failing in shear under reversed cyclic loading. The main variable in this research was shear reinforcement ratio (ranging from 0.22% to 0.54%) and all the beams were designed to fail in shear before flexural reinforcement yields. The shear span-to-depth ratio (a/d) of all beams was kept constant at a value of 2.5. The beams were loaded in a series of load controlled cycles with three full cycles performed at each load level.

Shear resistance was calculated by superposition of the contribution of the concrete and the transverse reinforcement as in most shear design equations (ACI 318, Turkey earthquake code). Two strain gauges were attached at two different stirrups and their average value was used to compute stress in the transverse reinforcement from stress strain curve. The contribution of the concrete (V_c) was computed by subtracting the average contribution of the transverse reinforcement (V_s) from the shear force due to the applied load (V).

The beam responds uniformly until the first shear crack extending up to mid height appears; however at this point an increase in the strain of the transverse reinforcement was observed

activating the stirrups to effectively carry additional load. The degradation in shear strength and stiffness is resolved to be from the fact that crack openings are unable to close due to yielding of transverse reinforcement. Despite degradation, a significant amount of contribution of concrete to the shear strength (18% - 69%) was observed in the ultimate state ranges. However, further research with diverse variables is recommended for a conclusive assessment of RC beam failing in shear. [22]

2.2.8 Ruggiero et al. (2016)

This research aimed to investigate the shear response of Reinforced Concrete panels under reversed cyclic loading; to lay the ground work for a rational, analytical model for reversed cyclic shear behavior. Three shear panels, with unequal reinforcement in x and y direction, were tested under reversed cyclic loading using University of Toronto's Shell Element Tester (SET). The transverse reinforcement ratio was varied from 0.23% to 0.68% in a ratio of 1:2:3; while the reinforcement ratio in the X-direction (longitudinal) was kept constant. The longitudinal (X-direction) and transverse (Y-direction) reinforcing was oriented at 45 degrees to the horizontal and vertical axis system to apply pure shear.

This paper builds on assertion made by Stevens et al.[17] on reduction of shear resistance even in regions where there's no flexural hinging. According to the strain gauge readings attached on the reinforcements, while Y-direction reinforcements yielded, X-direction reinforcement didn't yield prior to failure. Hence these experiments are analogous to structural elements outside of flexural hinging zones and add on the sparse experimental data available for such elements (or sections).

In this research, it is convincingly demonstrated that reversed cyclic shear loading of structures causes strength degradation with respect to their expected monotonic capacity even if longitudinal reinforcement has not yielded. This was accounted to the formation of two quasi-orthogonal systems of cracks significantly diminishing the capacity of the structure to carry shear. Moreover for the cycles before cracking has occurred, linear elastic behavior with no apparent degradation due to reversal of load was observed.

In its attempt to develop an analytical model for reversed cyclic shear behavior, the paper evaluates the suitability of Modified Compression Field Theory (MCFT), a rotating crack model, to predict shear strength under reversed cyclic loading. This assessment was undertaken by comparing the test results of the three cyclic shear tests with MCFT prediction and the

underlying assumptions of the model. The assumption of equal principal stress and strain angles ($\theta=\theta_c$) was refuted in the case of reversed cyclic loading according to the test results. A 20^0 difference between the angles was observed; which is double the maximum noticed in monotonic tests by Vecchio and Collins[16].

Finally, it is concluded rotating crack models are ill-suited for reversed cyclic shear. Considering the material behavior in a fixed coordinate system oriented along the crack directions is recommended for better modeling of structures under reversed cyclic loading. [23]

2.2.9 Research gap

Shear strength degradation of Reinforced Concrete members under cyclic loading is a vital topic of research since most design codes are still based on empirical equations derived from monotonic tests. To account for this disparity, most of them make conservative consideration of the concrete contribution for shear strength (V_C); to the point where V_C is taken as zero in most design codes. However, according to numerous researches[19], [22] a small residual contribution of concrete (V_r) at large ductility levels is observed in experiments. Although many modes have been developed based on a database of tests, an analytical model fully explaining cyclic behavior of shear resistance is yet to be established.

There had been a huge supposition in the research community, on the existence of cyclic shear degradation within flexural plastic hinge regions only. Therefore, there's a sparse database for experiments done on structures failing in shear, before longitudinal reinforcement yields in flexure, under cyclic loading. However studies ranging from Stevens et al.[17] to current papers such as Arslan and polat[22] and Ruggiero et al.[23] concur on degradation of shear resistance in regions where there's no flexural hinging or structures failing in shear. This recent assertion clearly requires further study to add to the scant database and develop conclusive analytical models. Moreover due to the continuous development and modification of many design equations, many aged structures are at risk of being shear critical; hence the correct evaluation of their cyclic shear degradation is of paramount interest for retrofitting efforts.

The suitability of rotating angle models for the study of degradation of shear strength under cyclic loading has been investigated by numerous researches[17], [20], [23]. Rotating angle models such as MCFT were found to be ill-suited for such experiments displaying large variation from theoretical assumptions. Several researchers recommend fixed angle theory as a better alternative to study cyclic shear degradation. Moreover Vecchio[12] on his paper 'Analysis of

Shear-Critical Reinforced Concrete Beams' suggests rotating crack models do not adequately model the shear response of shear-critical RC beams, which are the subject of this research. Besides rotating angle theories inherently neglect the contribution of concrete for shear resistance as previously discussed. [5] Hence in this context, fixed angle theory is the best possible alternative for analysis of cyclic shear degradation of shear-critical members.

3 EXPERIMENTAL PROGRAM

The experimental program of this thesis consists the construction and testing of six shear-critical Reinforced Concrete beams under different loading protocols. All experiments were performed at the Construction Materials Laboratory of Addis Ababa Institute of Technology (AAiT). The main variable in the current study is type of loading (monotonic and one-side cyclic); other parameters are kept constant as much as practically possible. Shear failure was ensured by providing a theoretical flexure to shear over-strength of 1.39 and 1.33 for typical beams type 1 and type 2 respectively. Specific details of the specimens, their material property, test setup and instrumentation will be discussed in the following sections.

3.1 Specimen Summary

The primary goal of this study was to investigate the influence of cyclic loading on shear-critical, slender, Reinforced Concrete beams. Hence four beams lightly reinforced for shear were typically constructed with identical specifications. Moreover, to observe the degradation of the concrete contribution (V_C) without any influence from shear reinforcement, additional two beams with no transverse reinforcement were tested. Hence although the main variable was loading condition, shear reinforcement ratio, ϱ, was also varied (0.0 % and 0.13 %).

A total of six beams: two beams with no shear reinforcement (Type 1 beam) and four beams with minimum shear reinforcement (Type 2 beam) were tested under monotonic and one-side cyclic loading. All beams have 2.2 meter length, and identical rectangular cross section of 250 mm width and 300 mm depth. The beams are given special designations depending on their shear reinforcement ratio, loading protocol employed and the maximum amplitude of fatigue as a percentage of their ultimate capacity. For instance, a beam with shear reinforcement 0.13% (Type 2) tested under cyclic loading up to 90% of its expected capacity is designated as B2C90; where 2 stands for Type 2 beam, C stands for cyclic and 90 for 90% of its presumed capacity. A detailed summary of the six specimens is given on Table 3-1. Cylindrical compressive strength and tensile strength of the concrete are computed from cube compression tests and Split cylinder tests according to Eurocode specification; where tensile strength is determined as 0.9 times the splitting tensile strength, $f_{ct,sp}$.[2]

Table 3-1 : Summary of experimental specimens, as built

Beam designation	Cylindrical compressive strength, f_{cm} (MPa)	Tensile strength of Concrete, f_{ctm} (MPa)	Shear reinforcement ratio, ϱ_w	depth, D (mm)	Span to depth ratio, a/d	Type of loading
B1M	33.58	2.000	0.00%	300	3.502	Monotonic
B1C90	34.18	2.573	0.00%	300	3.502	One-side cyclic
B2M	31.98	2.403	0.13%	300	3.502	Monotonic
B2C90	32.34	1.853	0.13%	300	3.502	One-side cyclic
B2C85	32.81	1.893	0.13%	300	3.502	One-side cyclic
B2C80	33.59	1.836	0.13%	300	3.502	One-side cyclic

Typical beams for Type 1 and Type 2 are depicted in the following figure. Strain gauges are attached on the transverse reinforcements of Type 2 beams and are shown in Figure 3.1.

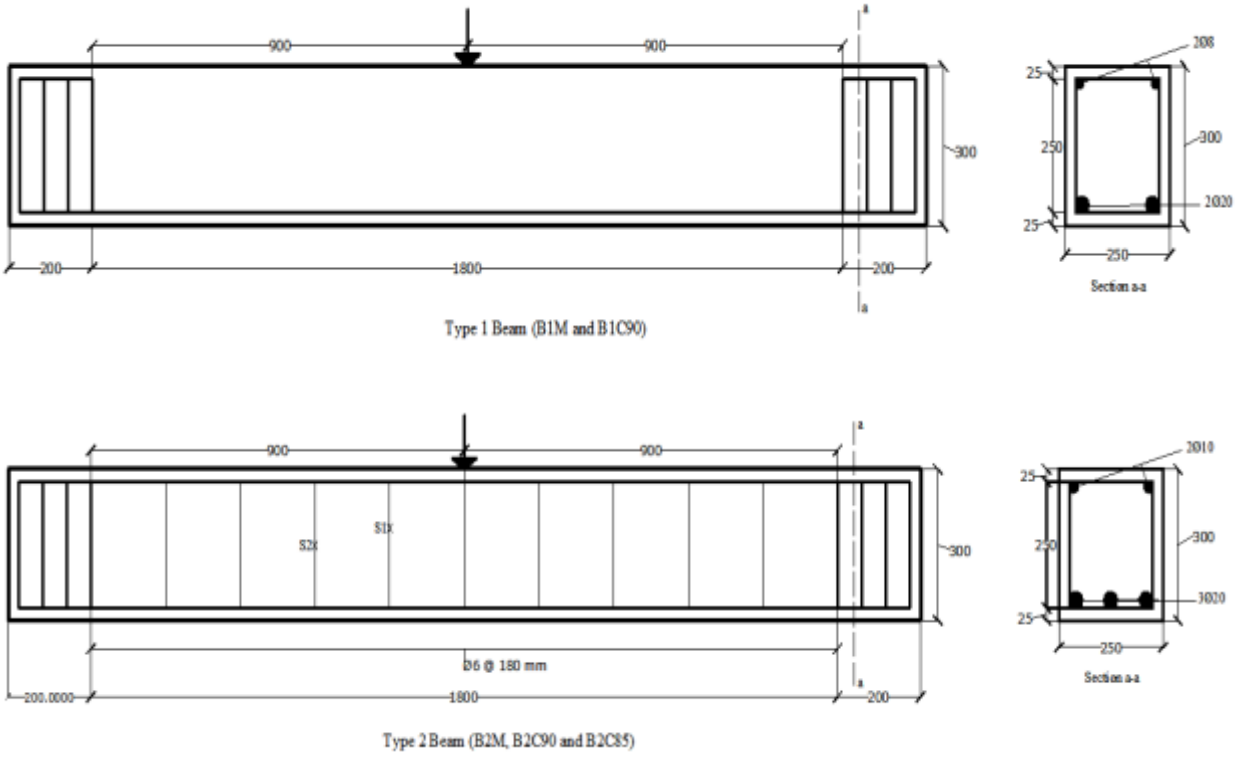

Figure 3.1 : Typical beam (Type 1 and Type 2) layout and strain gauge arrangement

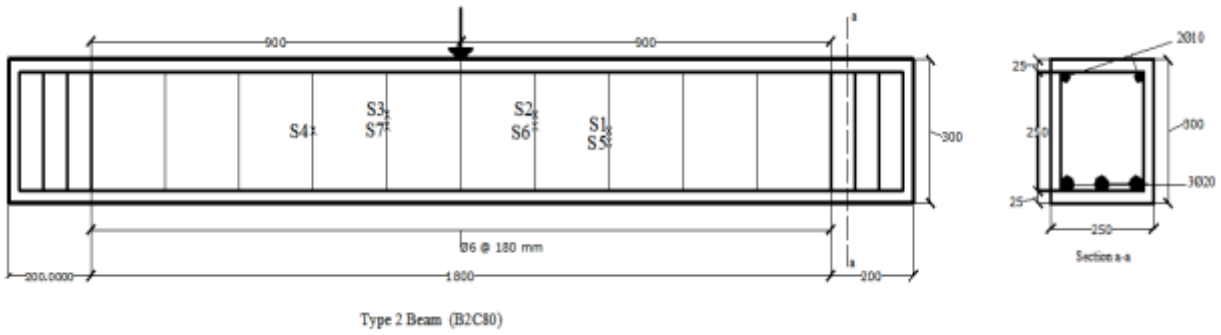

Figure 3.2 : Beam Layout and strain gauge arrangement for B2C80

Figure 3.2 shows the arrangement of strain gauges on B2C80; S5, S6 and S7 are attached at the backside of the stirrups. All shear reinforcements are anchored by 45^0 hooks according to Eurocode detailing specifications. [2]

3.2 Material properties

3.2.1 Concrete

Cast in situ concrete proportioned according to ACI mix design [24] was cast in a metallic formwork for all six beams. The concrete was specified to have a slump of 25 to 50 mm, a maximum aggregate size of 25 mm with a target compressive strength of 30 MPa and was mixed in the Construction Materials Laboratory of AAiT. Constant mix proportion of concrete was kept for all beams with little variations as possible. During the casting process, six cube samples (150 mm) and three cylinder samples of diameter 150 mm and height 300mm were prepared to determine the compressive strength and tensile strength of the concrete respectively. Samples were left to cure in the same environmental conditions as their respective beams.

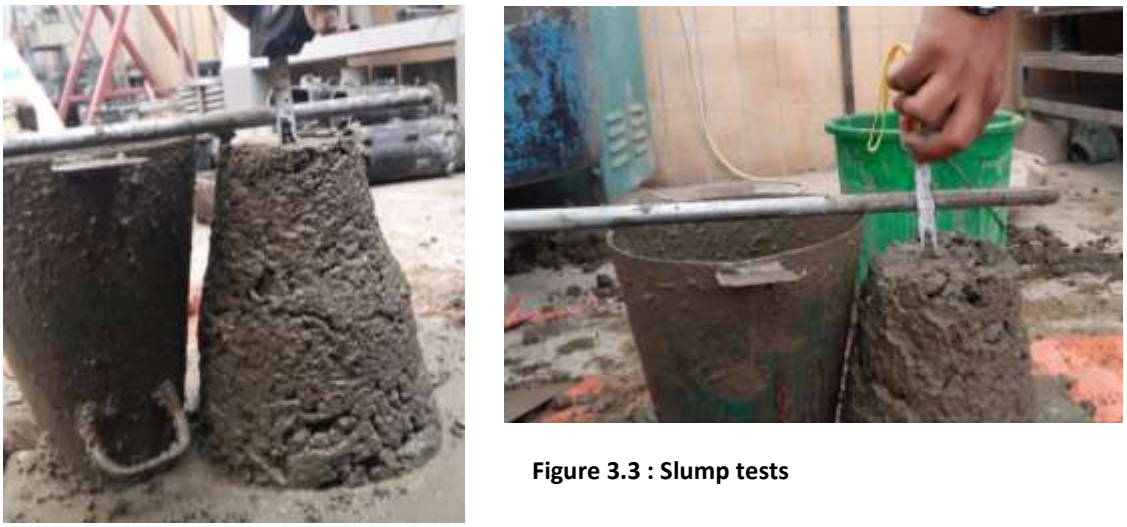

Figure 3.3 : Slump tests

Cubes were tested in compressive testing machines shown in Figure 3.4, while the concrete tensile strength was measured via split cylinder tests according to ASTM standard C496 – 96 as shown in Figure 3.5. [25] All samples were tested on the same day of one point loading tests on beams; or within a day difference.

Figure 3.4: Compressive Strength testing machine

Figure 3.5 : Split Cylinder testing machine

Concrete strengths at test day are given in Table 3-2 below. The splitting tensile strength of concrete was computed from the applied compressive force, P, by using equation (3.1); where l and d are the length and diameter of the concrete cylinder samples. Complete cube and cylinder test results are provided in ANNEX B.

$$\sigma_t = \frac{2P}{\pi l d} \qquad (3.1)$$

Table 3-2 : Average Concrete Strengths (Test day)

Specimen	B1M	B1C90	B2M	B2C90	B2C85	B2C80
Age at testing (days)	101	99	63	64	63	94
$f_{cm,cube}$ (MPa)	42.72	43.68	40.17	40.75	41.5	42.75
$_{fct,sp}$ (MPa)	2.222	2.859	2.670	2.059	2.104	2.040

B2C80 exhibited un-usual behavior during cyclic testing and was presumed to have fallen prematurely before attaining expected number of cycles. Since, the nine representative cube samples taken from the fresh mix during casting it, tested under compression showed relatively high variability with coefficient of variation 8.26%. Additional three core samples were extracted and tested according ASTM standard C42. [26] For comparison, similar samples were also taken from B2C85. The results obtained from the compressive cylindrical tests performed according to ASTM standard C39 are assumed to be better representatives of the actual concrete behavior in the beams and are presented below. The potential cylindrical strength of the core samples was predicted using ACI 214.4R-10 [27] and detailed discussion of core taking and testing is reported on ANNEX B.

Table 3-3 : Average Cylindrical Compressive Strength of core samples

Specimens	B2C85	B2C80
Age at testing (days)	139	135
F_{core} (MPa)	29.04	22.74
Equivalent in-place strength, F'c (MPa)	26.09	23.02

The concrete was proportioned according to ACI mix design to achieve cylindrical compressive strength of 30 MPa and was kept constant throughout the research. The mix design is performed by using weight method and absolute volume method which is displayed on Table 3-4. However, the proportion derived by weight method in the second column was eventually employed uniformly for all beams.

Table 3-4 : Mix proportion of Concrete

Material	**Mass**	**Percentage by mass**	**volume**	**Percentage by volume**
Coarse aggregate	1056.83 Kg/m^3	43.99%	0.38 m^3	37.88%
fine aggregate	916.63 Kg/m^3	38.15%	0.41 m^3	40.83%
Cement	331.48 Kg/m^3	13.80%	0.11 m^3	10.52%
Water	97.65 Kg/m^3	4.06%	0.10 m^3	9.76%
Air			0.01 m^3	1.00%
Concrete	2402.59 Kg/m^3	100.00%	1.00 m^3	100.00%
	water cement ratio =		**0.54**	

Material test on components of concrete such as: silt content, sieve analysis, moisture content of aggregates, unit weight of coarse aggregates and specific gravity and absorption tests have been performed and are reported on ANNEX A.

3.2.2 Steel

In all test specimens, normal strength deformed reinforcements available in the local market were used. Diameter 20 mm bars are used as bottom longitudinal reinforcement, diameter 10 mm and 8 mm bars as top reinforcement and diameter 6 mm bars as shear reinforcement for both typical beams. Tensions tests were performed on all reinforcements as shown in the Figure 3.6. Average tensile strength of all bar groups and other mechanical properties obtained from the tension tests are reported on Table 3-5.

Figure 3.6 : Tension test performed on Rebar

Table 3-5 : Mechanical properties of Reinforcement

Specimen	Average Diameter (mm)	Average Yield stress (MPa)	Average Fracture stress (MPa)	ultimate Strain, ε_u (‰)
φ 6	6.00	574.64	651.13	91.67
φ 8	8.10	539.53	613.98	100
φ 10	10.39	486.40	563.14	55
φ 20	19.81	603.47	696.26	175

3.3 Specimen Fabrication

In this section, preparation of the reinforcement cage, placement and casting shall be discussed. All specimens were constructed at the backyard of the materials laboratory of AAiT due to space deficiency.

3.3.1 Preparation of the rebar

The reinforcement cages were first assembled outside the form work. Spacing of shear reinforcement and detailing provisions was closely monitored. All shear reinforcements were anchored by 45^0 hooks placed on alternating sides as shown in Figure 3.8.

Figure 3.7 : Rebar preparation

Figure 3.8 : Reinforcement cage for Type 2 Beams

Figure 3.9 : Strain gauge installation for B2C80

3.3.2 Installation of the rebar cages into the formwork

Metal sheet formworks constructed in the Mechanical Engineering laboratory of AAiT were used for casting. Since thin metal sheets were used, the sheets were bent in an angle and bolted to stiffen the corners. To eliminate bulging of the concrete during casting, the formwork was gripped at two positions. However for the first beam cast, B1M, was only gripped at mid-span as shown in Figure 3.12. The reinforcement cage was placed in the formwork keeping a 25 mm clear distance by using concrete spacers as shown in Figure 3.8.

Figure 3.10 : Reinforcement cage placement in formwork

3.3.3 Casting of the concrete

The concrete proportioned according to Table 3-4 was mixed in a mechanical mixer at materials laboratory of AAiT as shown in Figure 3.11. Due to the small size of the mixer, it took four batches of concrete mix to cast the entire beam, cube and cylinder samples.

Figure 3.11 : Concrete Mixer

Figure 3.12 : Casting Concrete in Metal formwork

An electric vibrator was used to consolidate the concrete during casting. Once the formwork was removed, a day after casting, the beam and concrete samples were covered by wet cotton for moist curing. Plastic casing was also placed on top, to reduce evaporation of water as the beams were cast outdoor.

3.4 Test Setup

All beams were tested under one point loading supported by steel plates with a roller on both sides. A concentrated force was applied at mid span by a hydraulic jack of maximum capacity around 300 KN. Since the load was applied manually by using a hydraulic Jack (shown in Figure 3.14); loading rate could not be kept constant. Though the loading rate varied randomly for each experiment, it was kept below 0.325 mm/s or 11.5 KN/s for all experiments. Therefore the effect of increase in loading rate was somehow controlled but not consistently regulated as with an automatic actuator. Although consistent loading rate would have been preferred for this research, due to limitation in laboratory equipment, it could not be so.

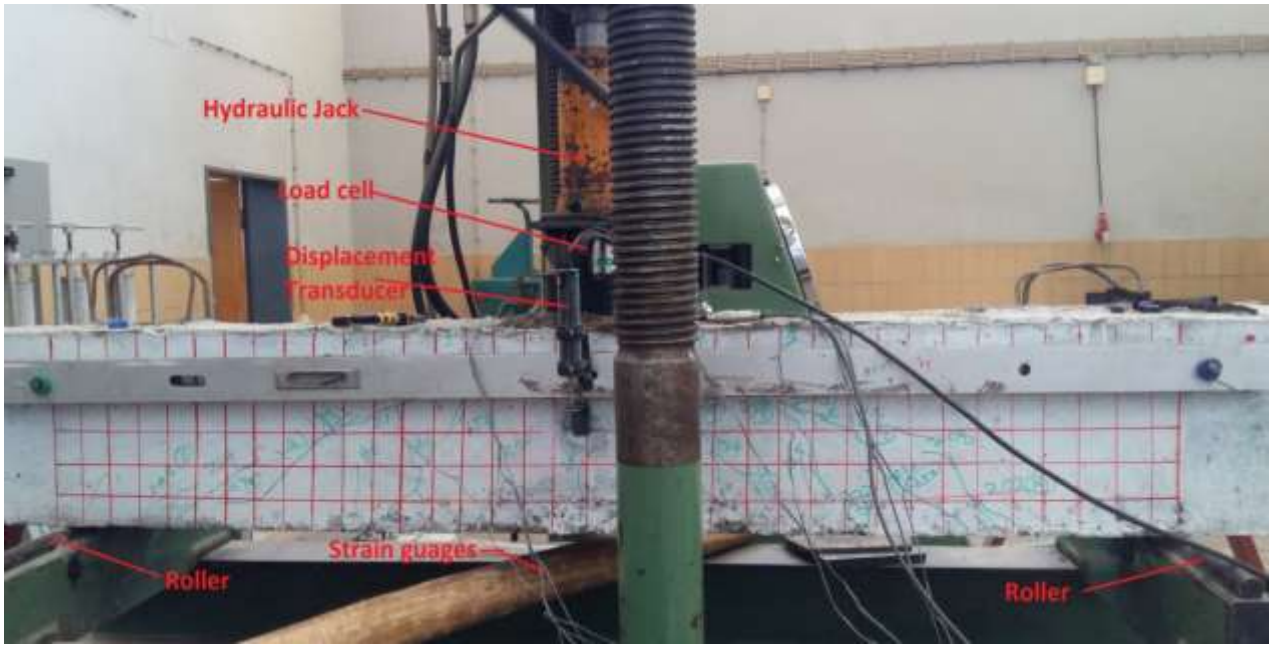

Figure 3.13 : Test Setup

3.5 Instrumentation and data acquisition

Instruments indicated in Figure 3.13 are mainly employed for data acquisition and load application. The load applied by the hydraulic Jack (Figure 3.14) is measured by a load cell (Figure 3.15) linked to a data logger (Figure 3.16). A Linear variable displacement transducer (LVDT) is used to measure the mid-space displacement of the beam throughout the experiment. The LVDT is attached to a static horizontal rod fixed on the beam at support position as shown

in Figure 3.17. Strain gauges attached to some of the stirrups were used to measure strain in the web reinforcements. All instruments employed were connected to the data logger and a comprehensive data: entailing load, displacement and strain measurements, is obtained using a USB stick from the data logger.

Figure 3.14: Hydraulic Jack

Figure 3.15 : Load Cell

Figure 3.16 : Data logger

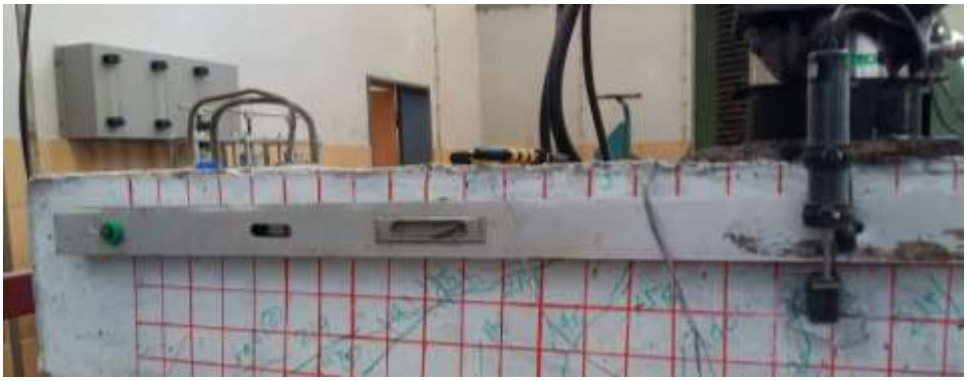

Figure 3.17 : Linear variable displacement transducer (LVDT)

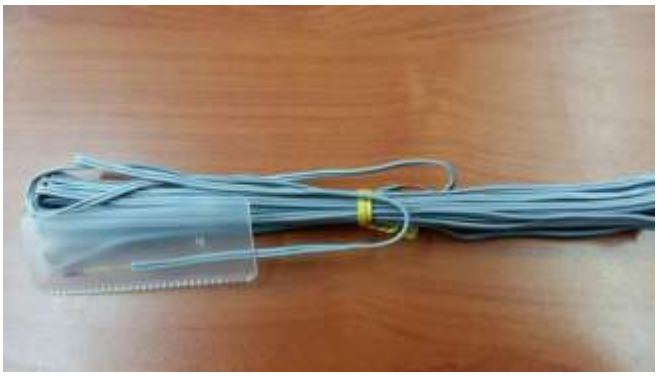

Figure 3.18 : Strain Gauge

3.6 Loading Pattern

Either monotonic or one-side cyclic loading was applied on all beams. One-side cyclic loading was applied basically by monotonically increasing the load to a certain percentage of the presumed capacity of the beam and unloading instantly when this maximum load is reached. Since load was applied manually by a hydraulic jack: when the aforementioned maximum cyclic load is reached, the beam is unloaded by unbolting the hydraulic jack. Thus some inconsistencies are to be expected.

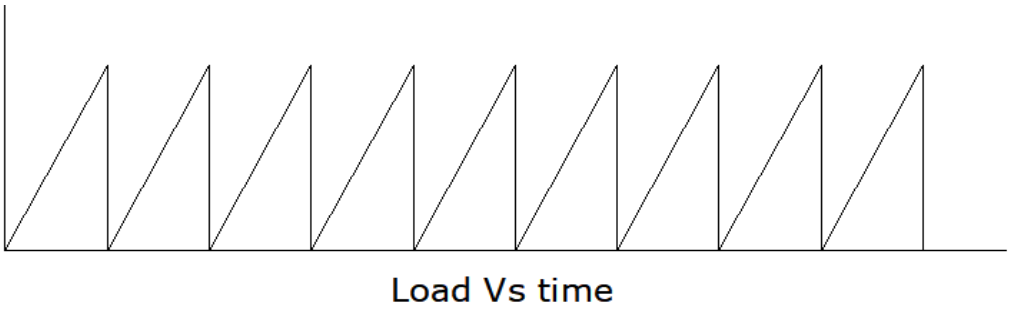

Figure 3.19 : Loading Pattern

4 FEM ANALYSIS USING DUCOM-COM3

4.1 About the software

For computational simulation and analysis of this research, DUCOM-COM3 - a finite element analysis platform is used. The software is intended to be a computational environment for integrated safety and durability assessment of reinforced concrete structures and is a result of an ongoing research in the University of Tokyo. DUCOM-COM3 is the integration of a three dimensional nonlinear FE analysis system, COM3 (**Co**ncrete **M**odel for **3**Dimensional problems), and DUCOM (**D**urability **M**odel of **CO**ncrete). DUCOM is a computer program that uses Finite Elements to solve the heat and mass transport problems of a porous media. It is based on a microstructure model of inorganic composite material substance balance/ migration analysis system which consists of C-S-H gel particle. COM3 undertakes simulation and nonlinear FEM analysis of concrete structures comprising short and long-term time-dependent high nonlinear mechanics under static and dynamic loads. Hence, with computational integration of these two components a homogenous system of concrete service life span simulation could be achieved.

4.2 Specimens

A three-dimensional finite element analysis was carried out for six specimens analogous to the experimental beams. There are two types of typical beams depending on shear reinforcement as formerly described in section 3.1. After both types of beams were analyzed under monotonic loading, a certain percent of their maximum capacity was applied for fatigue analysis. The nomenclature used for experimental beams shall be implemented for the respective specimens only adding A (i.e. Analytical) as prefix. Hence A-B2C90 is the equivalent specimen for B2C90 for analytical simulation in DUCOM-COM3. Summary of all specimens studied under finite element analysis shall be listed below.

Table 4-1 : Specimen Description

Beam designation	Cylindrical compressive strength, f_{cm} (MPa)	Tensile strength of Concrete, f_{ctm} (MPa)	Shear reinforcement ratio (ϱ_w)	depth, D (mm)	Span to depth ratio, a/d	Type of loading
A-B1M	33.58	2.000	0.00%	300 mm	3.502	Monotonic
A-B1C90	33.58	2.000	0.00%	300 mm	3.502	One-side cyclic
A-B2M	31.98	2.403	0.13%	300 mm	3.502	Monotonic
A-B2C90	31.98	2.403	0.13%	300 mm	3.502	One-side cyclic
A-B2C85	31.98	2.403	0.13%	300 mm	3.502	One-side cyclic
A-B2C80	31.98	2.403	0.13%	300 mm	3.502	One-side cyclic

Unlike the experimental beams, all type one and type two beams are modelled exactly identical as shown in Table 4-1 as is the original intent in this study. During the experimental study, it was inevitable that there should be some variations in specimen fabrication. However such discrepancies weren't encountered during analytical simulation; hence a more accurate output is expected.

The specimens, as modelled in DUCOM-COM3, are displayed in the following diagrams. The reinforcement cage is modelled with different colors for longitudinal and shear reinforcements. Better clarification on the modeling process shall be discussed in following sections.

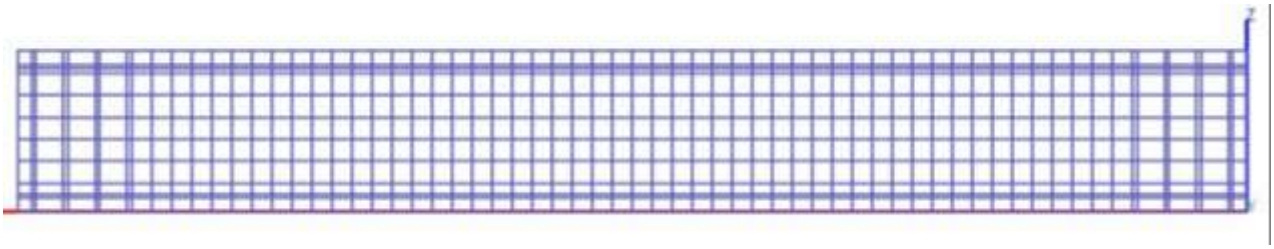

Figure 4.1: Type one beam Finite Element mesh

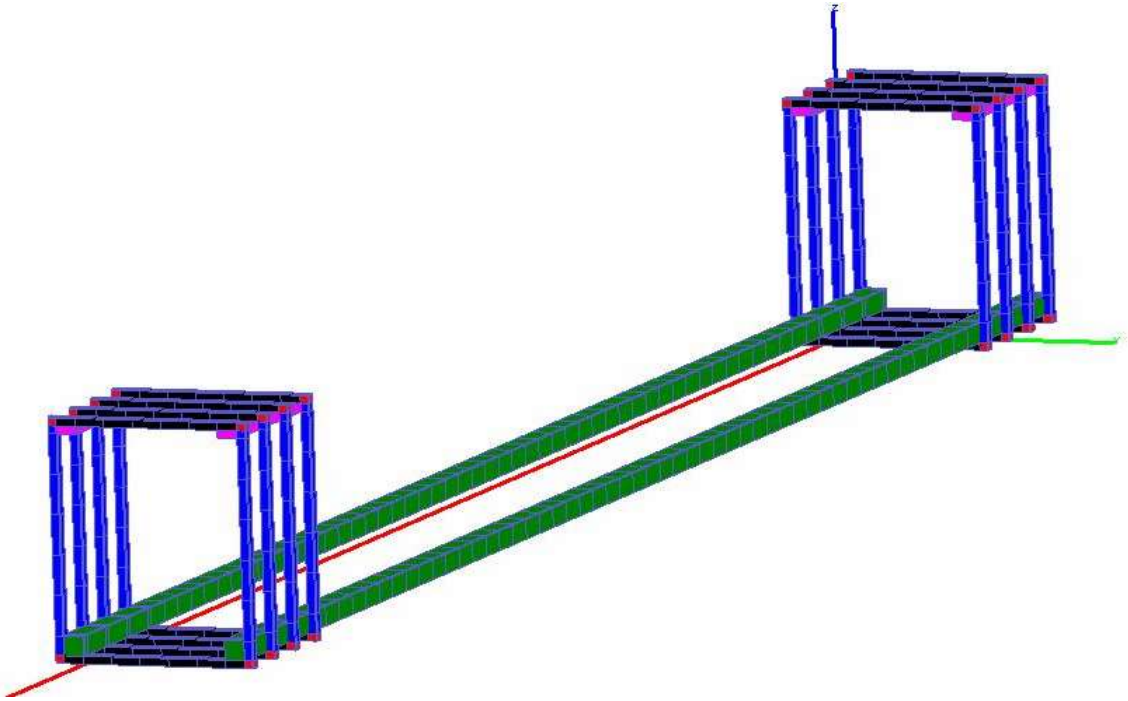

Figure 4.2 : Reinforcement cage of Type one beam

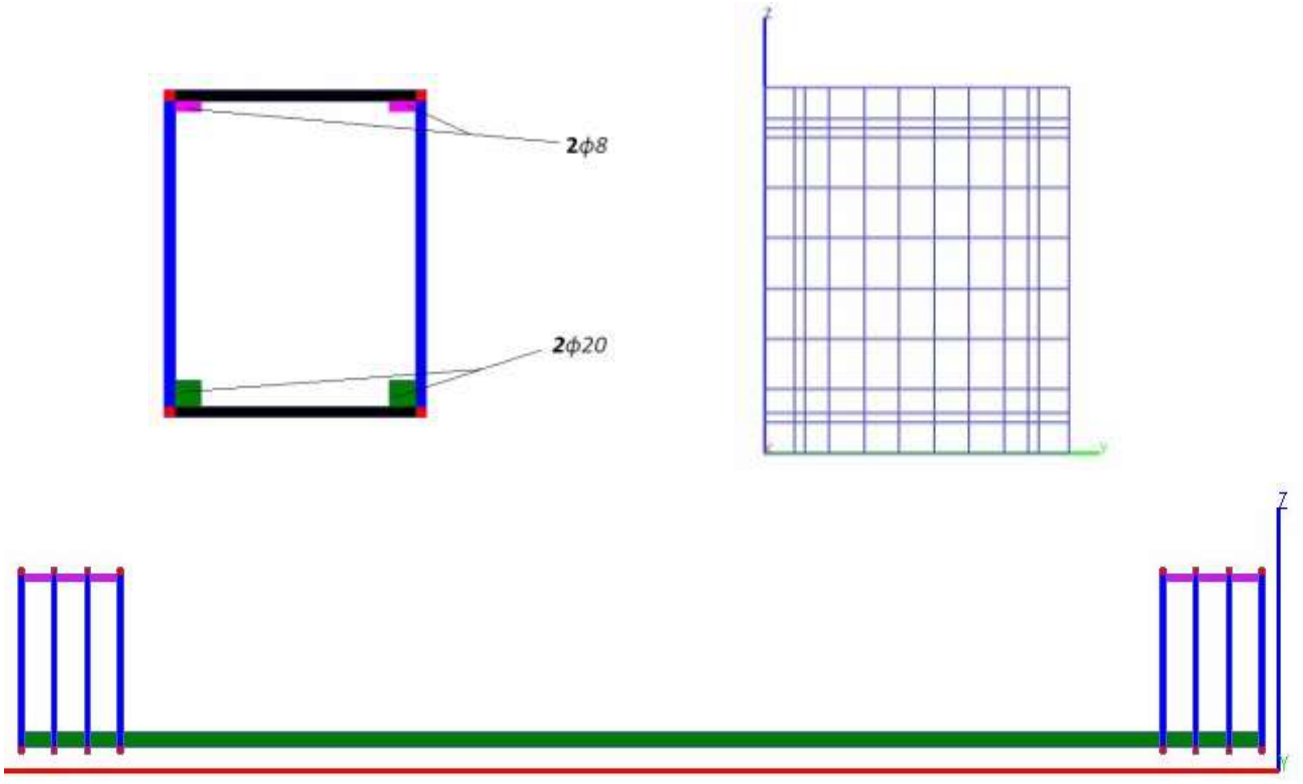

Figure 4.3: Reinforcement cage of Type 1 beam on DUCOM-COM3

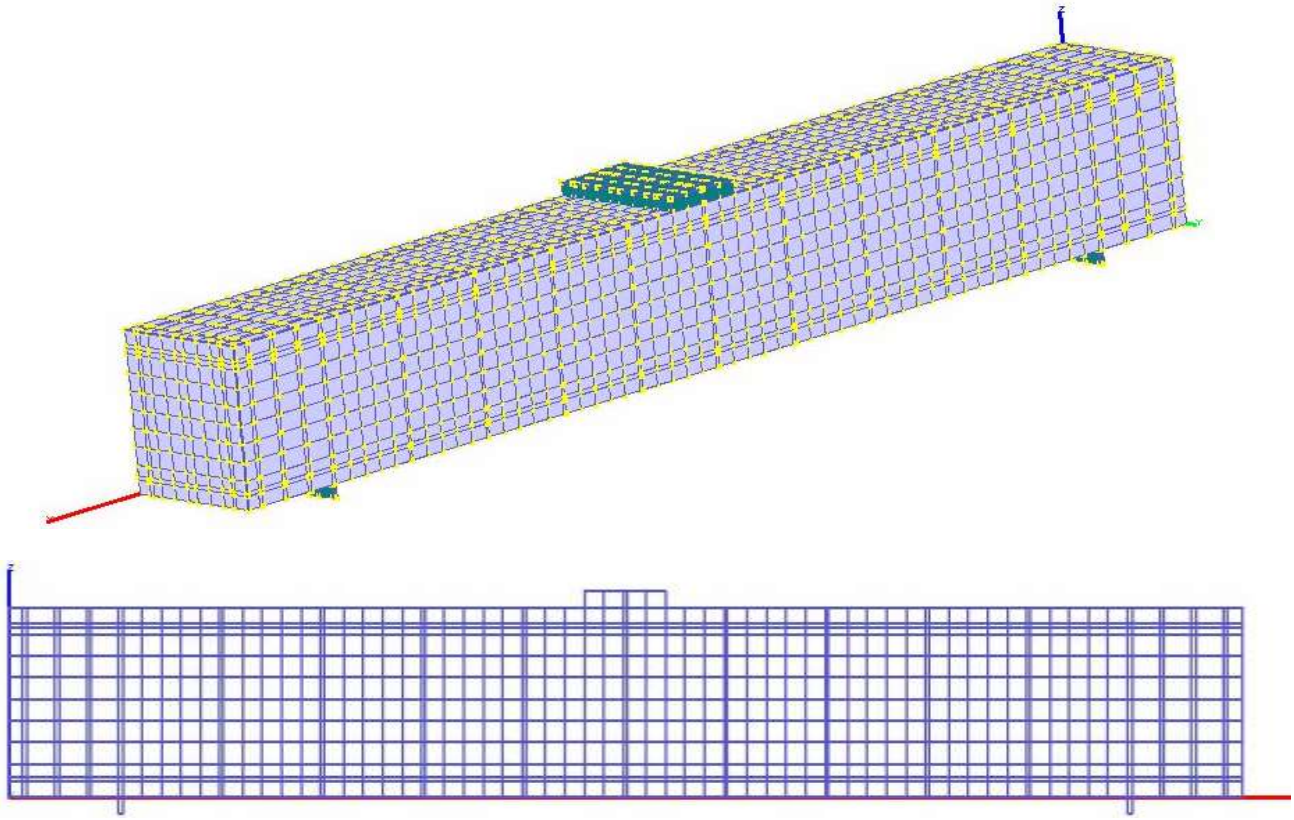

Figure 4.4: Type two beam finite element mesh

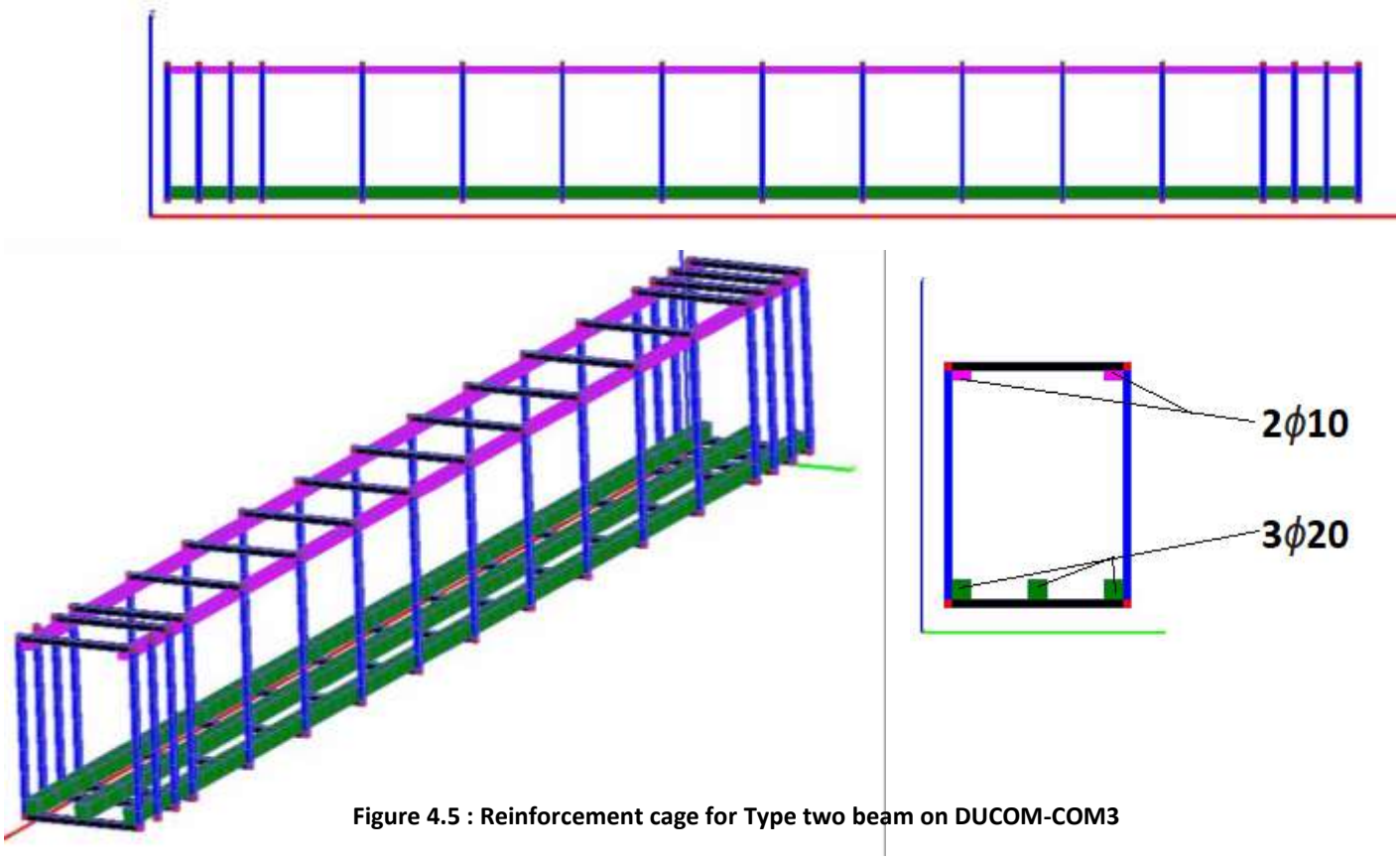

Figure 4.5 : Reinforcement cage for Type two beam on DUCOM-COM3

4.3 Materials

Since the analytical model was expected to confirm to the experimental test results, the concrete strength obtained from compression test on 150 mm cube samples and tensile strength of reinforcements experimentally obtained from tension test were directly used as input for the analytical model. The cylindrical strength, modulus of elasticity and tensile strength of concrete were all computed according to Eurocode specification. The cylindrical strength was determined by multiplying the cubic strength with a variable coefficient (crudely varying from 0.78 to 0.86) interpolated from Table 3.1 of Eurocode 2. The modulus of elasticity of the concrete was computed according to equation (4.1); while the tensile strength of concrete was computed from splitting tensile strength according to equation (4.2) per Eurocode specification. [2] Mechanical property of concrete in both typical specimens is reported in Table 4-2 below.

$$E_{cm} = 22\left[\frac{fcm}{10}\right]^{0.3} \qquad (4.1)$$

$$f_{ct} = 0.9 \times f_{ct,sp} \qquad (4.2)$$

Table 4-2 : Mechanical Property of Concrete

Specimens	Type 1 Beam	Type 2 Beam
Initial Stiffness (MPa)	33,715.42	33,396.04
Compressive Strength (MPa)	33.58	31.98
Tensile strength (MPa)	2.000	2.403
Poison's ratio	0.2	0.2
Unit weight (Kg/m^3)	2294.42	2352.198

Normal strength reinforcements of different diameters were used as reported in the experimental program. Yield strength, ultimate strength and ultimate strain determined from tension tests were directly inserted in the analytical model. A smeared reinforcement model was used for analysis; hence reinforcement diameter wasn't an important parameter for analytical simulation.

Table 4-3: Mechanical property of Reinforcement bars

Specimen	Average Yield stress (MPa)	Average Fracture stress (MPa)	ultimate Strain, ε_u (‰)
φ 6	574.64	651.13	91.67
φ 8	539.53	613.98	100
φ 10	486.40	563.14	55
φ 20	603.47	696.26	175

4.4 Modeling

A three dimensional multi-directional smeared crack model was utilized for analysis. This model comprises cracking strains from multi-directional cracks (primary and secondary cracks) that simultaneously occur at a sampling point. All steel reinforcements were modelled as smeared reinforcements in concrete elements. The finite elements were categorized to plain concrete region (PL zone) and reinforced concrete region (RC zone) based on recommendations for embedment zone of reinforcements from CEP-FIP (1990). The Modeling of average tensile behavior of concrete after cracking is based on a proposed model by Shima and Okamura. [28] Hence the relationship between average stress and average strain for concrete under tension is expressed by equation 4.3; where ε_{tu} is the cracking strain and c is the parameter describing the inclination of the descending branch.

$$\sigma_t = f_t \left(\frac{\varepsilon_{tu}}{\varepsilon_t} \right)^c \qquad (4.3)$$

This coefficient C is varied in RC and PL Zones to describe the gradual release or sharp release of normal stress after crack respectively. Consequently, C is taken as 0.4 for tension stiffening in RC zone and 2.0 for tension softening in PL zone. Moreover, anisotropic tension stiffening/ softening scheme was employed since the relative orientation of the crack and bar axis affects post cracking stress transfer. [28]

The two specimens, A-B1M and A-B2M, under monotonically increasing load were loaded using displacement-based approach to determine the ultimate capacity of the beams. Afterwards, a force-based approach was utilized for one-side cyclic loading simulation. For high cycle fatigue simulation the direct path integral method was employed to reduce runtime. [29] Time dependency effect was incorporated in all the models.

4.5 Support condition and loading

The beams were simply supported with 1.8 m span distance between supports. The loading plate and support bearing were modelled as elastic materials; with analogous size to the actual loading plate. For A-B1M and A-B2M, a displacement controlled analysis was performed to capture the post-peak phase of the experiments. A loading rate of 0.02 cm per min was employed with 76 steps. The rest of the beams underwent force controlled fatigue analysis with a frequency of 1 Hz. The input file was manipulated by applying a progressive magnification factor on the loading data based on the direct path integral scheme. [29]

5 RESULT AND DISCUSSION

5.1 Results

5.1.1 Test summaries

All beams fail in shear with crushing of concrete at the point of load application prior to yielding of longitudinal reinforcement. Shear tension failure was observed in all specimens with no evidence of anchorage failure. However, loss of bond due to splitting crack along the longitudinal reinforcement was observed after peak load. Though it was a priority to be consistent with specimen fabrication and testing, there were occasional variations in material properties and testing protocol. A qualitative summary of each experiment is reported to offer an insight to such variations. Table 5-1 displays a numerical overview of the entire experimental program and its results. The cracking load reported in the table is recorded as seen by the researcher and/ or inferred from the load deflection graph for each beam.

Table 5-1 : summary of experimental results

Specimen	Cylindrical compressive strength (F'_c)	Shear reinforcement ratio (ϱ_w)	Cracking Load (P_{cr})	Maximum load (P_{max})	Number of cycles (n)
B1M	33.58	0.00%	21.51	181.57	monotonic
B1C90	34.18	0.00%	43.77	163.07	4
B2M	31.98	0.13%	32.01	275.86	monotonic
B2C90	32.34	0.13%	54.27	250.35	21
B2C85	32.81	0.13%	70.28	301.62	220
B2C80	33.59	0.13%	53.27	224.84	216

5.1.1.1 B1M

B1M is a typical Type 1 Beam (shown in Figure 3.1) with no shear or top longitudinal reinforcement and was the first beam cast in this research. Nonetheless web reinforcements were provided outside the region of load application to avoid anchorage failure. It was initially planned to test the beam under one point loading on the 63rd day. However, due to a sudden accident during manual transportation, the beam fell of the testing equipment and cracked around its mid-span (shown in Figure 5.1). This incident created a significant setback; since better technique and more man power was needed to transport the rest of the experimental

beams: which were around the same size and weight. Moreover, the extent of damage incurred by the beam had to be assessed and a methodology had to be employed to circumvent the effect of the damage on the experiment.

Figure 5.1 : Damage on B1M

After considering several options and observing tests performed on the other beams, it was concluded that it was better to proceed with the specimen as it was. This was because the crack occurred at the top center of the beam; it was expected to close at the onset of loading due to compression under flexure. Moreover, since the beam was designed with a high flexure to shear over-strength, the neutral axis depth was expected to be below the crack. Hence, the beam was finally tested under monotonically increasing load 38 days later, 101 days from casting.

At the onset of loading, at 21.51 KN, a slightly diagonal crack appeared right next to the initial crack from the damage. This crack didn't widen; yet the crack initially from the damage extended to the bottom reinforcement and halted. After the formation of minor slightly diagonal cracks sparsely spaced throughout the length of the beam, the beam reached its diagonal cracking load. A major diagonal crack started growing wider and the beam fail suddenly at 181.57 KN. Specimen B1M exhibited brittle shear failure with no crack redistribution after diagonal cracking.

Figure 5.2 :B1M after failure

5.1.1.2 B1C90

Specimen B1C90 was tested under one-side cyclic loading 99 days after casting. This beam is analogous to B1M in size, percentage of reinforcement (both longitudinal and transverse) and concrete strength. Although the mentioned parameters were to be kept constant, slight variations were noticed. For instance, compressive and tensile concrete strength measured for B1C90 was slightly higher than B1M. Moreover, high variability in compressive test of cube samples was observed in B1C90 with a coefficient of variation of 16.3%. This was explained due to a single bad mix with a higher water cement ratio from the four batches during casting.

B1C90 exhibited a very stiff response at the onset of loading, yet micro-cracks started appearing right away. The stiffness of the beam decreased simultaneously with the onset of flexural cracks around 40 KN load. As the test progressed during the first cycle, flexural cracks started extending to inclined flexural shear cracks. The first cycle was stopped at 163.82 KN, which is 90% of the shear capacity of B1M, and unloaded. Since B1M and B1C90 were hypothetically identical, their maximum shear strength is assumed to coincide. At the end of the first cycle, specimen B1C90 was still intact with few slightly inclined cracks sparsely distributed.

The diagonal tension cracks formed on the first cycle started extending to the point of load application with each cycle. The beam fell suddenly on the fourth cycle right before it reached the amplitude of cyclic loading. The flexural shear crack on one side gaped wider and extended to a splitting crack along the longitudinal reinforcement as shown in Figure 5.3.

Figure 5.3 : B1C90 after failure

5.1.1.3 B2M

Specimen B2M was tested under a monotonically increasing load, 63 days after casting. It was the first beam to be tested; after a failed attempt to test specimen B1M. Casting was closely regulated and a consistent mix was obtained throughout the four batches of mix. Subsequently, very small variation was observed during compressive strength and splitting tensile strength tests performed on cube and cylinder samples respectively. The entire experimental result for cube compression tests and splitting tensile strength tests is reported on ANNEX B.

Specimen B2M exhibited typical shear failure with crack redistribution. Flexural cracks first appeared at the bottom of the mid span and spread evenly in both directions. As the test progressed and load was monotonically increased, these flexural cracks began bending in a diagonal direction towards the point of load application; hence flexure-shear cracks were formed. A few web-shear cracks were also initiated near support. First inclined crack was observed at 168 KN. Strain gauges S1 and S2 attached to shear reinforcements as shown in Figure 3.1, indicated yielding of stirrups in the range 200 KN to 250 KN.

In this range, diagonal tension cracks also kept on extending towards point of load application until the maximum load of 275.86 KN was reached. At this ultimate fracture load, brittle shear failure occurred with concrete crushing both at support and point of load application as shown in Figure 5.4.

Figure 5.4 : B2M after failure

5.1.1.4 B2C90

Specimen B2C90 was tested under one-side cyclic loading 64 days after casting. This beam is analogous to B2M in size, percentage of reinforcement (both longitudinal and transverse) and concrete strength. Since all Type 2 beams are expected to be identical theoretically, the mentioned parameters were to be kept constant. However in practice, slight variations were inevitable. The compressive strength of the concrete in beam B2C90 was nearly equivalent to B2M; but the tensile strength of the concrete obtained from splitting tensile test was much less. The coefficient of variation in splitting tensile results was also large, 13.48%, in between the three samples for B2C90. This was associated to minor variations in water-cement ratio among the batches during mix.

Specimen B2C90 was monotonically loaded up to 90% of the maximum capacity of B2M and exhibited a slightly stiffer response in the first cycle of loading than B2M. Apart from that, similar behavior with an analogous load deflection response to B2M was observed. Evenly distributed flexure-shear cracks were initiated in the first cycle, traced in blue as shown in Figure 5.5. From the strain gauges attached at two stirrups, it can be seen that the shear reinforcements nearest to the mid-span has started yielding during the first cycle. However the strain measurements recorded were oddly small throughout the experiment. This might be because strain gauges measure local strain, instead of average strain; at the specific location they're attached. Nonetheless, the strain gauges were attached to two stirrups near point of load application and the beam eventually fell on the side where strain gauges were attached. Graphical representation of load deflection response and load versus strain will be displayed and thoroughly discussed on section 5.1.2.

Stiffness degradation and crack development was intensified with every cycle until the beam had a brittle shear failure on the 21st cycle. Starting from the fourth cycle, the initial stiffness of

the beam was highly reduced with a nearly flat load deflection curve. But as center loading was increased stiffness recovery was noticed in the middle stages of every cycle after the fourth cycle. At failure, concrete crushing at point of load application and at the support was accompanied by spalling of concrete as shown on Figure 5.6. The shear reinforcements on the side of failure have fully fractured with a wide gaping crack.

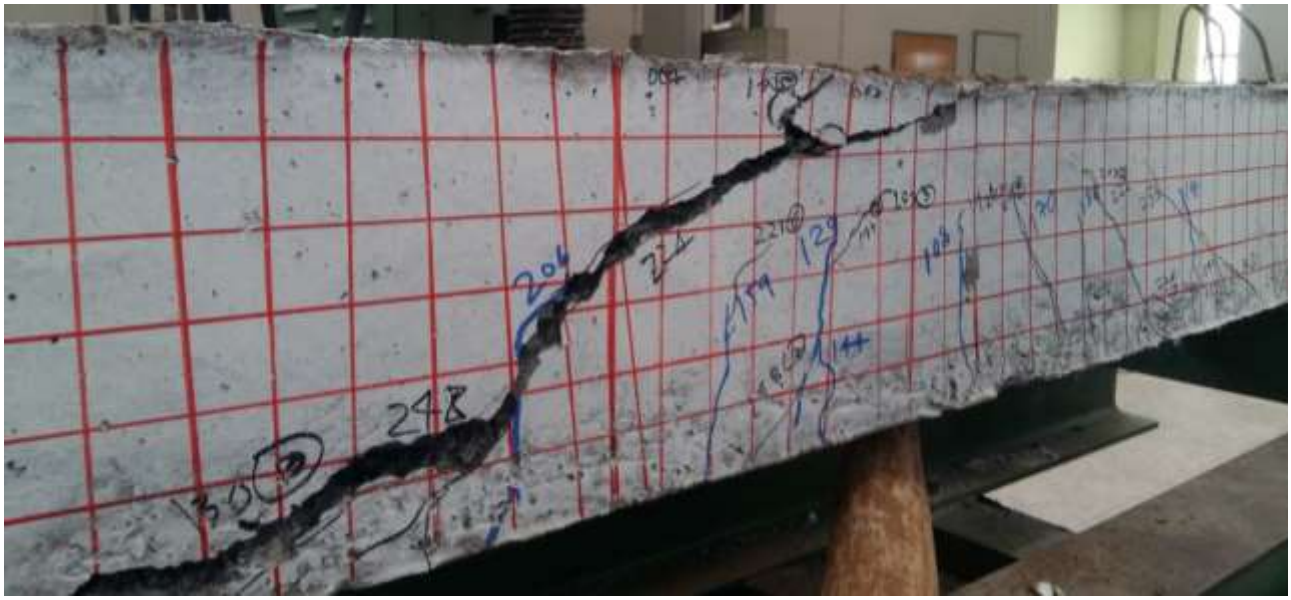

Figure 5.5 : B2C90 after failure

Figure 5.6 : B2C90 after failure (half view)

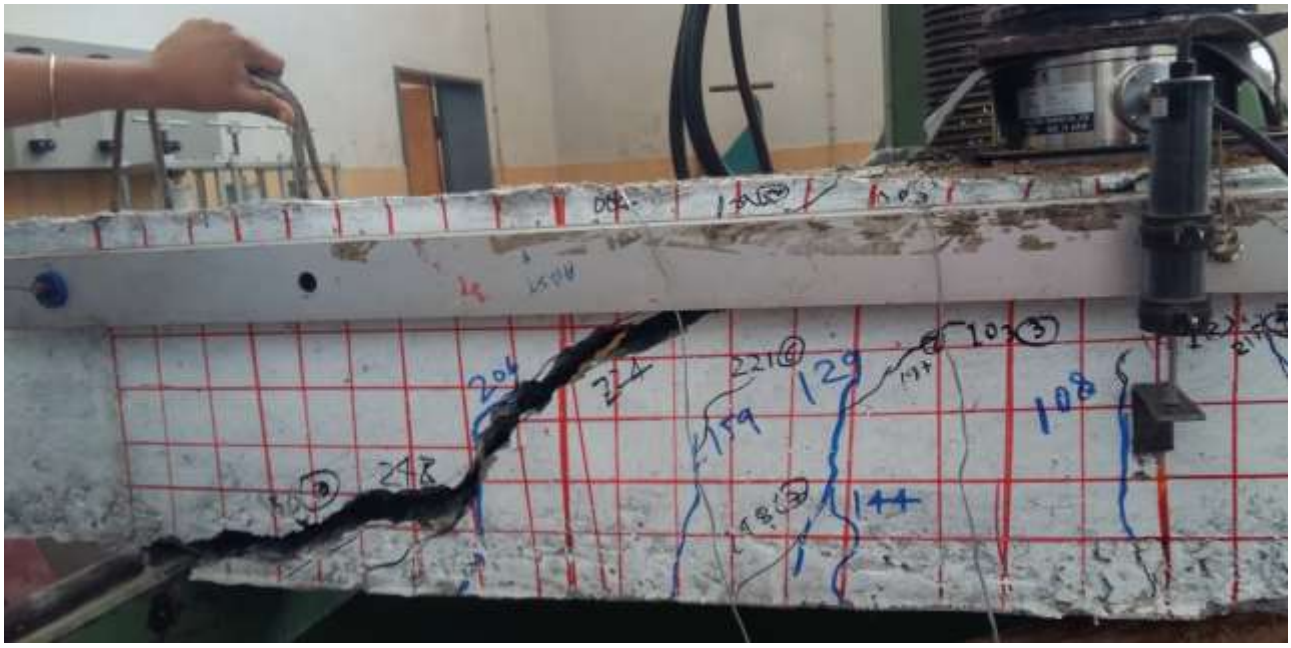

Figure 5.7 : B2C90 after failure (half view)

5.1.1.5 B2C85

Specimen B2C85 was tested under one-side cyclic loading 63 days after casting. Only 200 cycles could be performed on the day of testing; so the experiment had to be resumed 2 days later, after the weekend, for 20 more cycles. This beam is a Type 2 beam with similar material properties, size and detailing as B2M. However, the compressive strength of the concrete in beam B2C85 was slightly higher than B2M while the tensile strength of the concrete obtained from splitting tensile test was much less. The coefficient of variation in splitting tensile results was also large, 8.79%, in between the three samples for B2C85. This was associated to minor variations in water-cement ratio among the batches during mix.

Since specimen B2C85 and B2M are hypothetically identical, specimen B2C85 was monotonically loaded up to 85% of its maximum capacity; which was assumed to coincide with the maximum capacity of B2M. It exhibited a nearly identical response with B2M in the first cycle of loading with similar stiffness and an overlapping load deflection curve. One out of the two strain gauges attached was damaged during casting; hence strain gauge reading only from S1 was obtained. Although yielding of shear reinforcements began in the first cycle, the stirrup didn't fully yield for several cycles.

In the initial stages, evenly distributed flexure-shear cracks initiated in the first cycle extended towards the point of load application with every cycle. Yet after the 15^{th} cycle, there seemed to be hardly any change in response of the beam from cycle to cycle. Slow and steady stiffness

degradation was observed with a slightly higher deflection at the end of each cycle. Permanent deformation was also slightly increased at the beginning of every cycle. However there was no apparent crack development and cracks completely close when the beam is unloaded. After 219 such monotonous cycles, the beam was monotonically loaded to failure on the 220^{th} cycle. Surprisingly, the ultimate capacity of B2C85 after 220 cycles exceeded the maximum capacity of B2M by 9.34%.

A maximum load of 301.62 KN was achieved right before brittle shear failure. The shear reinforcements on the side of failure have fully fractured with a wide gaping diagonal crack. Concrete crushing at the point of load application and support coupled with spalling of concrete at the bottom was observed as shown in Figure 5.9. The compression strut inclination or crack angle was observed to have a lower gradient compared to previous tests on type 2 beams. Moreover internal degradation of the concrete was apparent due to the maximum crack width and considerable concrete spalling at failure.

Figure 5.8 : B2C85 after failure

Figure 5.9 : B2C85 after failure (bottom)

5.1.1.6 B2C80

Specimen B2C80 was tested under one-side cyclic loading 94 days later from casting. Only 66 cycles could be performed on the first day of testing; so the experiment had to be resumed 2 days later, after the weekend, for 150 more cycles. Since this beam is a Type 2 beam, it is analogous to B2M in size, percentage of reinforcement and concrete strength. However, the compressive strength of the concrete in beam B2C80 was higher than B2M; while the tensile strength of the concrete obtained from splitting tensile test was much less. Moreover the coefficient of variation in cube compressive test and splitting tensile test results was as large as 8.26% and 6.54% respectively between the samples for B2C80. This was associated to minor variations in water-cement ratio among the batches during mix and possible inconsistency in curing.

Specimen B2C80 was monotonically loaded up to 80% of its maximum capacity which was assumed to coincide with the maximum capacity of B2M. It exhibited a slightly stiffer response in the first cycle of loading than B2M. Apart from that, similar behavior with an analogous load deflection response to B2M was observed. There were seven strain gauges attached to the shear reinforcement in the positions shown in Figure 3.2. According to these strain gauge readings, none of the stirrups had reached their yield point on the first cycle. Yet residual strain from each cycle kept on steadily increasing until some strain gauges, mainly S1 and S4, revealed yielding of stirrups in later cycles.

Initially, this beam exhibited similar response as typical type 2 beams with flexure-shear cracks evenly distributed in both sides from the center loading. Web-shear cracks were initiated and flexure-shear cracks extended towards the point of load application with every cycle. Similar to B2C85, an uneventful intermediate stage with no apparent crack development where cracks completely close when the beam is unloaded was observed. When the 200^{th} cycle was reached, a pronounced degradation with faster crack propagation and stiffness degradation started being observed. The beam had a brittle shear failure on the 216^{th} cycle; much earlier than expected.

Failure was highly un-anticipated since estimations based on the response of B2C85 predicted a much higher number of cycles. Moreover the beam fell on the side which was least expected, since crack development and propagation was faster on the other side initially. Loss of bond due to splitting crack along the longitudinal reinforcement was also observed (shown in Figure 5.10). Moreover, core samples were taken from the beam to ascertain the concrete strength of B2C80. Although a lesser compressive strength is to be expected from core samples, a lesser

result was obtained compared to compressive strength results obtained from representative samples. The cylindrical compressive strength obtained from the core samples has been reported prior on Table 3-3 and the entire experimental data is reported on ANNEX B.

Figure 5.10 : B2C80 after failure (half view)

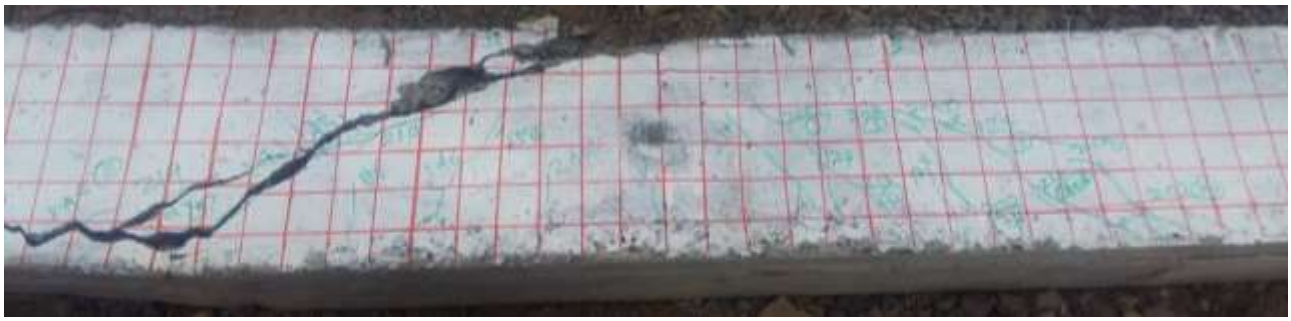

Figure 5.11 : B2C80 after failure

5.1.2 Experimental results

5.1.2.1 Load deflection curves

All experimental beams exhibited typical brittle shear failure as can be concurred from their load deflection diagrams. The experimentally obtained load deflection diagrams are presented below for all six specimens.

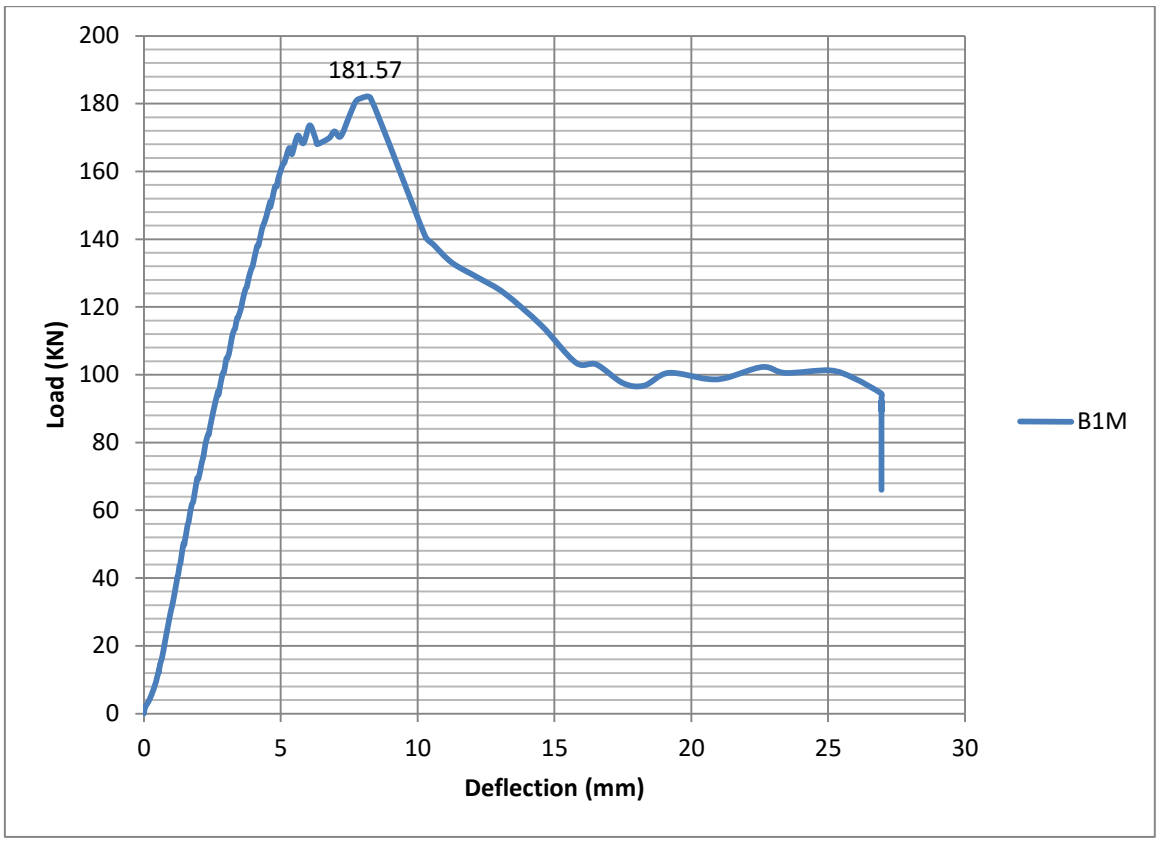

Figure 5.12 : Load deflection diagram for specimen B1M

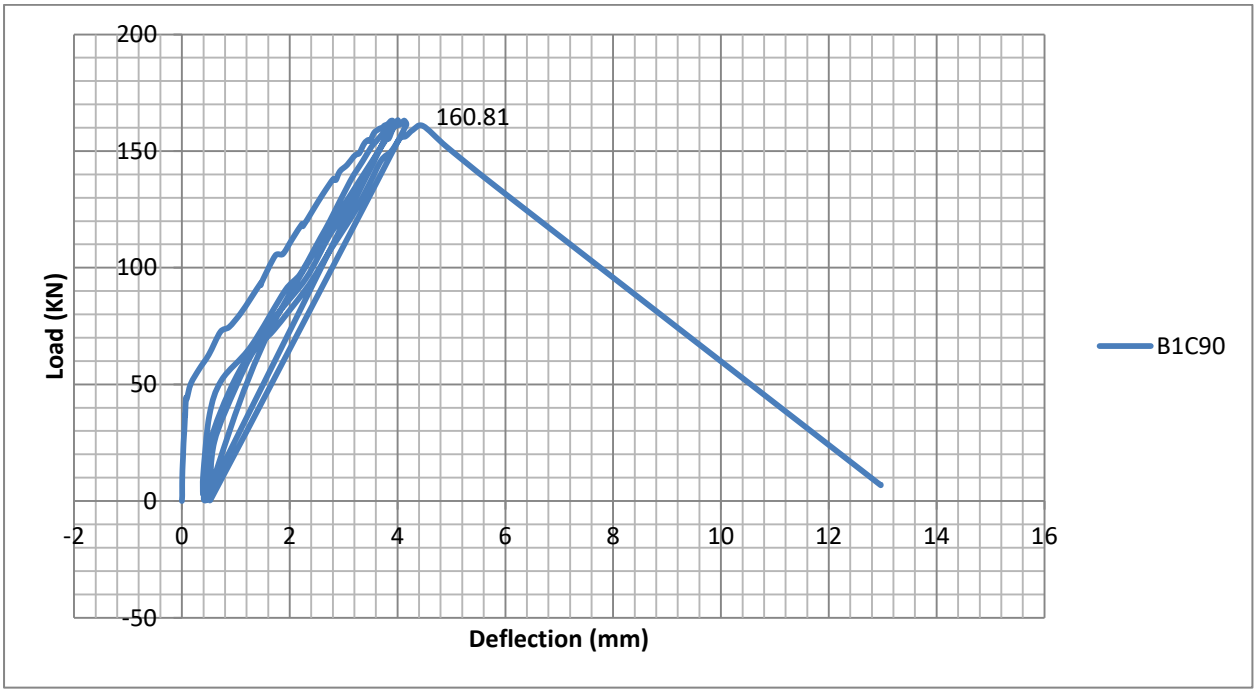

Figure 5.13 : Load deflection diagram for specimen B1C90

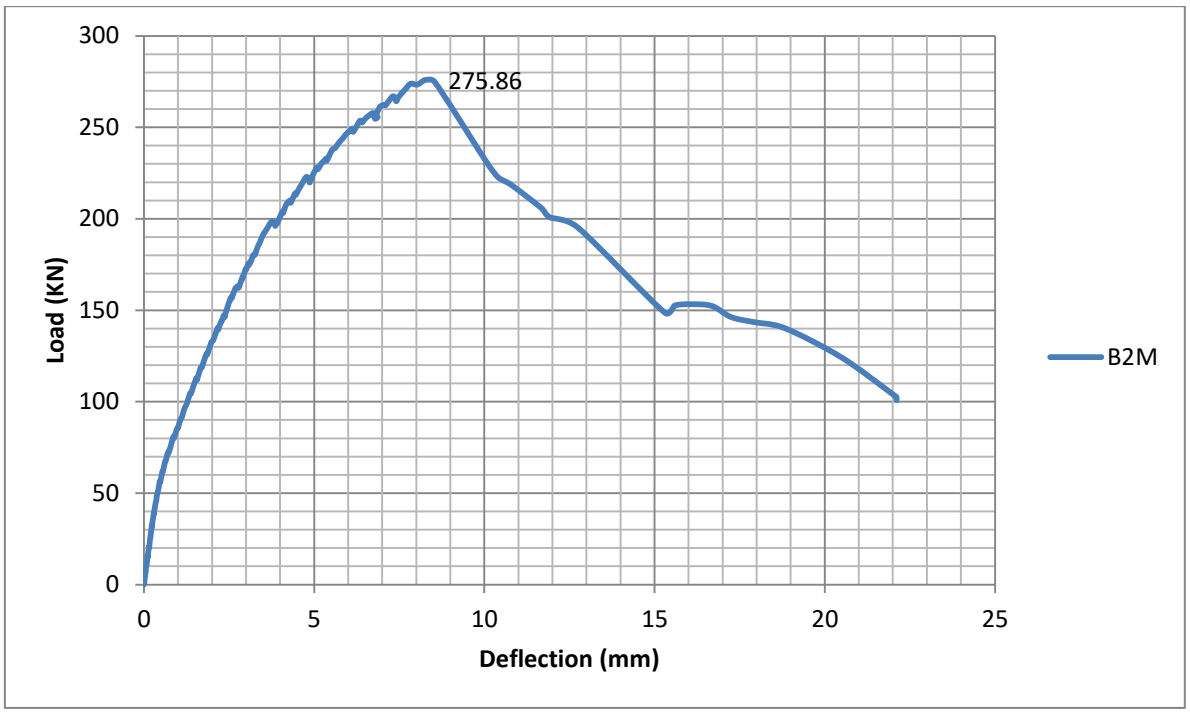

Figure 5.14 : Load deflection diagram for specimen B2M

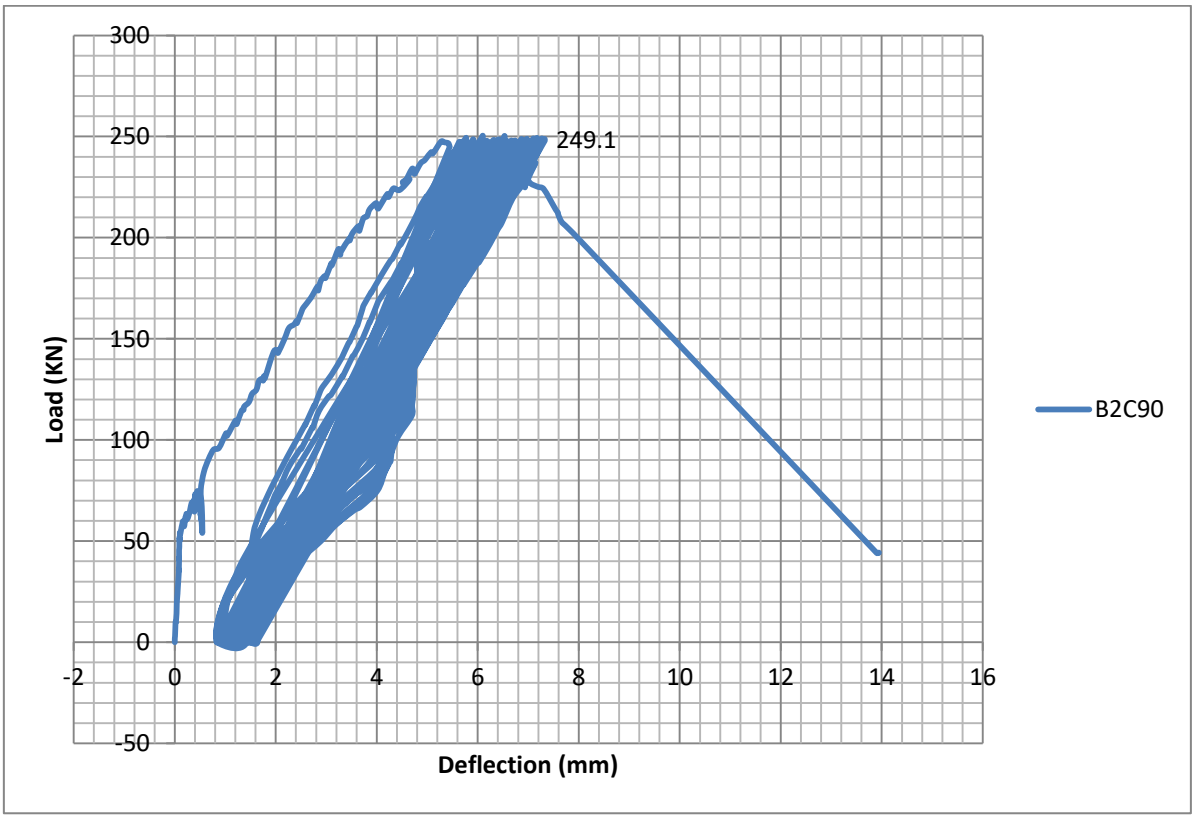

Figure 5.15 : Load deflection diagram for specimen B2C90

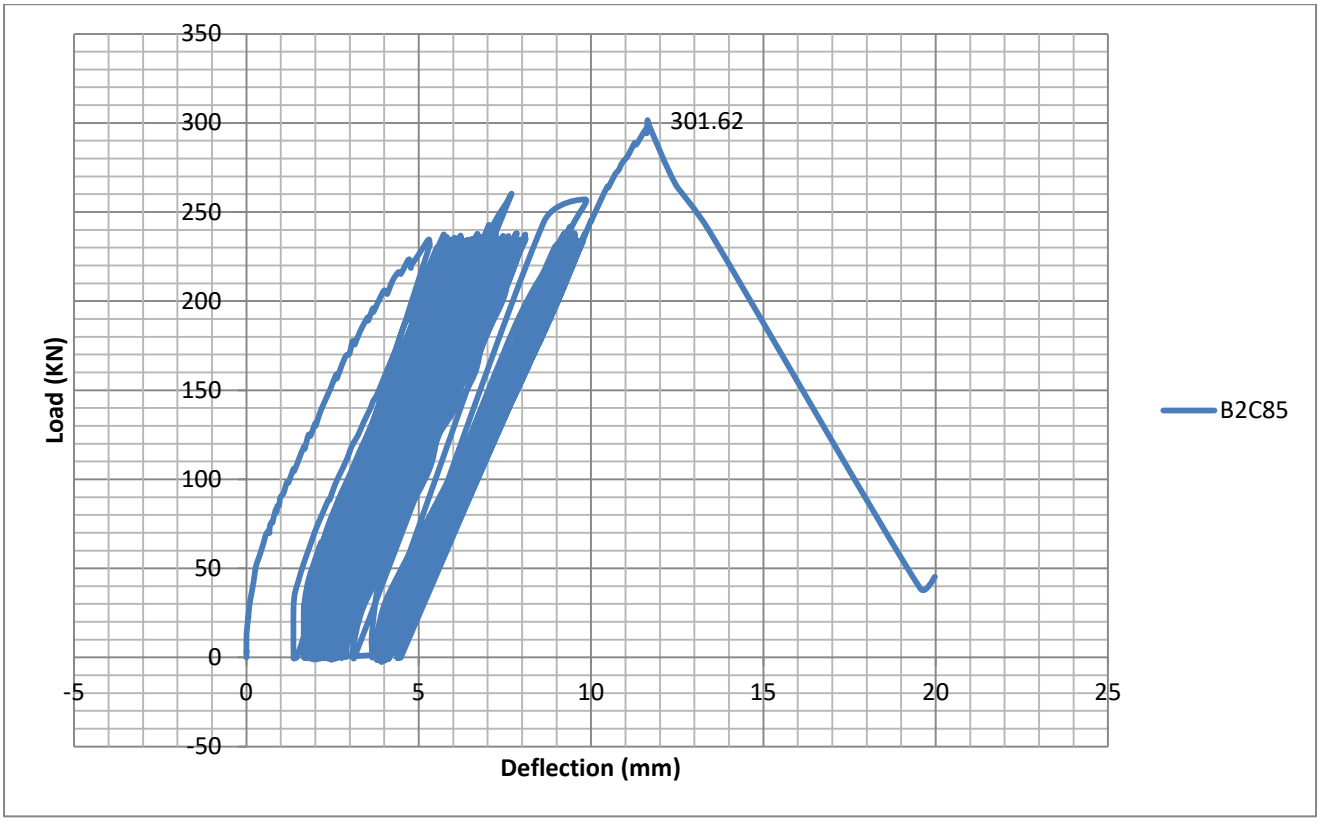

Figure 5.16 : Load deflection diagram for specimen B2C85

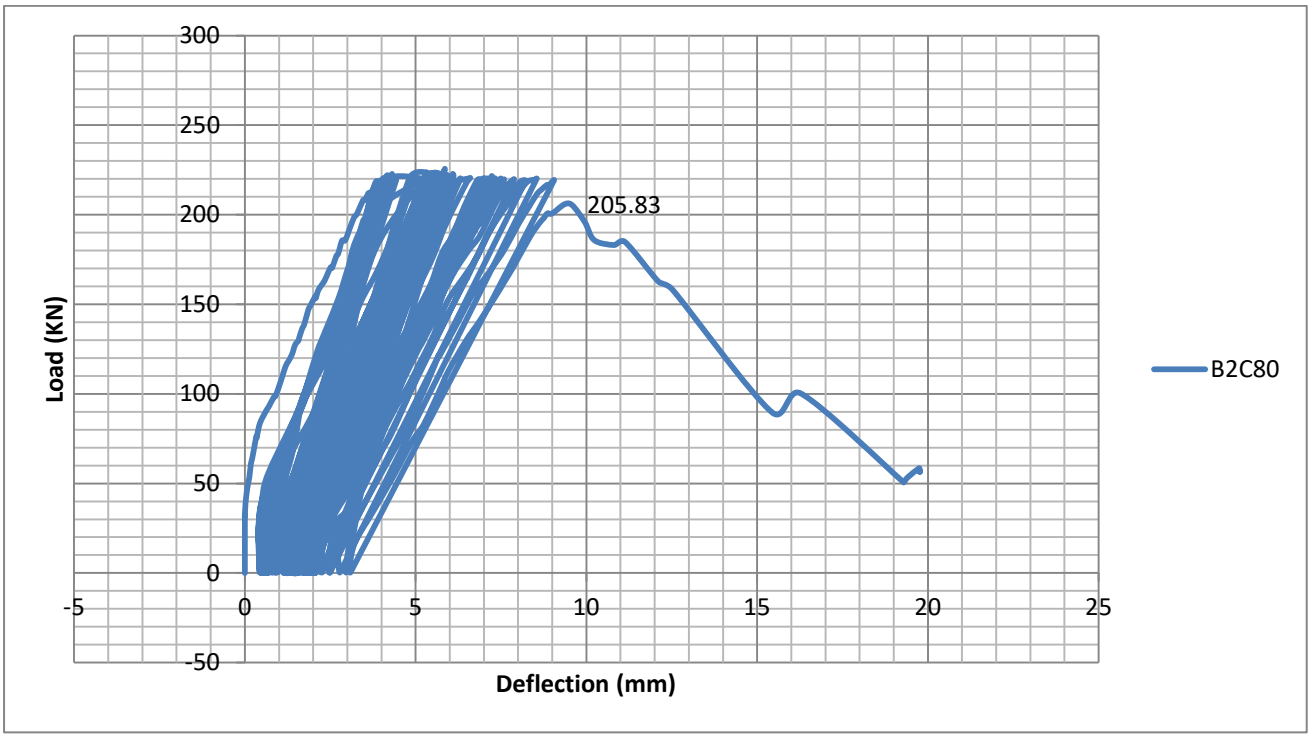

Figure 5.17 : Load deflection diagram for specimen B2C80

All Type 1 and Type 2 beams exhibited similar behavior in initial stiffness and cyclic degradation of stiffness as can be grasped from their load deflection diagrams. However, a few

apparent deviations have been noted and a rational explanation for these disparities is attempted herein.

Specimen B2C90 exhibited a lower initial stiffness with a nearly flat deflection curve and stiffness recovery in the middle stages of each cycle starting from the fourth cycle. Such kind of variation in stiffness on the same cycle has not been displayed by all other specimens. This is best understood and explained by observing the load vs strain curves of each specimen which shall be particularly discussed in section 5.1.2.2. Since specimen B2C90 was cyclically loaded to 90% of its capacity; it's presumed yielding of stirrups and extensive cracking has occurred in the first four cycles. Hence major stiffness degradation was observed in initial stages of each cycle after the fourth. However as the load is increased new crack formation and crack extension are initiated, the intact concrete exhibited a stiffer response in this middle stages. Moreover, strain hardening of shear reinforcement after their yield point can also be another reason for stiffness recovery in the middle stages of each cycle. Yet more importantly, this observed eccentricity in the load deflection diagram of B2C90, has no serious implication on the subject of this research; which is cyclic shear behavior

Specimen B2C85 exhibited typical property of Reinforced Concrete beams under cyclic loading. Yet, on the 132nd cycle plastic deformation of the beam was abruptly increased which is better demonstrated by the mid-span deflection versus number of cycles chart (Figure 5.18). This is presumed to be because of fracture of shear reinforcement since yielding of shear reinforcement has started as early as the 62nd cycle (Figure 5.23). Since loading was performed manually the amplitude of the cyclic loading has been greatly surpassed on two occasions, 61st and 181st cycle due to human error. In these two cycles the amplitude of fatigue loading has reached up to 94% of the presumed maximum capacity of the beam. After 220 cycles of loading, the capacity of the beam was increased by 9.34%. This phenomenon shall be better discussed on section 5.2.1.5.

Fatigue analysis of specimen B2C80 gave unexpected results in regards to fatigue life of the specimen. Hence, investigation on the concrete strength and technical integrity of the specimen was undertaken. Slight variations in concrete strength, dimensioning and reinforcement imperfections were observed and were assumed to be possible reasons of divergence. However the computational analysis of the specimen also delivered similar results addressing questions in the technical integrity of specimen B2C80.

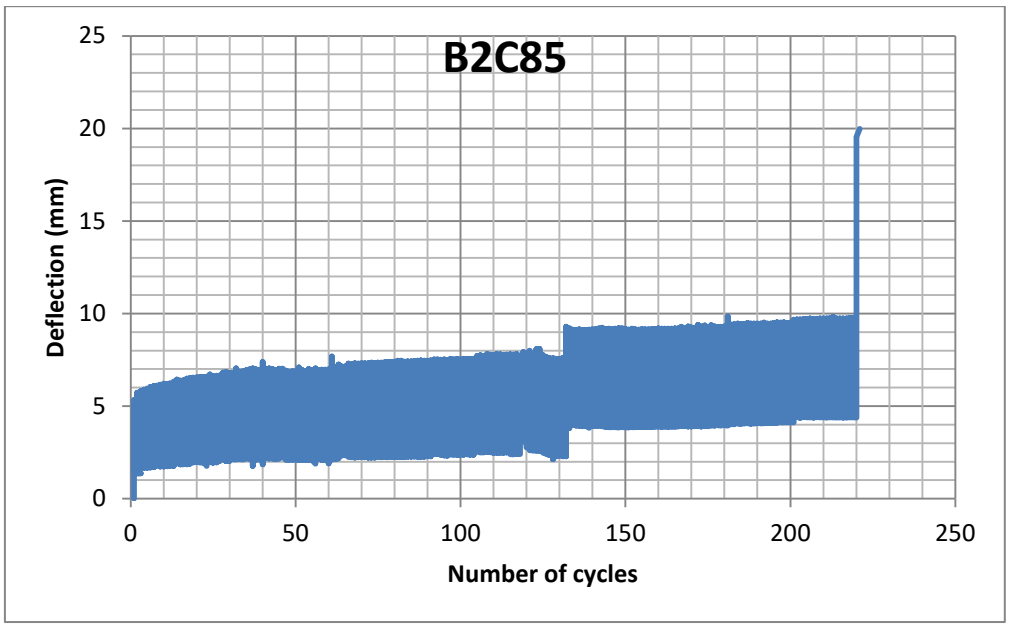

Figure 5.18 : Mid-span deflection history for specimen B2C85

5.1.2.2 Strain measurements

Load vs strain curves have been prepared based on the strain gauge readings attached on some of the stirrups near point of load application. This was done in an attempt to understand the internal shear transfer and the role of transverse reinforcements in carrying shear in fatigue loading. The load vs strain diagrams for Type 2 beams shall be presented below.

The position of the strain gauges is depicted on Figure 3.1 and Figure 3.2; hence the following graphs should be understood with the given locations in mind. It should be noted for Beams B2M, B2C90 and B2C85, the beams eventually failed on the side where strain gauges were attached

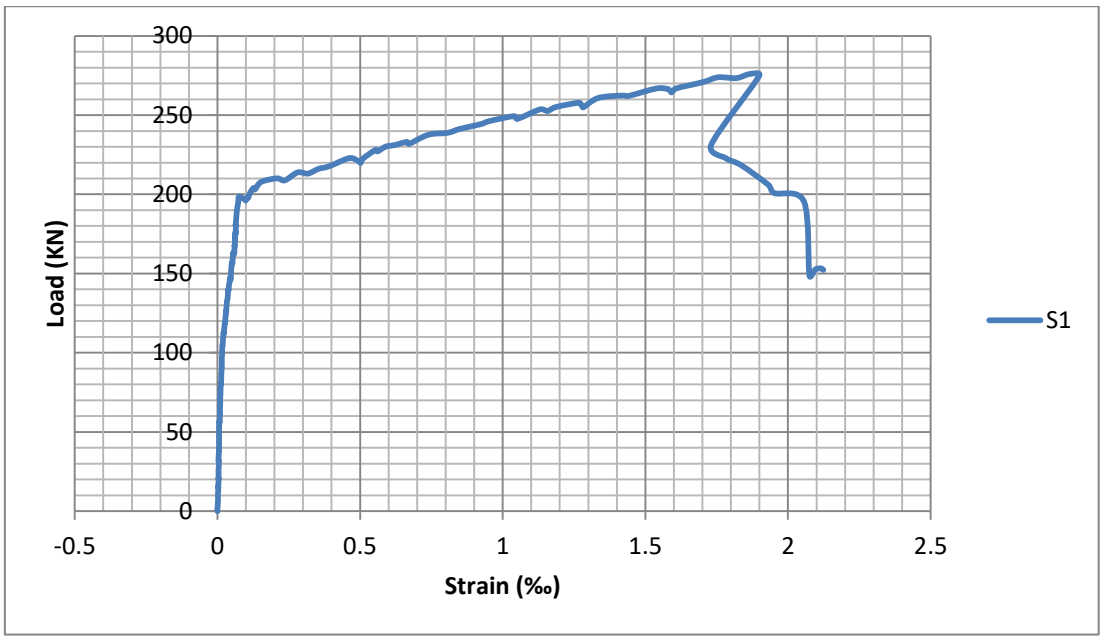

Figure 5.19 : Load Vs Strain from strain gauge S1 on B2M

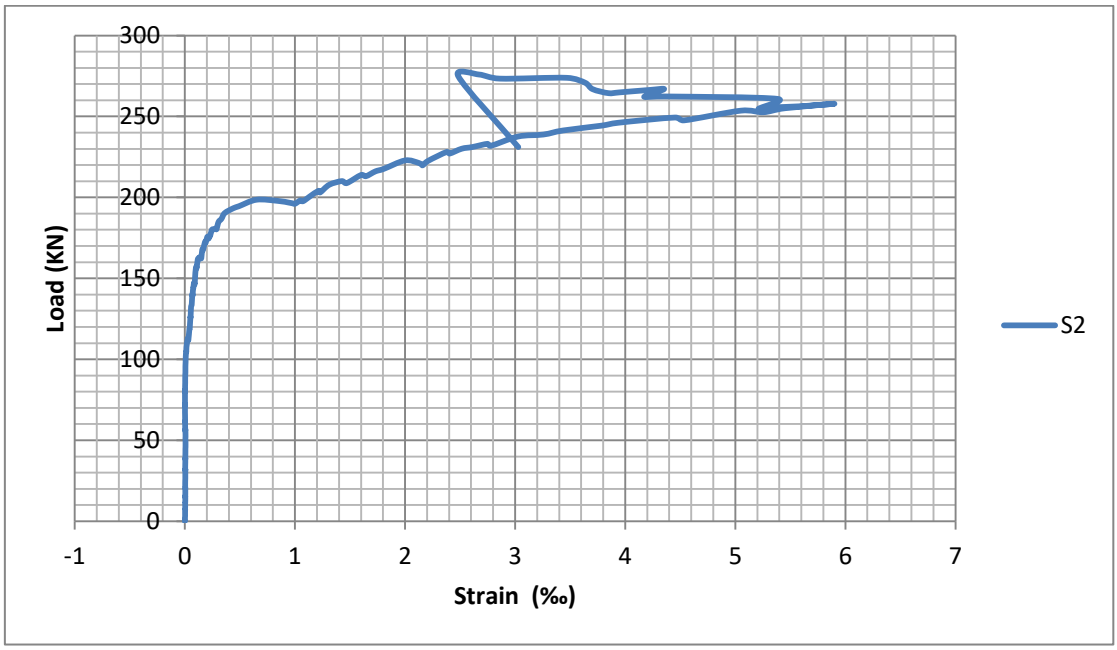

Figure 5.20 : Load Vs Strain from strain gauge S2 on B2M

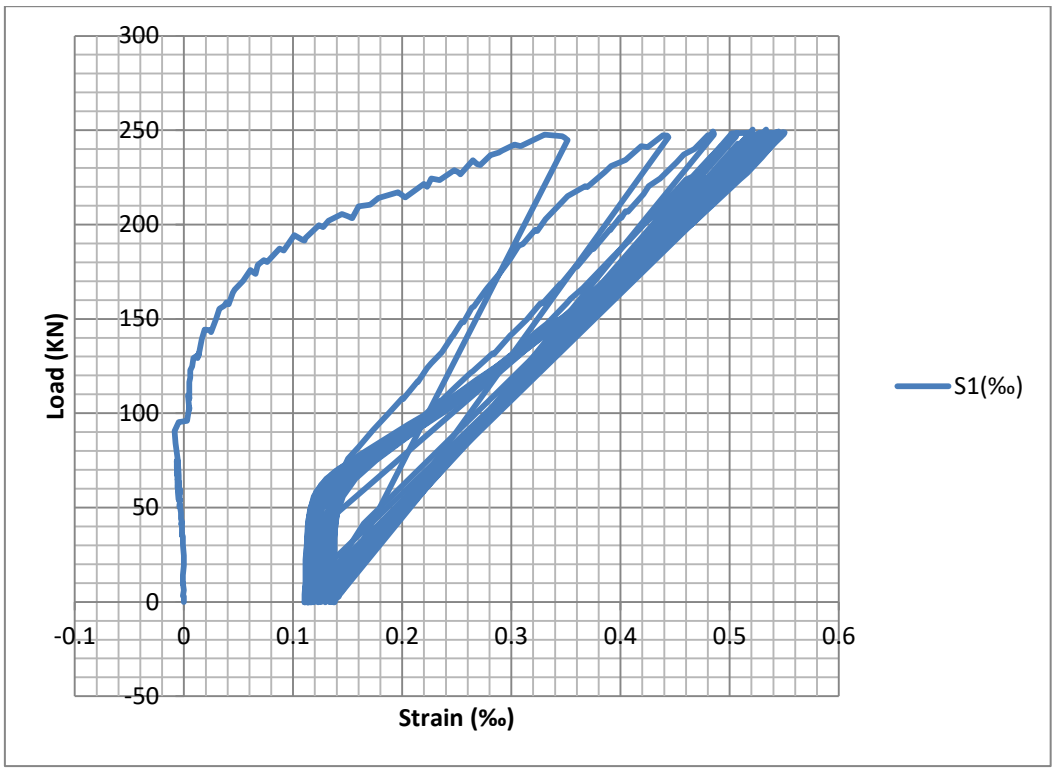

Figure 5.21 : Load Vs Strain from strain gauge S1 on B2C90

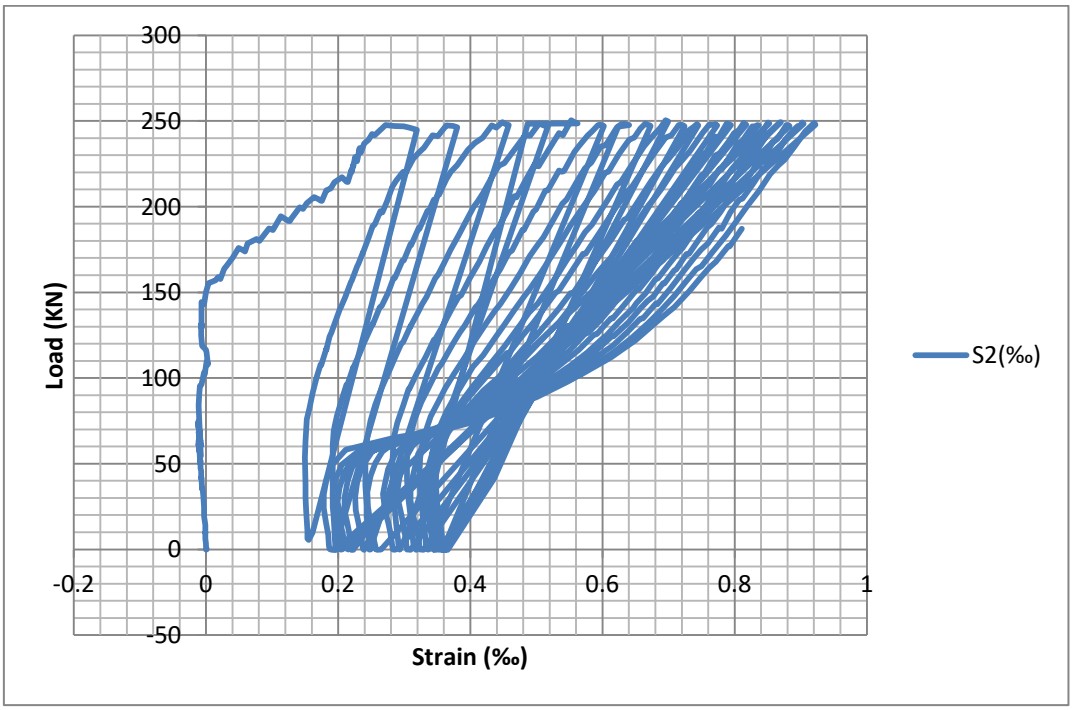

Figure 5.22 : Load Vs Strain from strain gauge S2 on B2C90

From the load vs strain diagrams for specimen B2C90, yielding of shear reinforcements can be observed. However, the strain measurements obtained are much below yielding strain in the entire loading history of the specimen. This can be explained by the location of the strain gauges or possible error during initialization of the data logger. Since the strain gauges measure local

strains (not average strain) in the reinforcements, even if the stirrup has yielded the strain gauge reading would depend on the specific location it's attached.

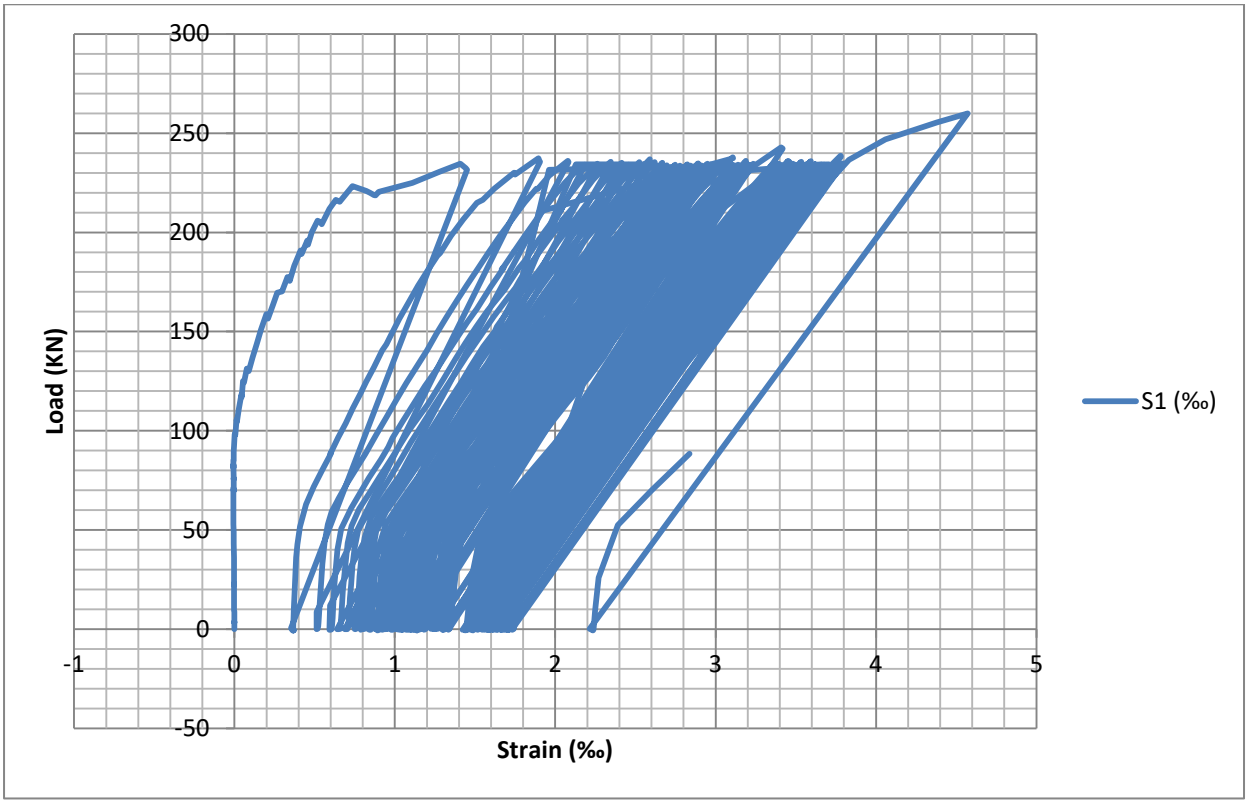

Figure 5.23 : Load Vs Strain from strain gauge S1 on B2C85

Although there were two strain gauges attached to specimen B2C85, S2 was presumably severed during casting and wasn't functional during testing. Thus strain reading from only S1 is available which is displayed on Figure 5.23. On the 61st cycle the load amplitude was accidentally exceeded by 10.82% during manual loading; and yielding of shear reinforcement was observed as shown in Figure 5.23. The strain gauge was detached on the 62nd cycle interrupting data inflow. However, more data was recorded sporadically whenever the strain gauge accidentally gets reattached and it exhibited continued degradation. But this was not incorporated in the above chart for it was not entirely reliable.

There were seven strain gauges attached to specimen B2C80 as shown in Figure 3.2. The beam failed on the side where strain gauges S3, S4 and S7 were attached. The load vs strain gauge diagrams for each strain gauge reading are presented as follows.

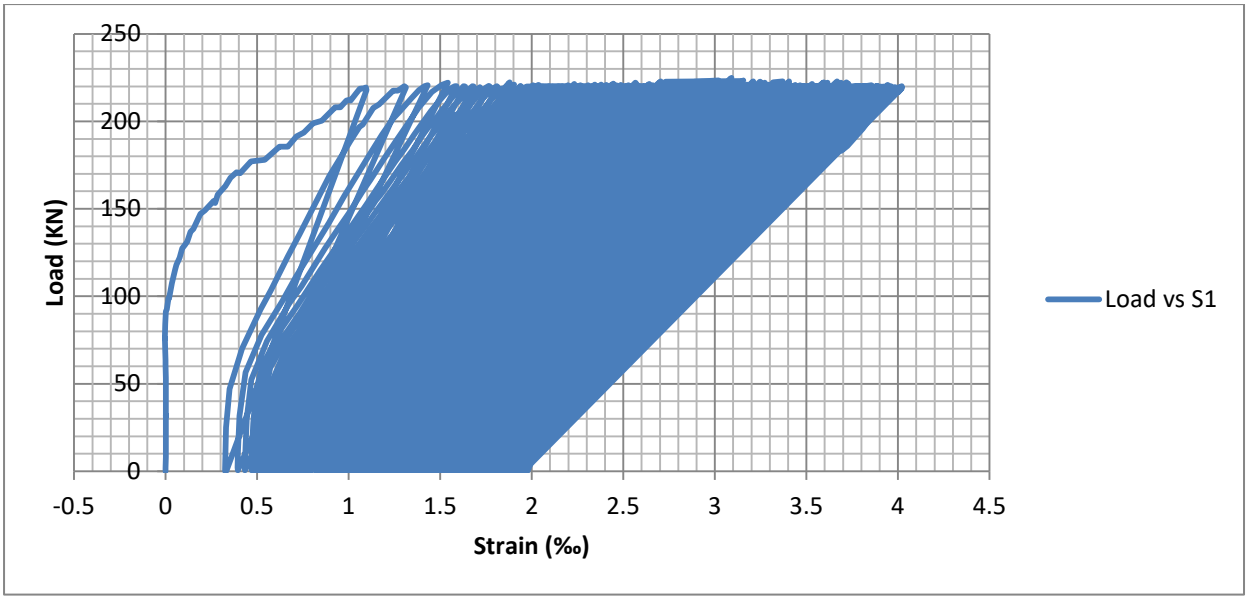

Figure 5.24 : Load Vs Strain from strain gauge S1 on B2C80

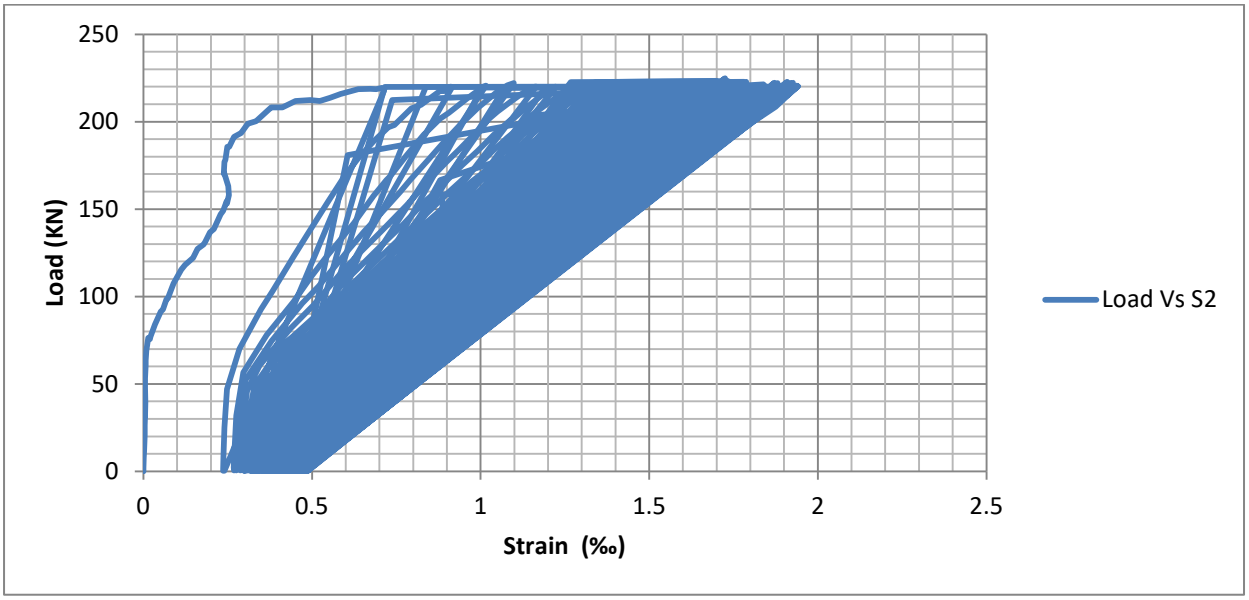

Figure 5.25 : Load Vs Strain from strain gauge S2 on B2C80

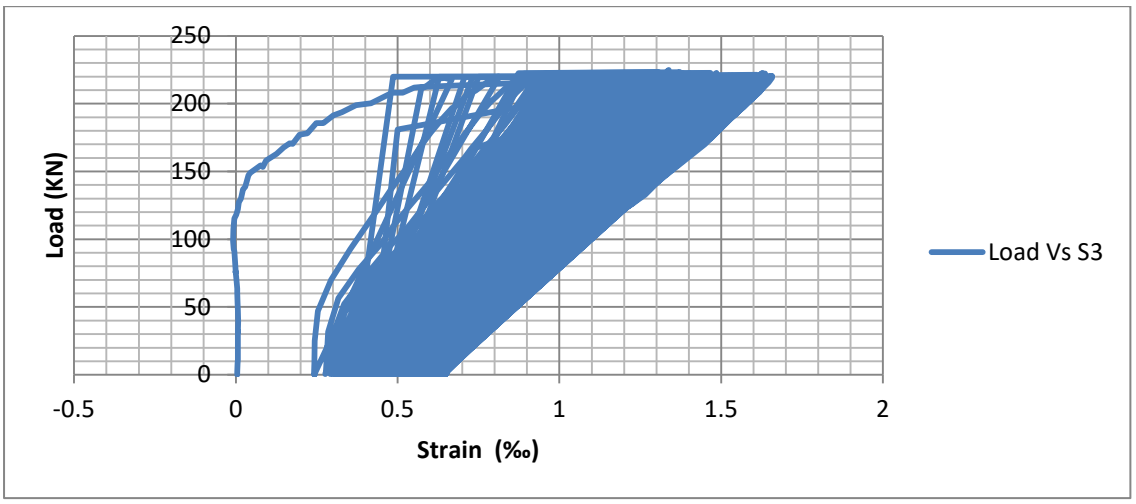

Figure 5.26 : Load Vs Strain from strain gauge S3 on B2C80

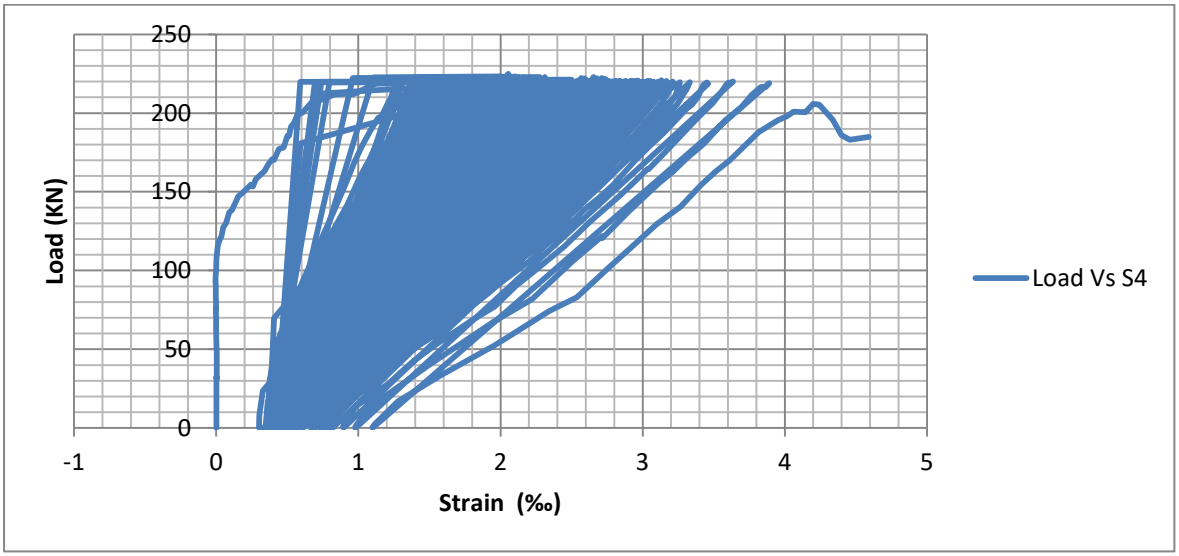

Figure 5.27 : Load Vs strain from strain gauge S4 on B2C80

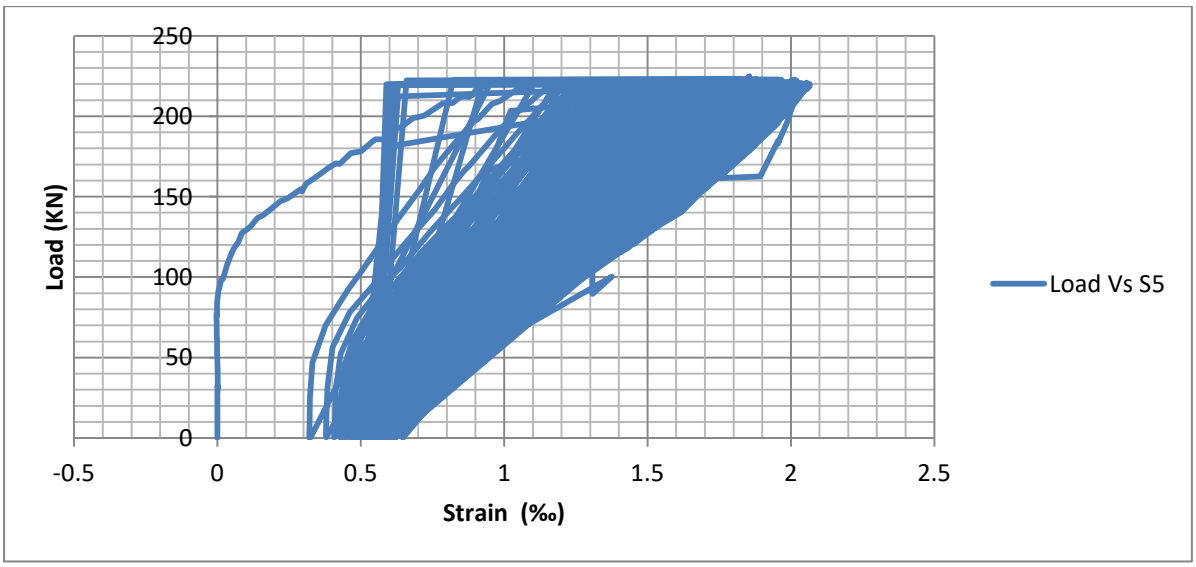

Figure 5.28 : Load Vs strain from strain gauge S5 on B2C80

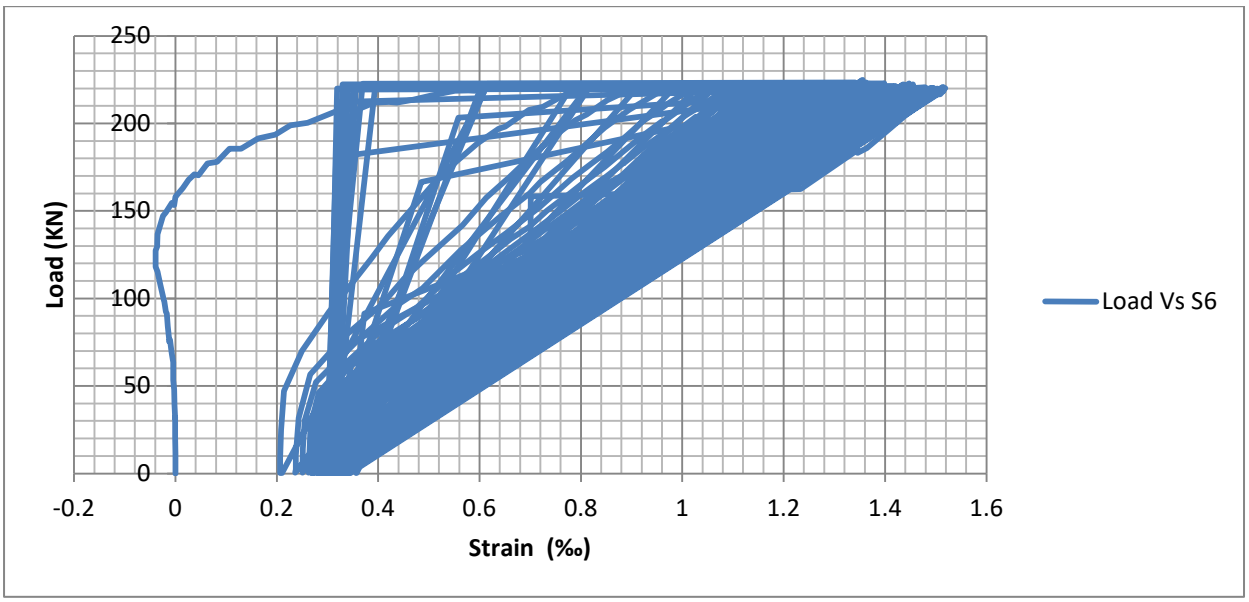

Figure 5.29 : Load Vs strain from strain gauge S6 on B2C80

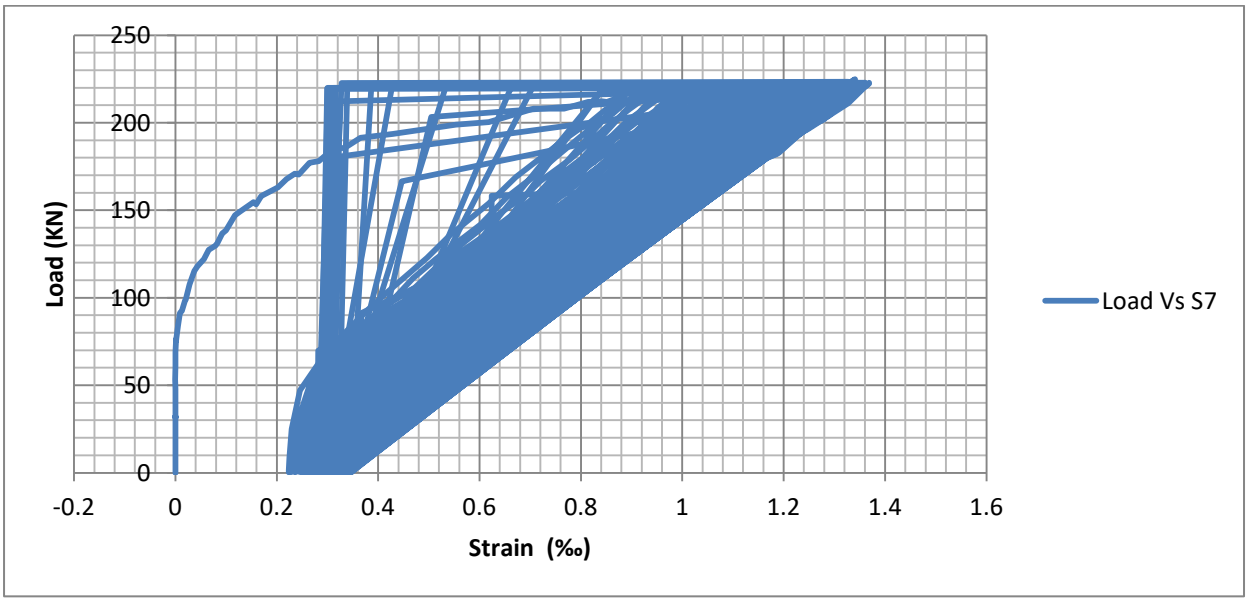

Figure 5.30 : Load Vs strain from strain gauge S7 on B2C80

From the above seven diagrams, it is observed strain gauge S1 recorded a gradual increase in strain with every cycle till the time of failure. Local stress concentration in the stirrup has reached well above its yielding point before failure and a steady degradation was observed throughout the experiment. However, strain readings recorded by strain gauge S4, on the opposite side of the beam, exhibited a substantial spike at the last stages of loading and failure occurred on this side with rupture of the stirrups.

Local strain readings of shear reinforcement per cycle shall be presented below, to clearly show accumulated damage with every cycle.

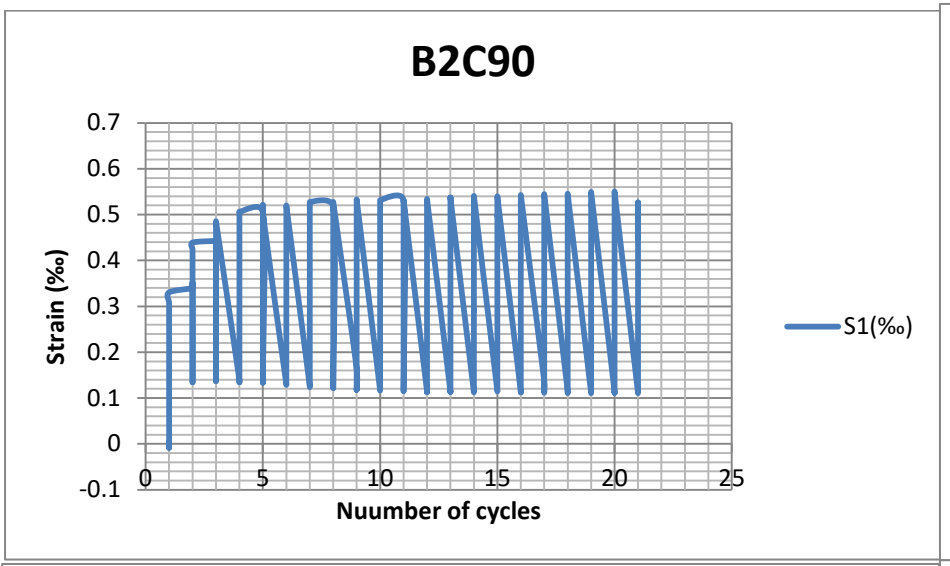

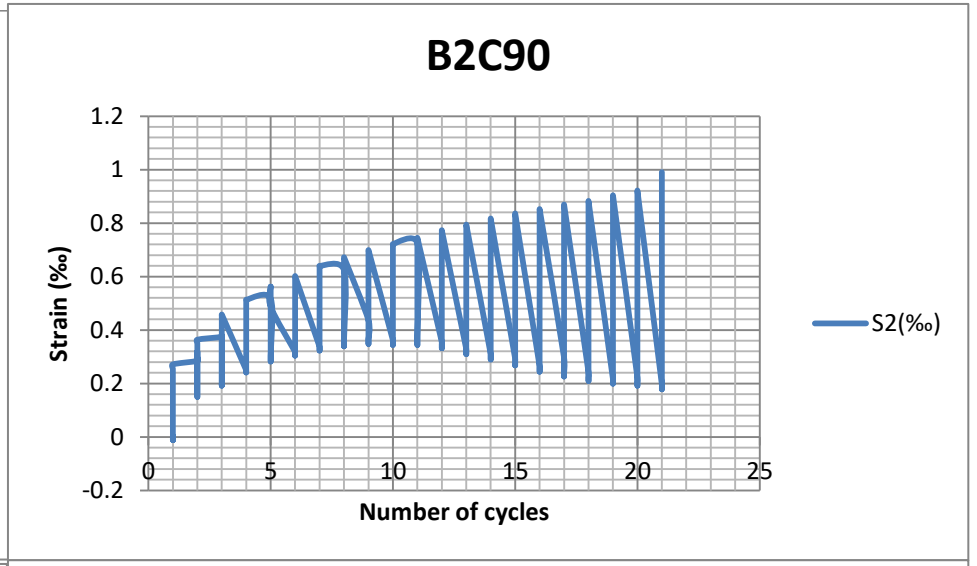

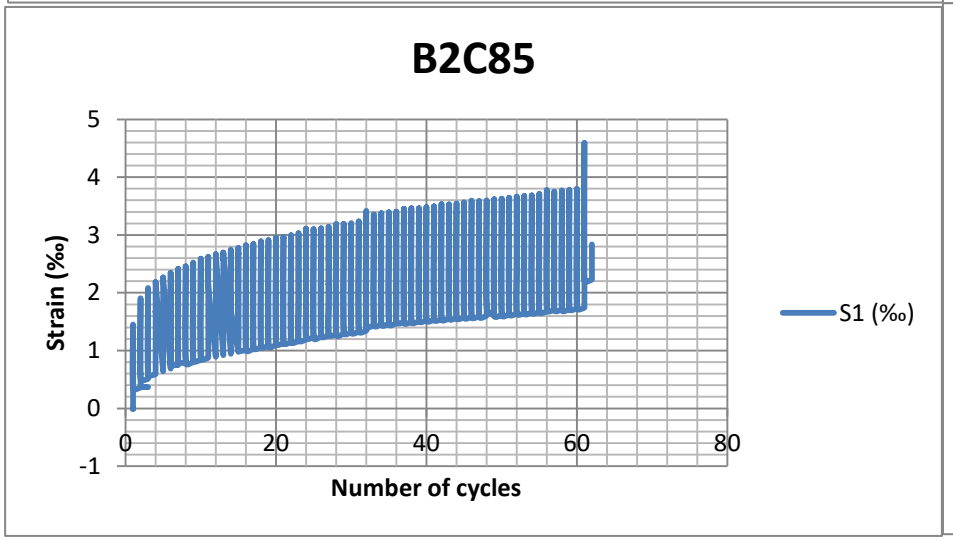

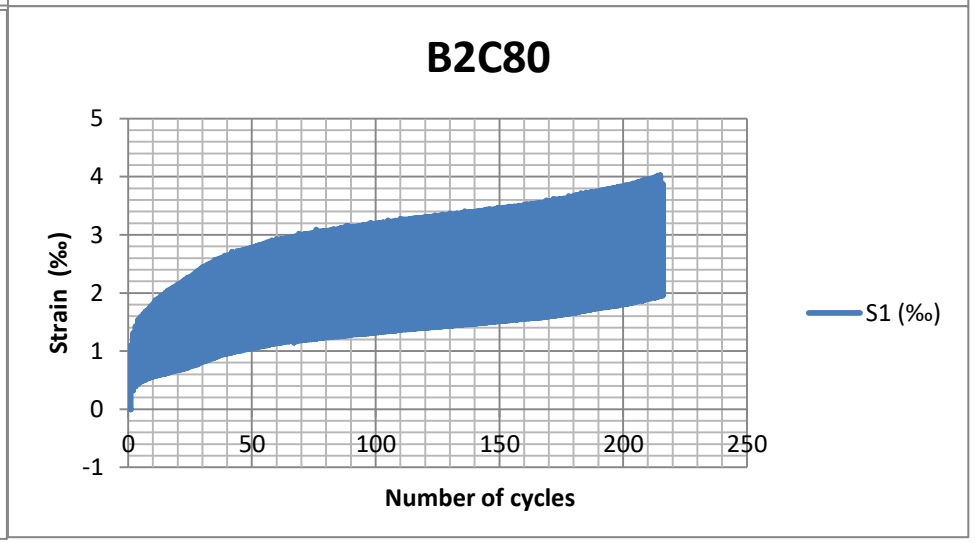

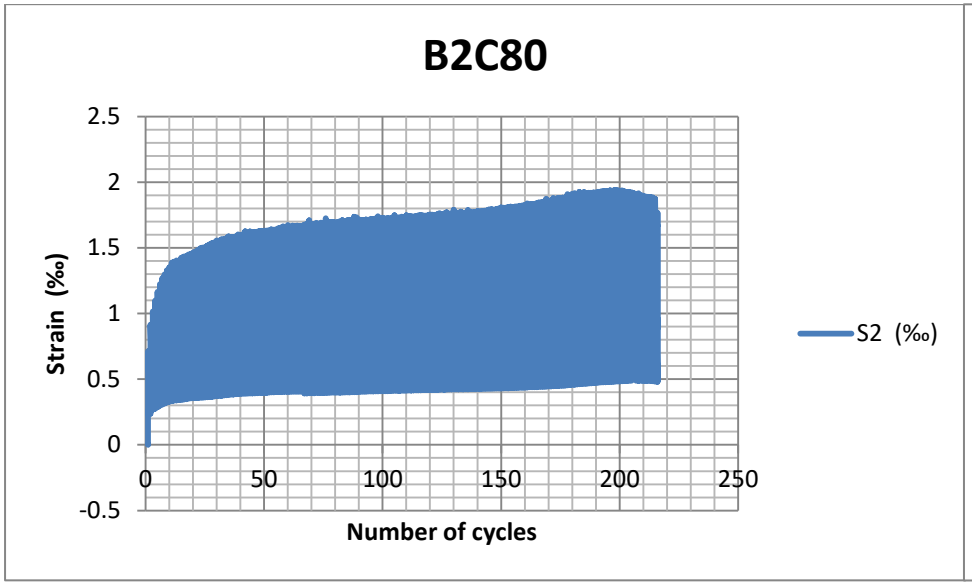
B2C80
Strain (‰)
2.5
2
1.5
1
0.5
0
-0.5
0
50
100
150
200
250
Number of cycles
S2 (‰)

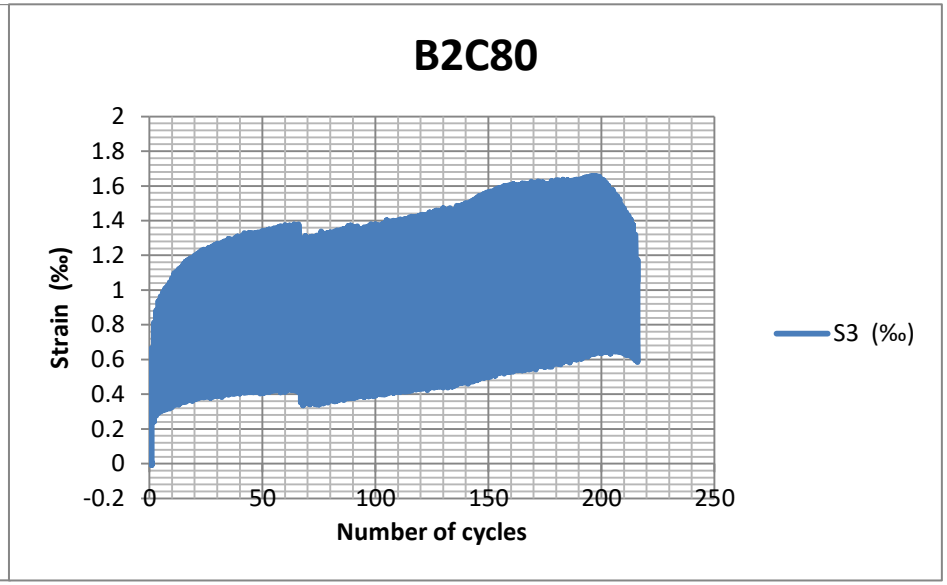
B2C80
Strain (‰)
2
1.8
1.6
1.4
1.2
1
0.8
0.6
0.4
0.2
0
-0.2
0
50
100
150
200
250
Number of cycles
S3 (‰)

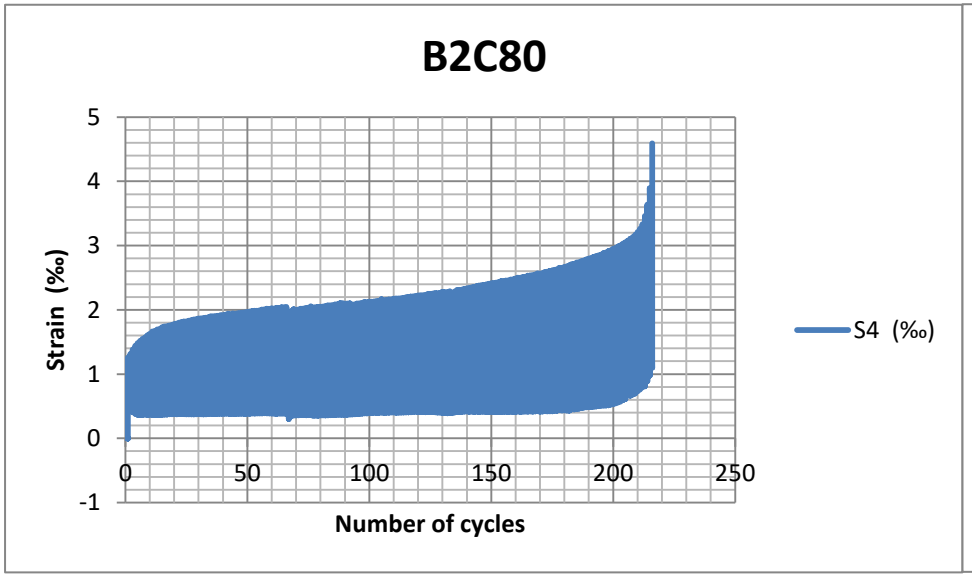
B2C80
Strain (‰)
5
4
3
2
1
0
-1
0
50
100
150
200
250
Number of cycles
S4 (‰)

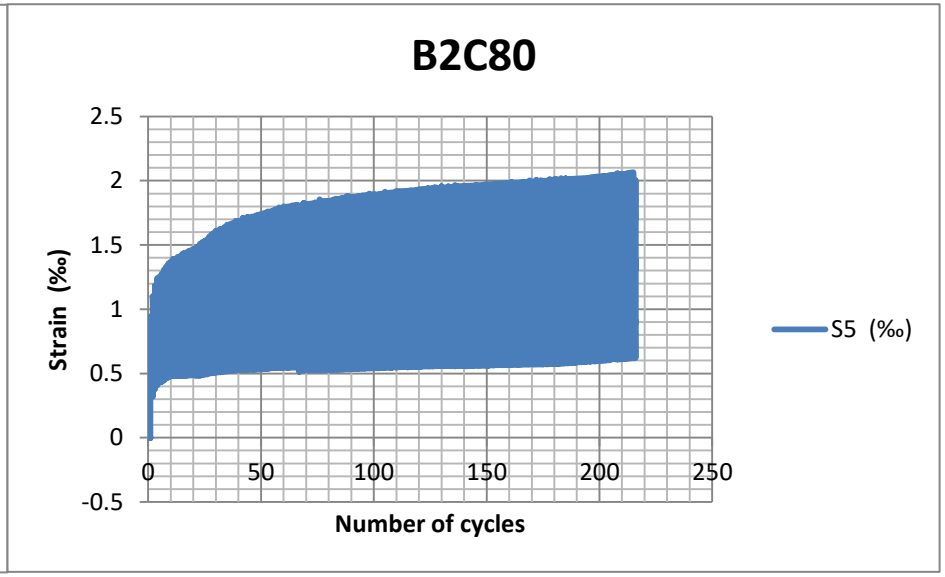
B2C80
Strain (‰)
2.5
2
1.5
1
0.5
0
-0.5
0
50
100
150
200
250
Number of cycles
S5 (‰)

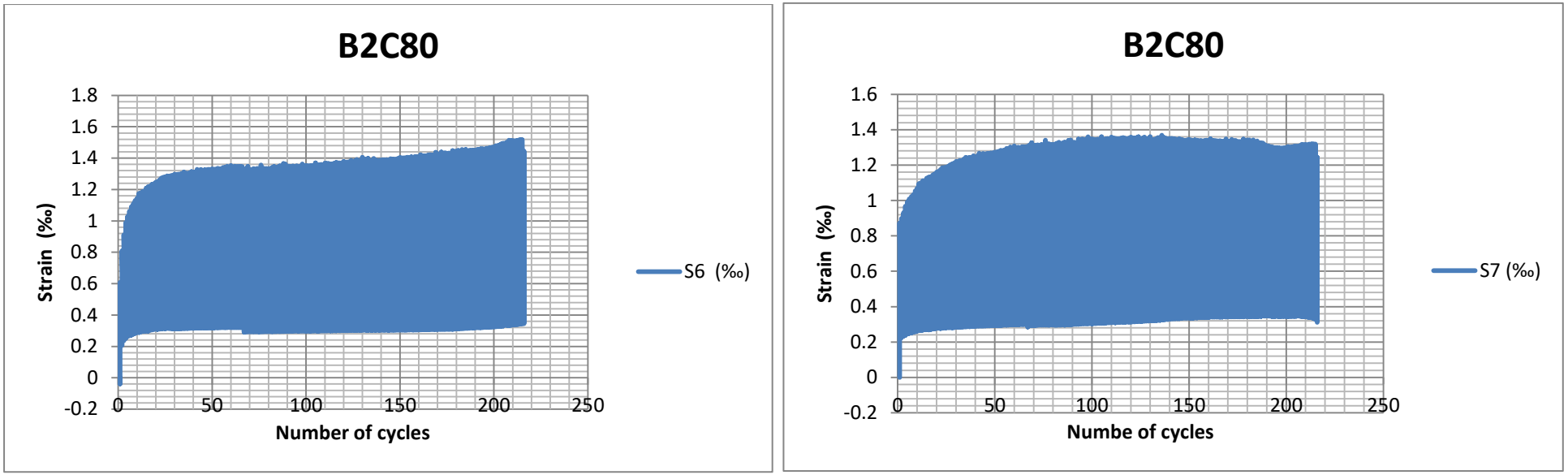

Figure 5.31 : Strain Readings from specimen B2C90, B2C85 and B2C80

From all the charts presented in this section, a consistent increase in strain, consequently stress, of the shear reinforcements with every cycle is observed. A higher strain is recorded for an identical Load with each consequent cycle. This can imply two things: concrete softening and/or reinforcement strength degradation due to repeated loading. The stiffness of the reinforcements was also gradually degrading; implying steel reinforcements undergo cyclic material softening. In this research, shear strength degradation is inferred to be the compound effect of cyclic material softening of both concrete and steel reinforcements; and no attempt has been made to isolate one from the other.

5.1.3 Analytical results

All specimens exhibited typical characteristics of shear failure based on their load deflection curves and strain contour. From the strain contours of the models in different load steps; maximum principal strain contour is observed diagonally from support to point of load application as shown in Figure 5.32 and Figure 5.33. Force-based approach was used for fatigue analysis while monotonic simulation was displacement controlled.

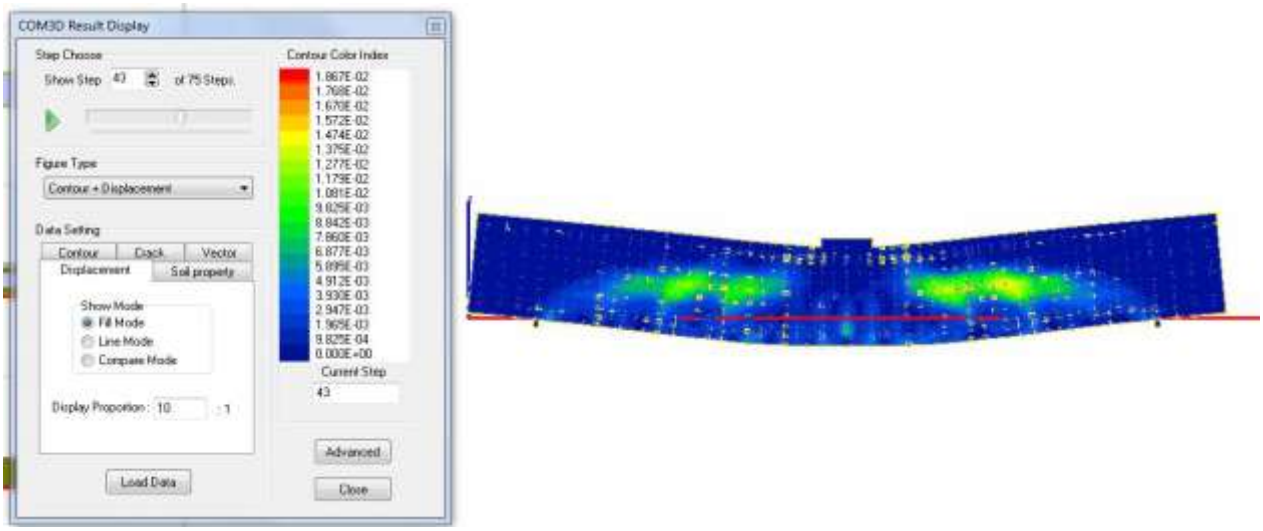

Figure 5.32 : Strain contour and displacement output of A-B2M in load-step 43

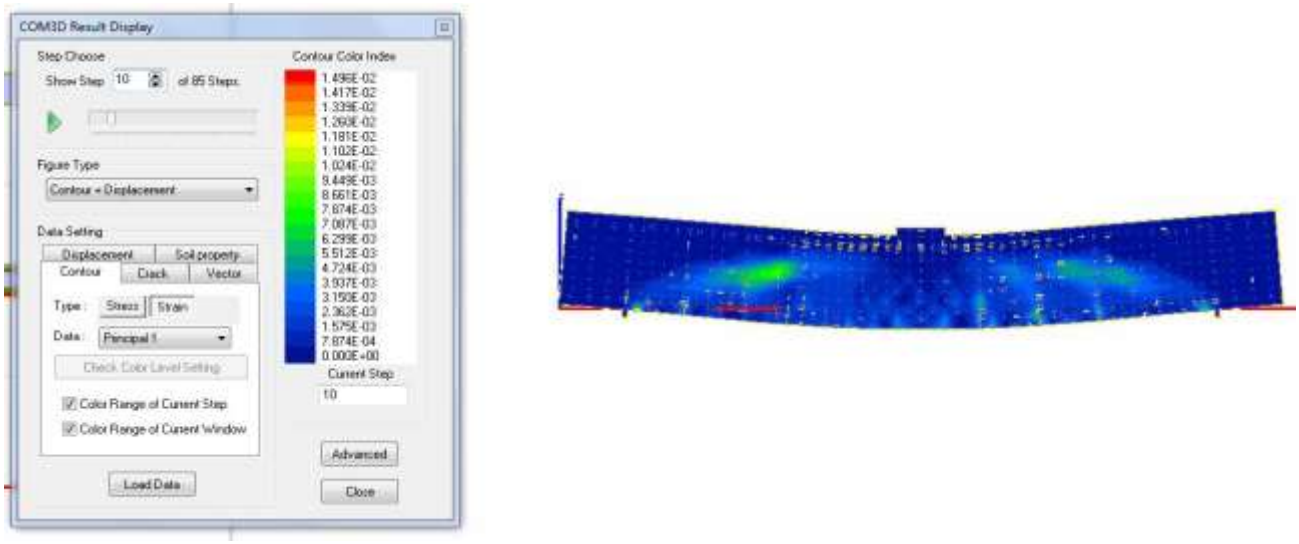

Figure 5.33: Strain contour and displacement output of A-B2C90 in load-step 10

Analytical computation outputs were verified by using experimental results of the beams in this research, under monotonic loading. After verifying analytical modelling as a close match to experimental results, loading pattern was the only parameter varied for the fatigue experiments.

Table 5-2 offers a numerical overview of the analytical simulation results, which shall be discussed in detail in the following sections.

Table 5-2 : Summary of analytical results

Specimen	Cylindrical compressive strength (F'_c)	Shear reinforcement ratio (ϱ_w)	Maximum load (P_{max})	Mid-span deflection at maximum Load (mm)	Life cycle (n)
A-B1M	33.58	0.00%	179.53	5.43	monotonic
A-B1C90	33.58	0.00%	161.58	6.36	30
A-B2M	31.98	0.13%	274.31	8.42	monotonic
A-B2C90	31.98	0.13%	246.88	22.63	19
A-B2C85	31.98	0.13%	233.16	19.79	110
A-B2C80	31.98	0.13%	219.45	19.06	200

5.1.3.1 Load deflection curves

The Load deflection diagrams obtained from analytical simulation on DUCOM-COM3 are presented as follows:

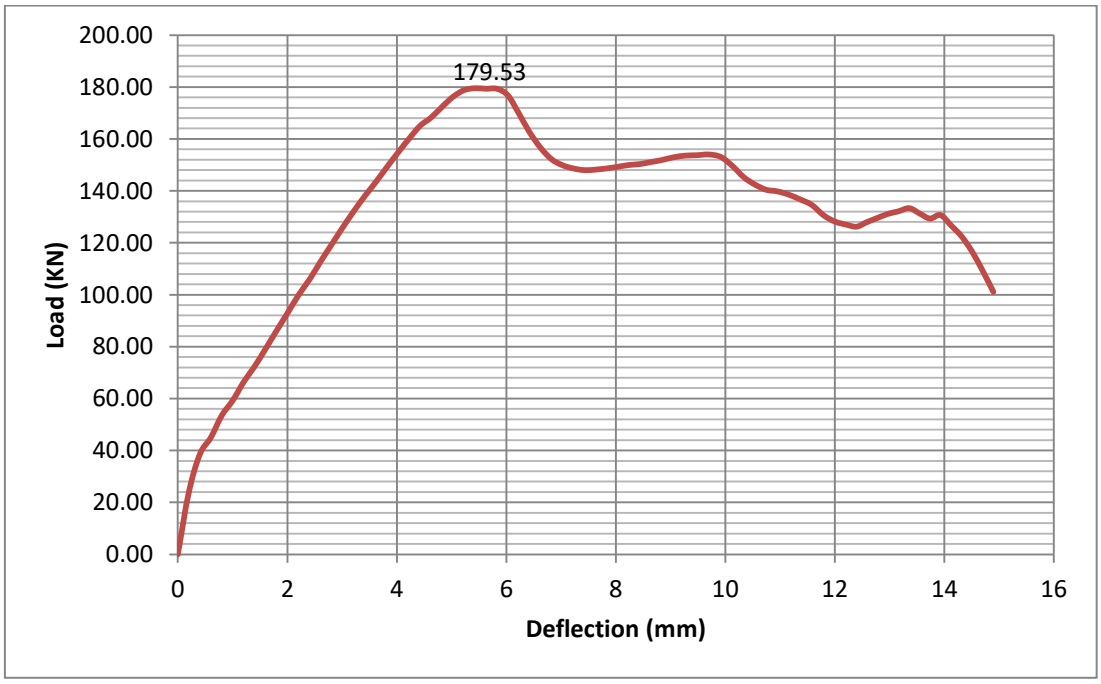

Figure 5.34 : Load deflection diagram for specimen A-B1M

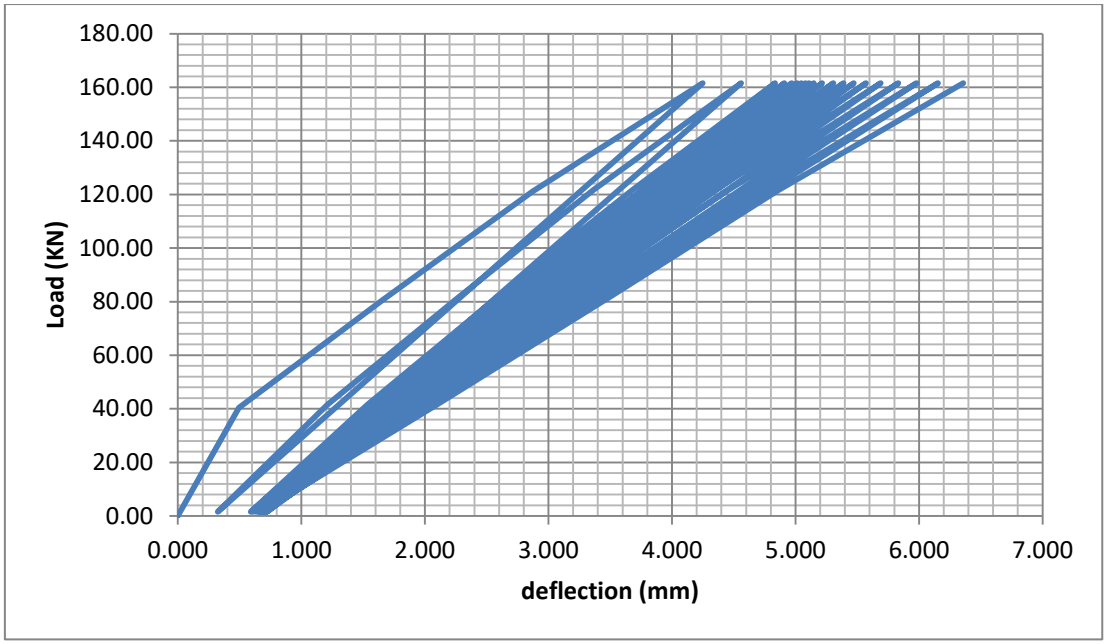

Figure 5.35 : Load deflection diagram of A-B1C90

Figure 5.36 : Load deflection diagram of A-B2M

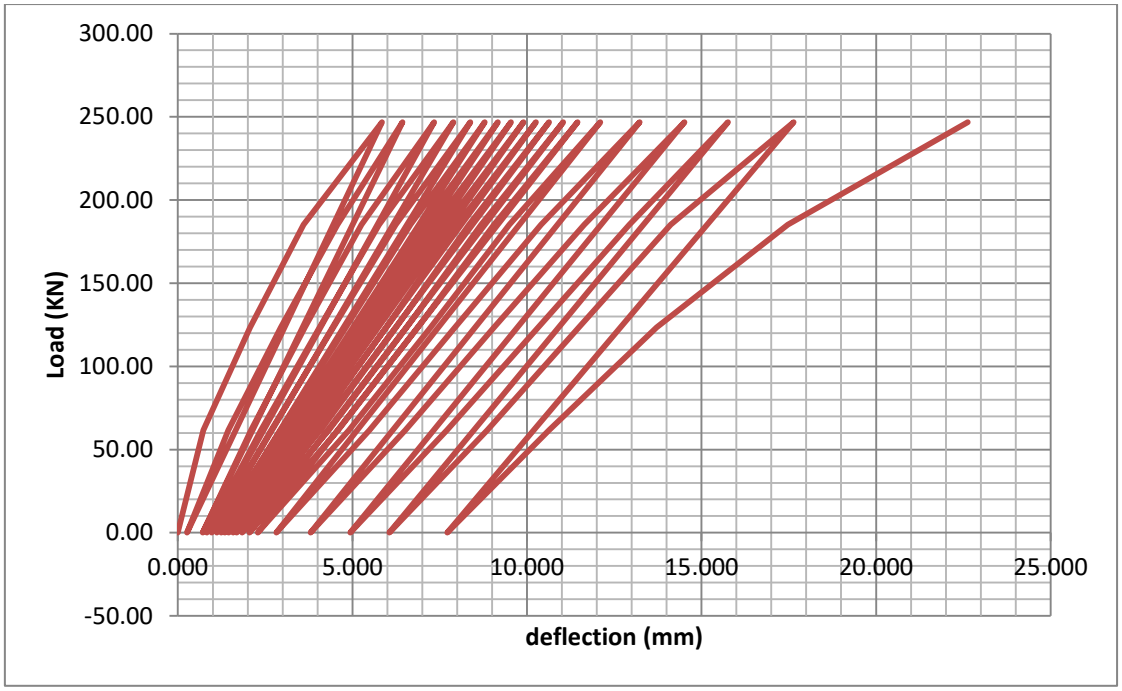

Figure 5.37 : Load deflection diagram of A-B2C90

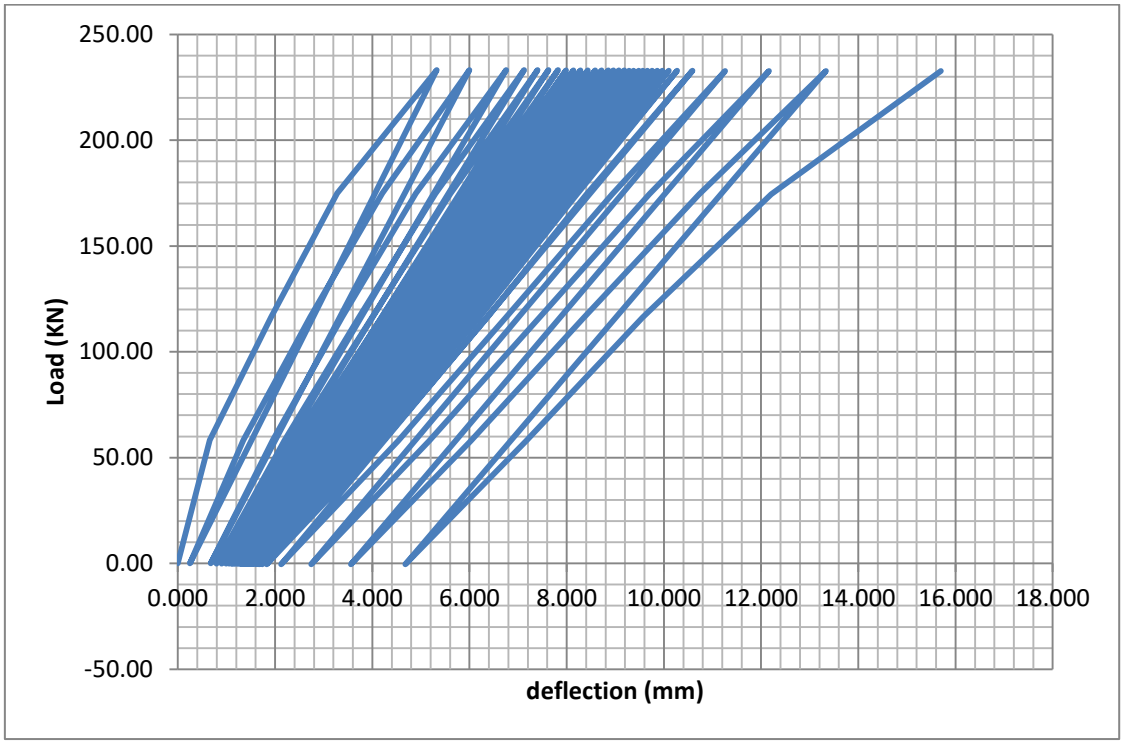

Figure 5.38 : Load deflection diagram of A-B2C85

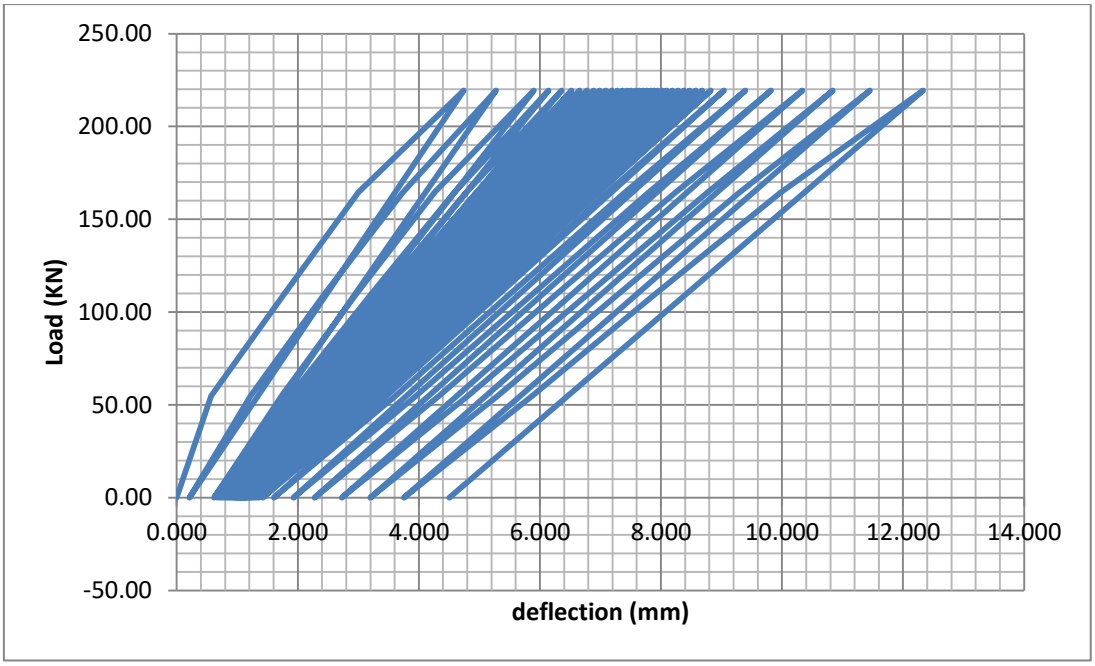

Figure 5.39 : Load deflection diagram of A-B2C80

5.2 Discussion

5.2.1 Shear behavior of experimental beams

Having a clear view of experimental and analytical simulation results, let's proceed to intent observation of this research's outputs and their implication on the shear behavior of shear-critical beams under cyclic loading. The following sections will compare the load deflection diagrams of both the experimental and analytical specimens and comment on their overall behavior.

5.2.1.1 Capacity prediction

The beams were design to fail in shear before yielding of longitudinal reinforcement according to Eurocode 2 (EN1992-1-1: 2004). [2] A theoretical flexure to shear over-strength in the range of 1.3 to 1.5 was employed during design. However after obtaining experimental data of the concrete and reinforcement strength, the theoretical capacity of each beam was predicted. The theoretically computed capacity of the typical beams as compared to experimental results obtained for the static tests is presented on Table 5-3. As can be observed, a theoretical flexure to shear over-strength of 1.39 and 1.33 for typical beams type 1 and type 2 respectively has been ideally employed.

Table 5-3 : Predicted capacity of experimental beams

Specimen Series		Theoretical prediction	Experimental Result
Type one Beam (B1M, B1C90)	Flexural cracking Load (P_{cr})	18.577 KN	21.51 KN
	Ultimate shear capacity (P_{ult})	137.381 KN	181.57 KN
	Flexural Yielding strength (P_y)	190.833 KN	____
	Mode of failure	Shear, Brittle	Shear, Brittle
Type two beam (B2M, B2C90, B2C85, B2C80)	Flexural cracking Load (P_{cr})	21.6 KN	32.01
	Ultimate shear capacity (P_{ult})	210.408 KN	275.86
	Flexural Yielding Strength (P_y)	279.83 KN	___
	Mode of failure	Shear, Brittle	Shear, Brittle

The flexural cracking and yielding load were predicted by using a moment curvature diagram and computing the moment at cracking strain of concrete and yielding strain of the longitudinal reinforcement respectively. The flexural cracking load theoretically computed and observed in the experiments are a closer fit compared to the ultimate shear capacity prediction. The ultimate shear capacity was computed based on Eurocode's provision for shear design using a rotating angle theory (or variable strut inclination). However, since the strut angle was bound within the range from 21.8^0 to 45^0 and the contribution of concrete is neglected; the ultimate capacity of the beams is underestimated. The inclination of the major diagonal crack had been observed to be less than 21.8^0 in the case of B2C85 only.

5.2.1.2 Comparison in response of Type one beams

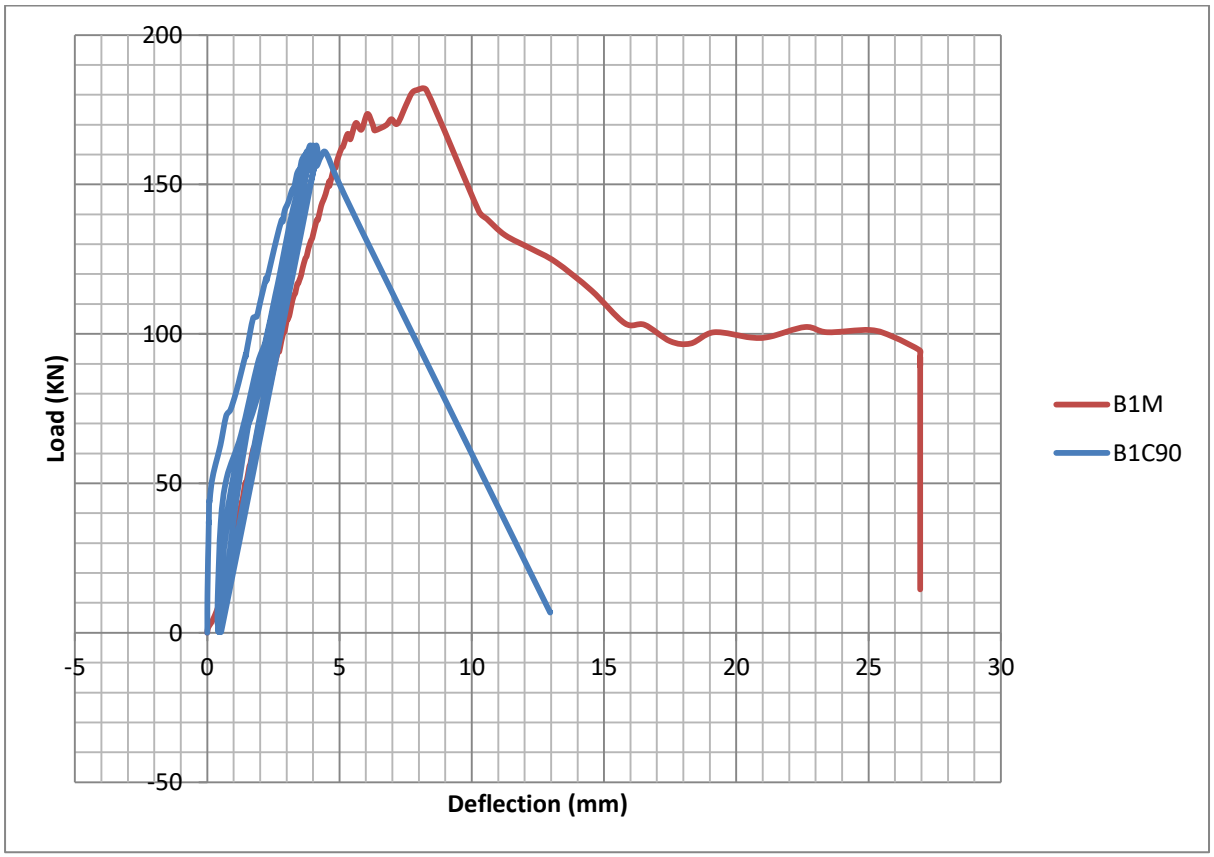

Figure 5.40 : Comparison between B1M and B1C90

Specimen B1C90 exhibited a slightly stiffer response than its monotonic counterpart B1M. Since compressive and tensile strength of the concrete in specimen B1C90 were higher than B1M as shown in Table 3-2, the stiffer response of the first cycle is understandable. However, the beam fell suddenly on the fourth cycle without showing adequate signs of stiffness degradation. Since type one beams don't have shear reinforcement, such brittle failure is to be expected. Once the diagonal cracking stress of the beam is reached, failure is imminent without any crack redistribution. Previous studies performed on beams without shear reinforcement under fatigue loading present a life cycle around 10^1. These results don't deviate much from that. Moreover, since a variable loading rate was employed during testing, such minimal deviations are to be expected.

In general, it can be observed beams without shear reinforcement are highly unstable under low-cycle fatigue analysis. Failure is extremely brittle with no apparent warning.

5.2.1.3 Comparison in response of Type two beams

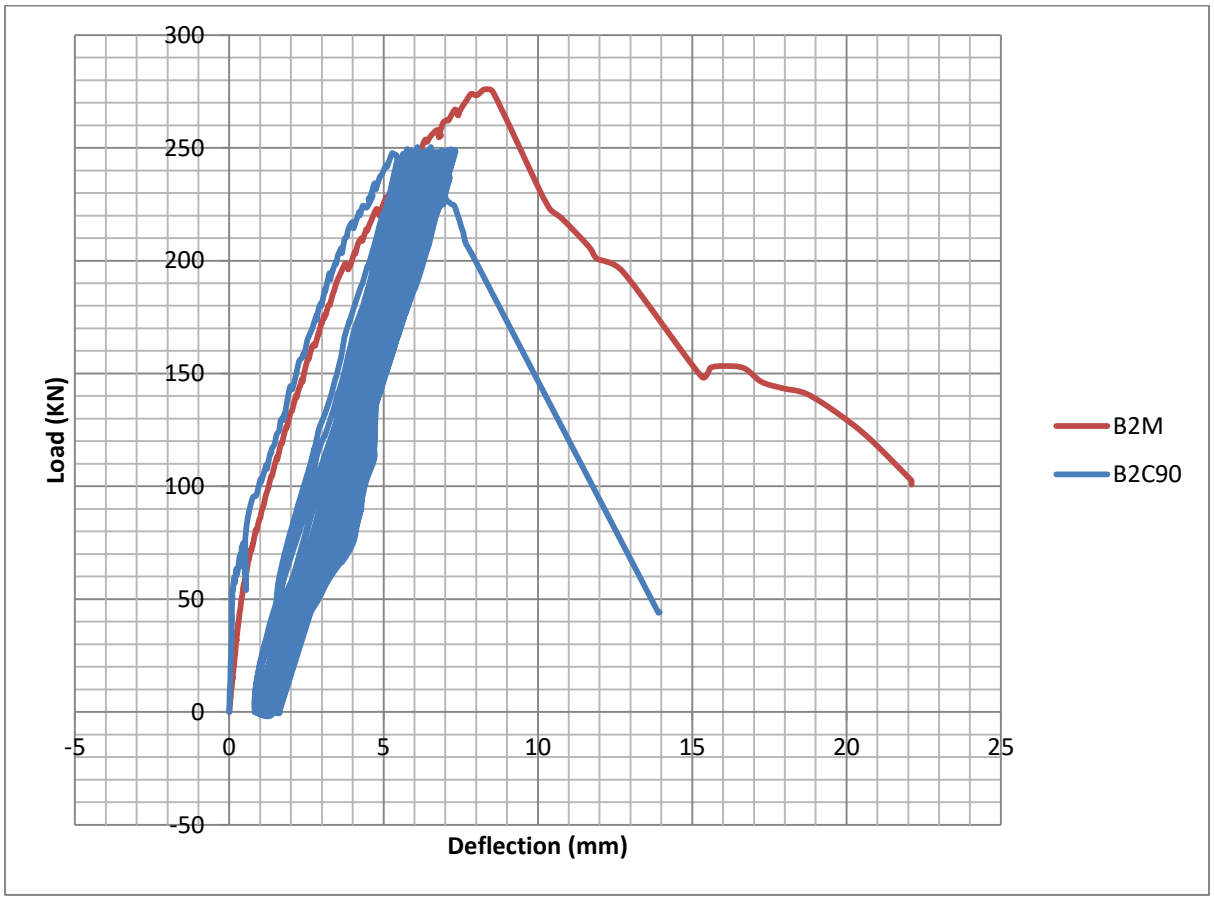

Figure 5.41 : comparison between B2M and B2C90

The load-deformation response measured under monotonic loading was observed to be an excellent envelope to the cyclic response of specimen B2C90 as shown in Figure 5.41. The life cycle of the specimen at 90% of its maximum capacity is observed to be 21 cycles. This is analogous to fatigue analysis of many Reinforced Concrete beams (failing in shear or flexure) in previous researches. [8], [10], [29], [30] Failure is quite brittle and abrupt under cyclic loading.

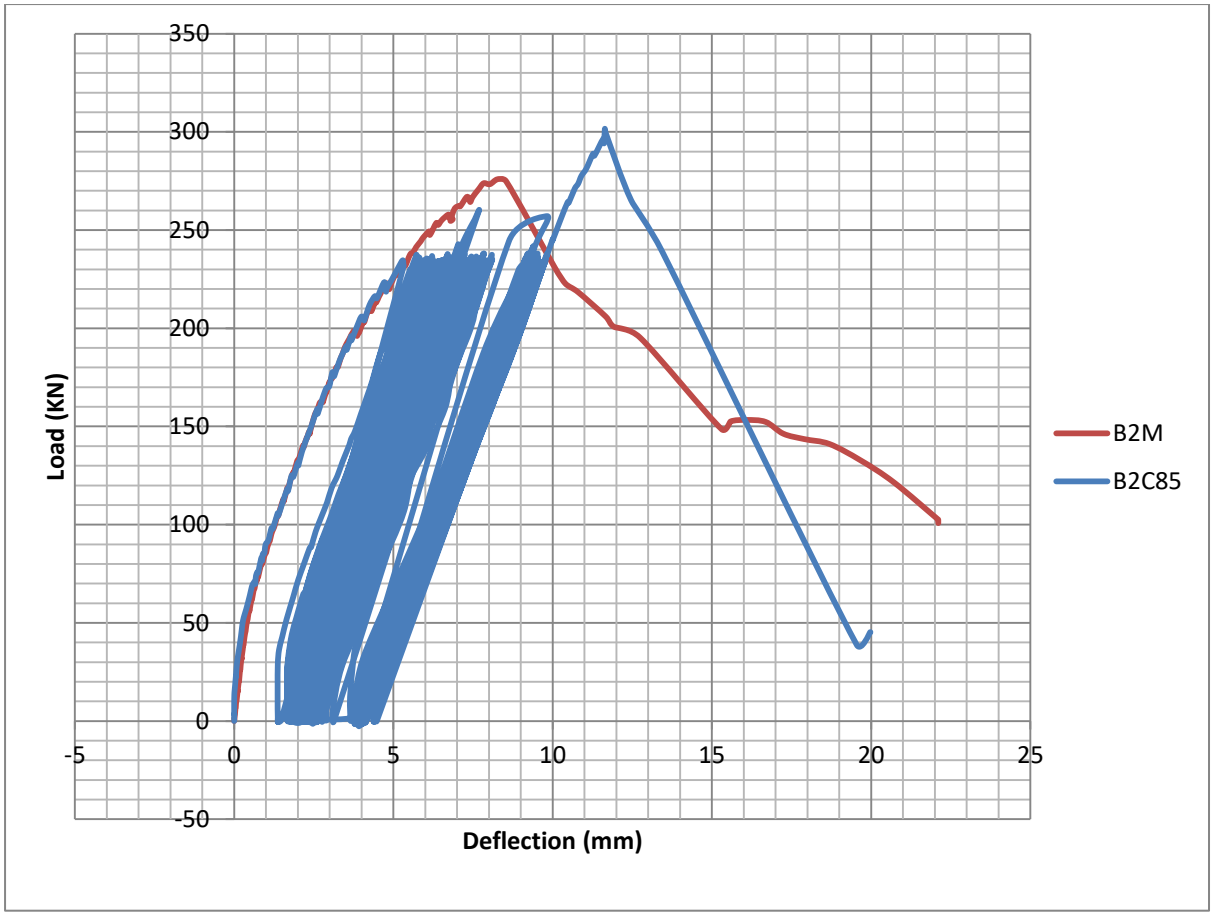

Figure 5.42 : Comparison between B2M and B2C85

The load-deformation response measured under monotonic loading was observed to be an excellent envelope to the cyclic response of specimen B2C85 as shown in Figure 5.42. Load deflection response of specimen B2C85 was in prefect agreement with B2M in the first cycle of loading. However after 219 cycles of fatigue loading, when the beam was loaded monotonically in the 220th cycle, it displayed a higher capacity as shown in the figure. This was an un-expected occurrence and has rarely been reported in other studies and mainly explained as an anomaly. [21] However in this study, a logical rationale for such capacity upsurge shall be put forth based on observation of test results in section 5.2.1.5.

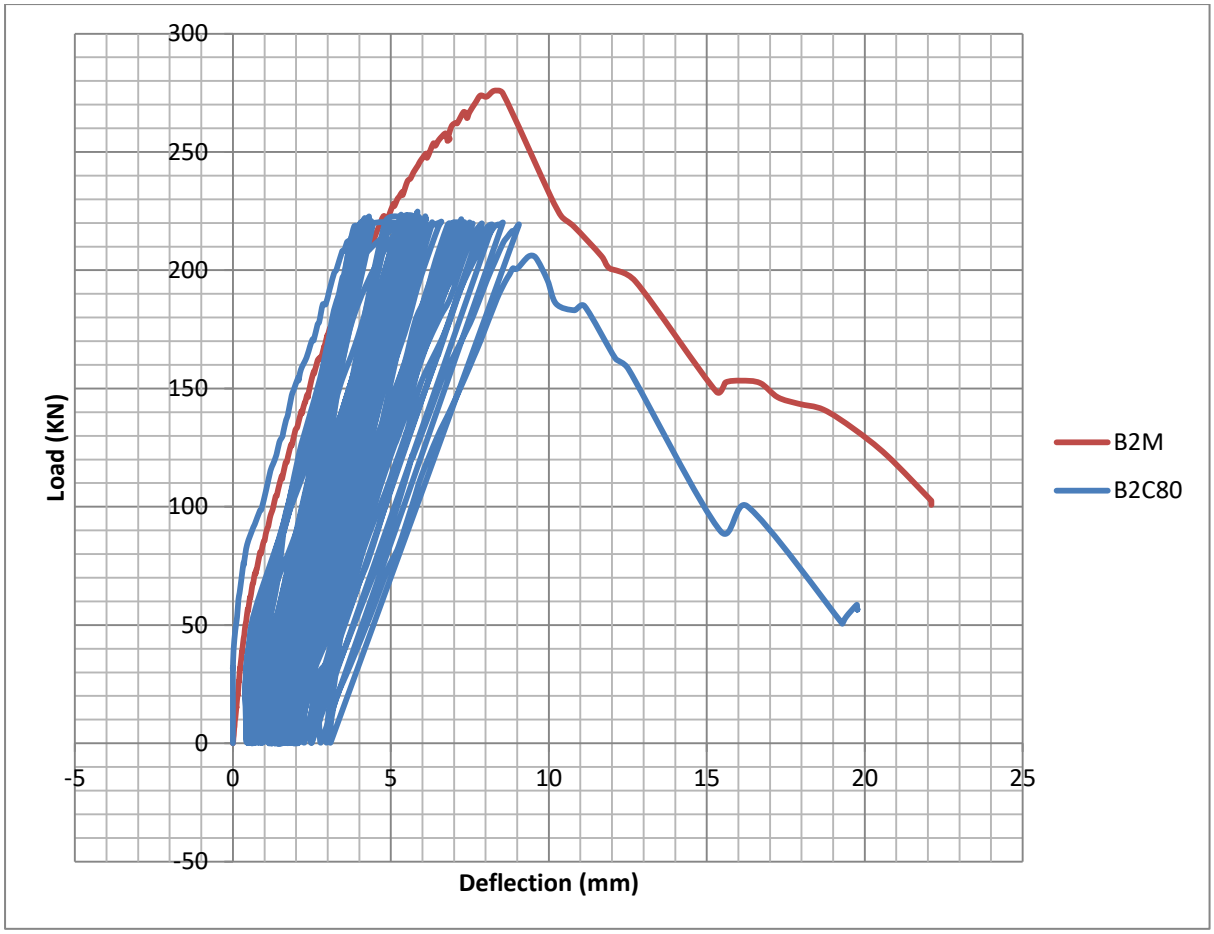

Figure 5.43 : Comparison between B2M and B2C80

The load-deformation response measured under monotonic loading was observed to be an excellent envelope to the cyclic response of specimen B2C80 as shown in Figure 5.43. However a faster degradation in capacity was observed unlike other experimental beams. As previously discussed, the beam was first presumed to have fallen prematurely due to random material variations and specimen fabrication defects. However, the close conformity of this result with the output of the analytical simulation has advocated validity of the results. Hence based on experimental and analytical results in this research, shear strength degradation is observed to be faster for shear-critical beams under low-cycle fatigue.

5.2.1.4 Comparison between type 1 and type 2 beams

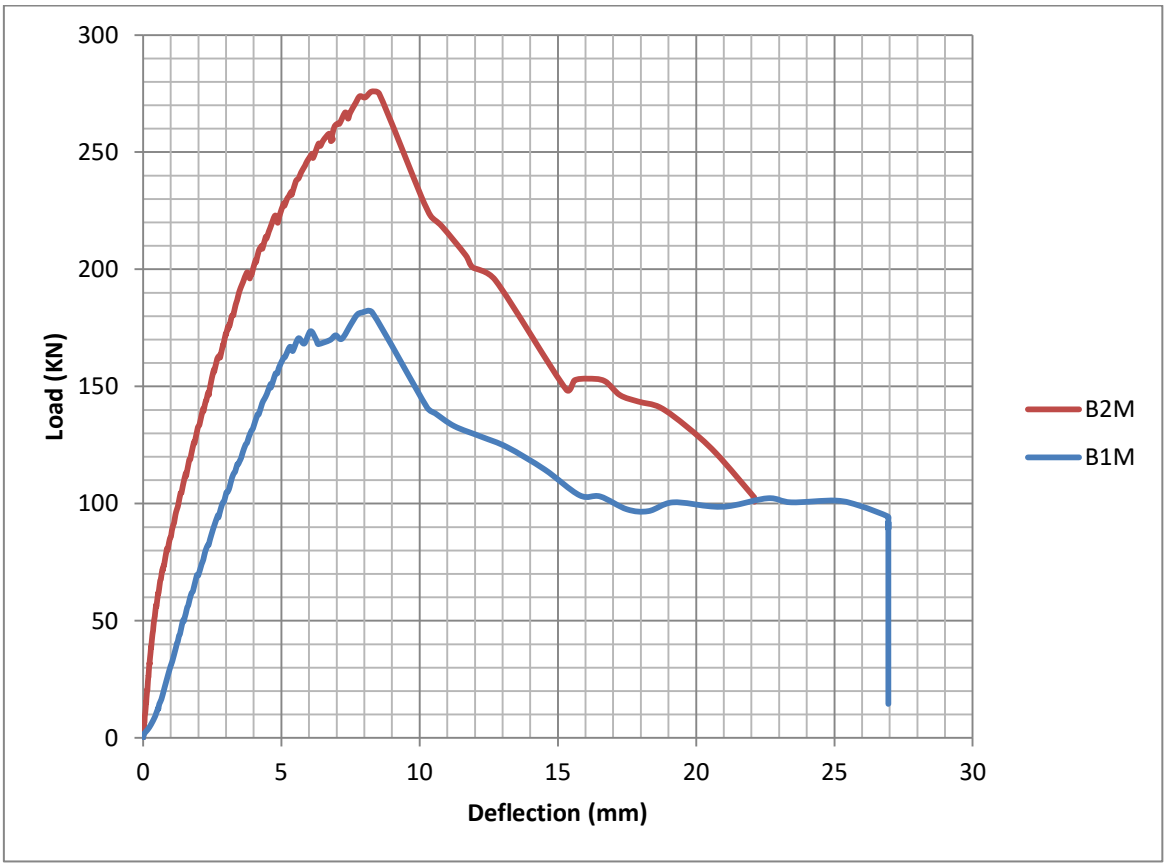

Figure 5.44 : Comparison between B1M and B2M

Specimen B2M exhibited a stiffer response with a higher maximum capacity compared to specimen B1M. Since specimen B1M and B2M have identical specifications except for shear reinforcement provision, an identical load deflection response was expected before diagonal cracking. However due damage incurred by specimen B1M before loading a weaker response with a lowered stiffness is observed. However the maximum capacity of the beam was not affected by this initial damage. The provision of shear reinforcement nearing the minimum requirement (0.12% according to Eurocode) has increased the capacity of the beam by 51.93%. Crack width is also observed to be narrower for beams with web reinforcement.

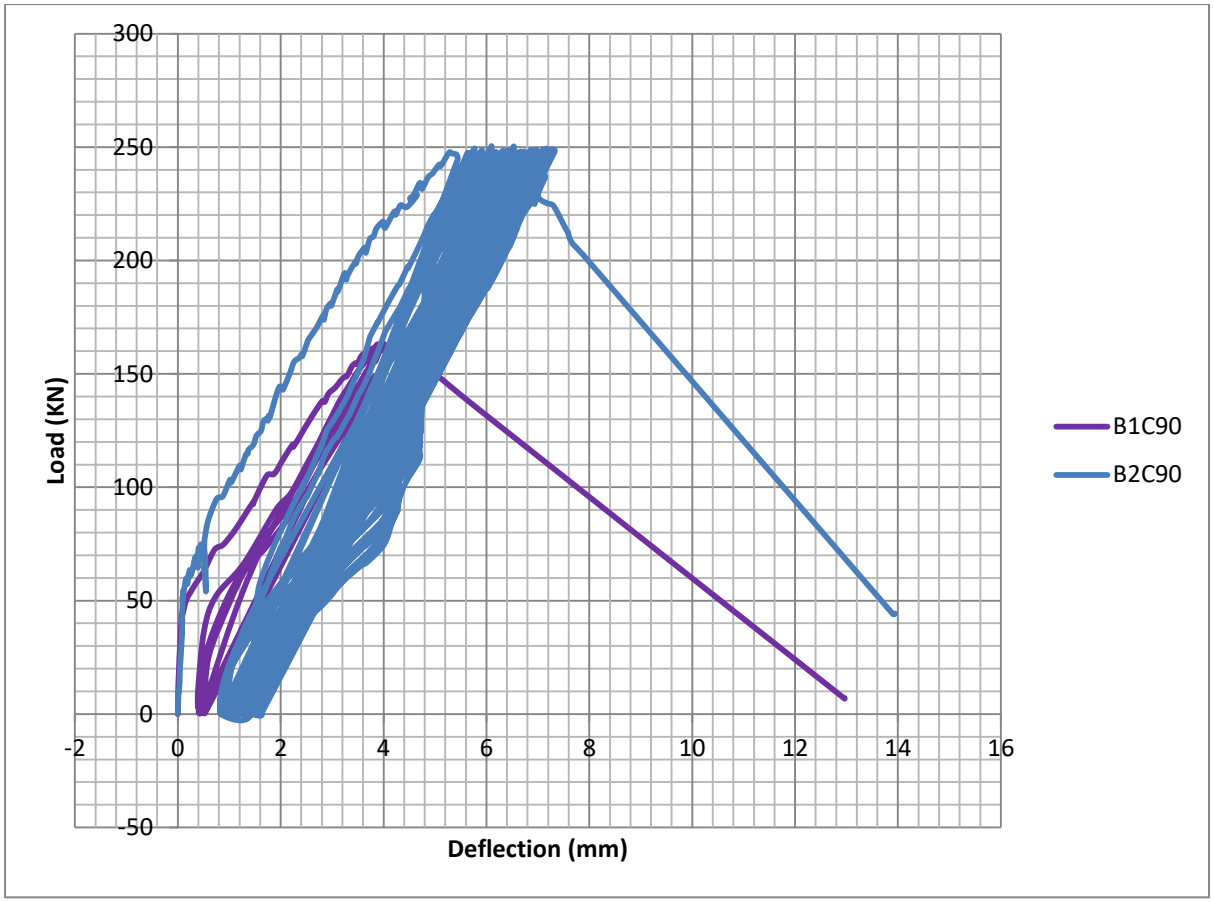

Figure 5.45 : Comparison between B1C90 and B2C90

Specimen B1C90 and B2C90 exhibited identical load deformation response up to diagonal cracking; where the stirrups were activated to carry the additional load in specimen B2C90. Both specimens were tested under low-cycle fatigue analysis with constant maximum amplitude of 90% of their ultimate capacity. Specimen B1C90 lasted only four cycles, much lesser than the fatigue life of specimen B2C90. This clearly showed the instability of beams without web-reinforcement under cyclic loading and the important role of stirrups in energy dissipation during seismic events.

5.2.1.5 Diagonal crack path

Fatigue damage process depends on several parameters such as loading history, time duration of loading, loading rate etc. Based on observations made on the major diagonal crack of specimens in this study, diagonal crack path is perceived to have influence on fatigue damage process. For beams with shear reinforcement, since there's redistribution of cracks, several inclined cracks are developed before failure. In one point loading tests, as load is increased, one of these inclined cracks will extend to the point of load application and a major diagonal

crack shall be formed right before brittle failure. 'Diagonal crack path' refers to the geometrical path of this major inclined crack where shear failure occurs.

A high percentage of shear stress is transferred across an inclined crack by aggregate interlock. For beams with web-reinforcements under fatigue loading, before yielding of stirrups, inclined cracks would remain narrow allowing for shear to be transferred by aggregate interlock. Hence the length of the cracked interface of the major diagonal crack would be one factor affecting shear capacity. Unfortunately there is no way of predicting the exact location of the major diagonal crack, since the formation of any crack alters the state of stress in the beam because of a stress concentration at the tip of the crack.

Yet under fatigue loading of Reinforced Concrete beams, the top section of the beam shall be stiffened by compression due to repeated loading. After a few cycles of loading, a permanent deformation in the beam is observed confirming the top section is under compression. This phenomenon makes extension of inclined cracks to the compression zone difficult. Therefore inclined cracks would grow more horizontal as they extend to the point of load application. Eventually, the diagonal crack path where failure occurs shall be an inclined crack from the point of load application to support; as in the case of deep beams. It has been observed that the diagonal crack grows flatter and longer with number of cycles for fatigue analysis of RC beams as shown in Figure 5.46.

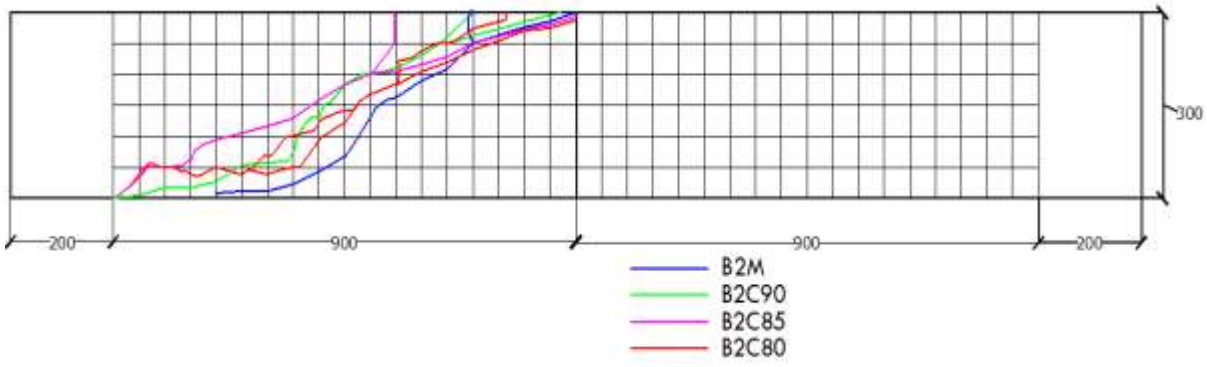

Figure 5.46 : Diagonal crack path of Type two beams

The increase in shear capacity of specimen B2C85 (Figure 5.47) after 220 cycles is attributed to this change in diagonal crack path. It can be observed from Figure 5.46, that specimen B2C85 had the longest diagonal crack path compared to the rest of the specimens. With such change in diagonal strut inclination, more stirrups will be engaged in carrying shear stress and aggregate interlock shall be maximized with a larger inclined crack interface. This in turn

shall increase the shear capacity of the beam as exhibited in specimen B2C85. Similar test results has been reported in previous research, Mihaylov et al.[21], where beams tested under cyclic loading exhibited a higher capacity than analogous beams tested under static loading. Usually such experimental outputs have been ruled out as outliers because of local material variability or other internal framework not understood by the researcher. However, this research suggests diagonal crack path inclination affects shear capacity of RC beams and therefore, beams that have undergone fatigue loading can exhibit higher capacity if they were loaded in a monotonically increasing load.

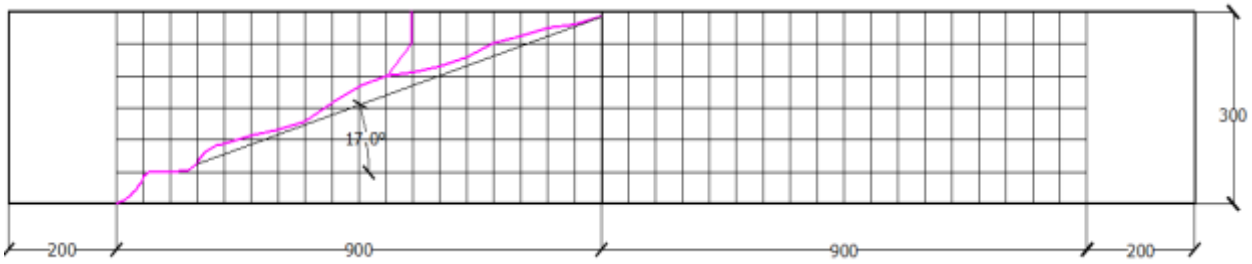

Figure 5.47 : Diagonal crack path of B2C85

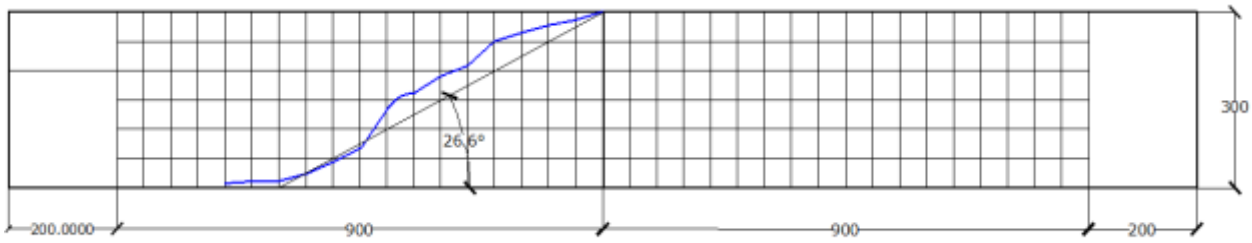

Figure 5.48 : Diagonal crack path of B2M

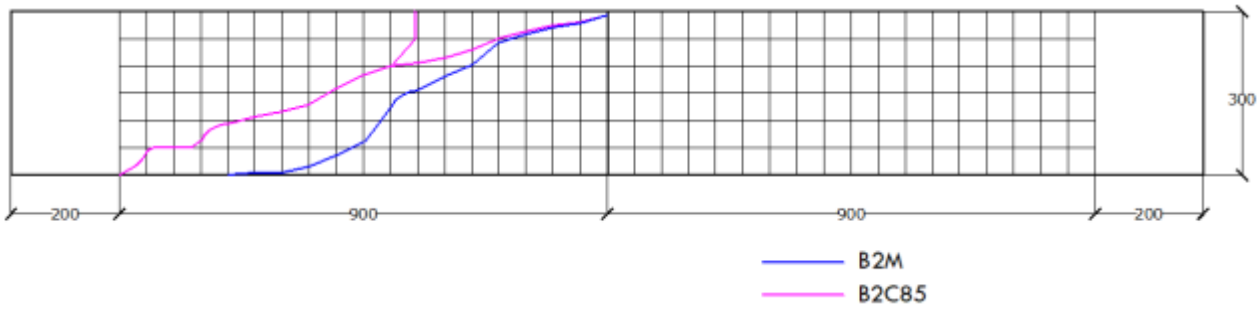

Figure 5.49 : Diagonal crack path of B2M and B2C85

In line with the above assertions, repeated loading during the service life of any structure can have a favorable effect on the capacity of its members by altering the state of stress in the members. This implies seismic analysis and simulation of structure should be undertaken after comprising the effect of repeated loading during the service life of the structure.

Structural simulation and analysis of structures neglecting prior service load and its effect are unrealistic and could yield erroneous outputs. Observations from this research clearly suggest the importance of incorporating preceding repeated load (fatigue) during service of the structure in future analysis.

5.2.2 Comparison between experimental and analytical results

The analytical simulation has fully captured the monotonic response of the experimental beams and confirms cyclic shear degradation of the experimental specimens. There's a strong correlation in analytical and experimental outputs with regards to initial stiffness of beams, maximum capacity of beams, mode of failure, crack pattern and fatigue life. However with regards to cyclic response, stiffness and shear degradation is observed to be slightly faster in analytical simulation. The load deflection diagrams of the specimens obtained from experimental and computational analysis are presented below for comparison.

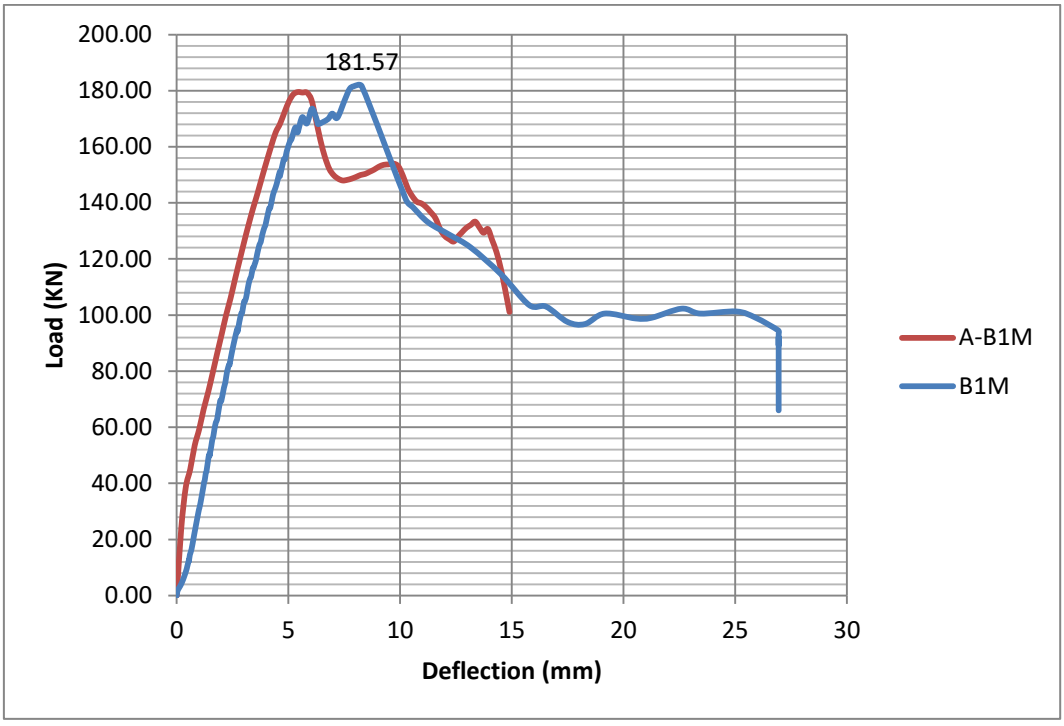

Figure 5.50 : Analytical and experimental load deflection diagram of specimen B1M

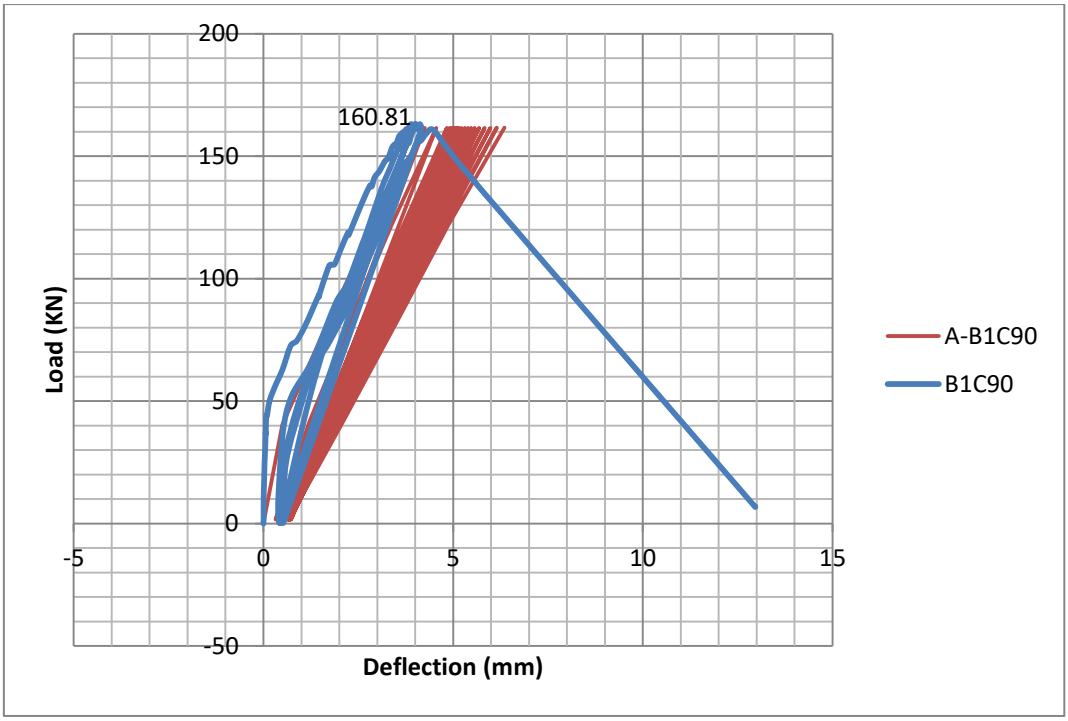

Figure 5.51 : Analytical and experimental load deflection diagram of specimen B1C90

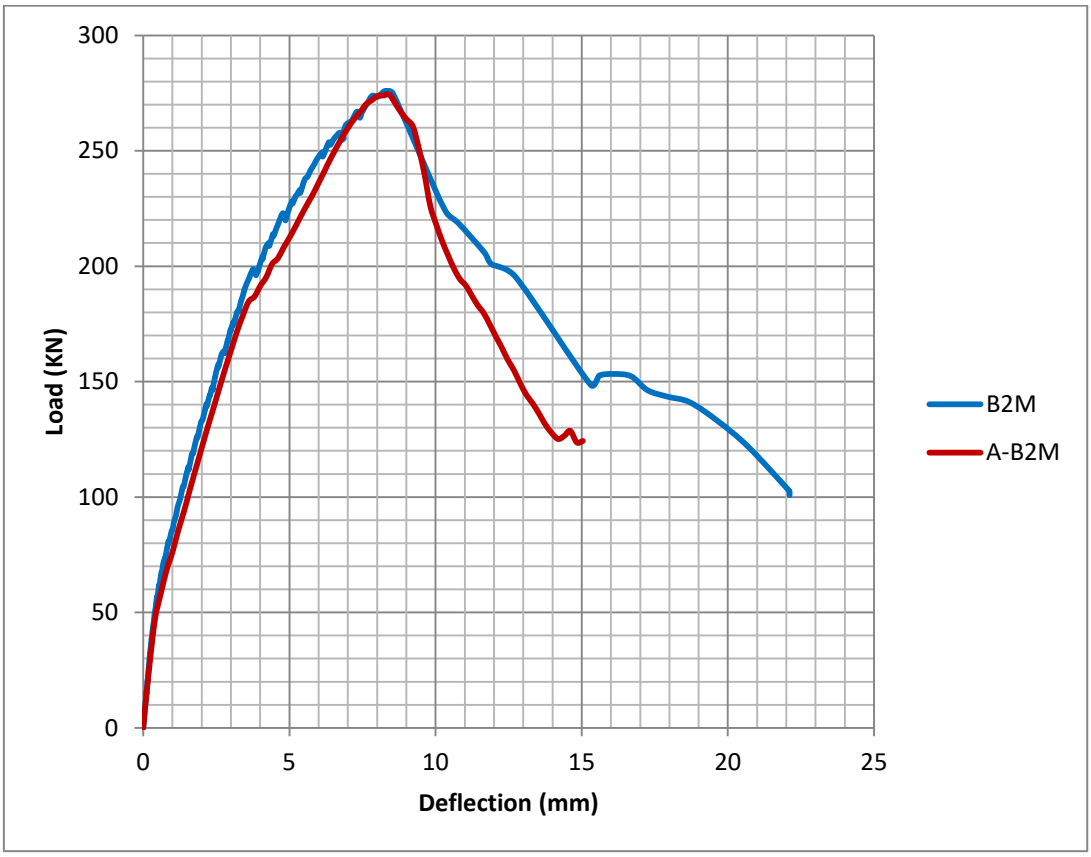

Figure 5.52 : Analytical and experimental load deflection diagram of specimen B2M

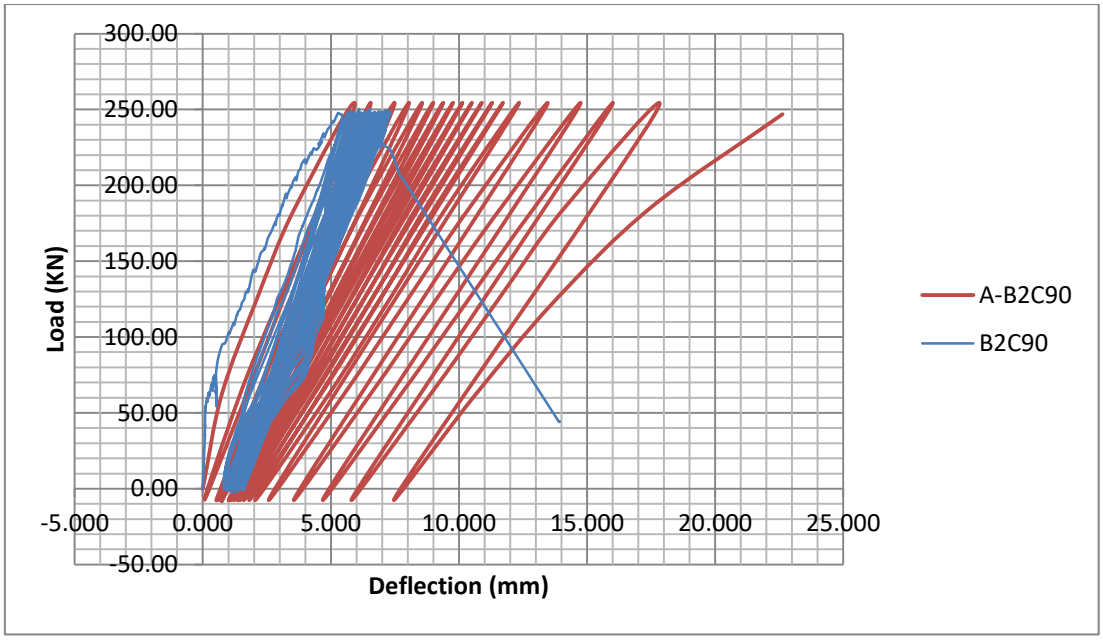

Figure 5.53 : Analytical and experimental load deflection diagram of specimen B2C90

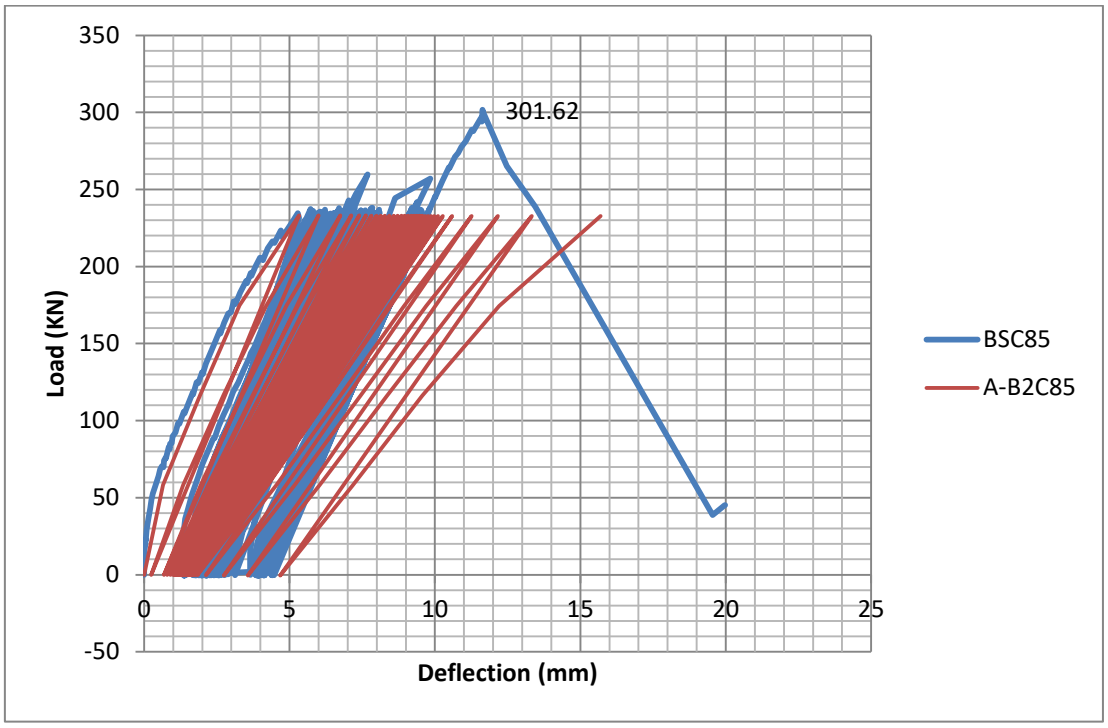

Figure 5.54 : Analytical and experimental load deflection diagram of specimen B2C85

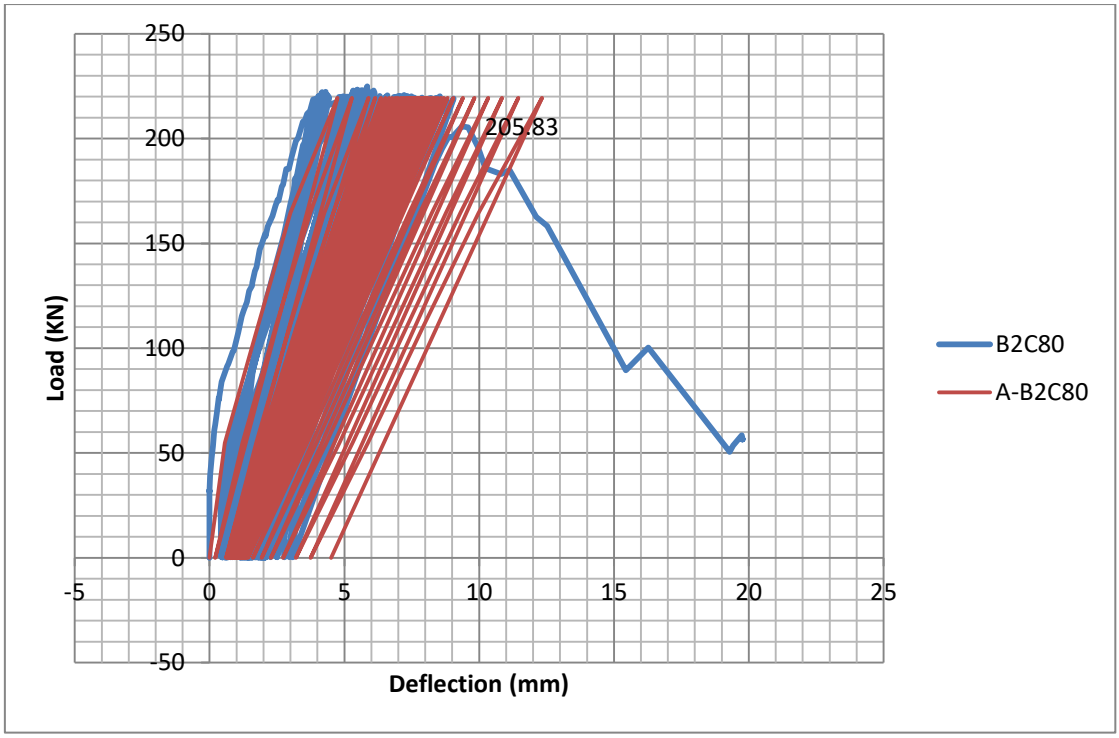

Figure 5.55 : Analytical and experimental load deflection diagram of specimen B2C80

Specimen B2C85 exhibited failure at the 110th cycle in the analytical simulation; hence it's speculated the diagonal crack path alteration, by increasing the shear strength of the specimen, may consequently have increased its fatigue life. However, a close correlation is observed between analytical and experimental load-deflection diagram of specimen B2C80 (Figure 5.55).

5.2.3 S-N Curve

The relationship between the fatigue strength of materials (frequently referred to as S) and the number of cycles of repeated loading (referred to as N) is commonly reported in the so-called SN curve (or Wohler curve). A logarithmic scale is generally employed to incorporate high cycle fatigue. If N is plotted in a logarithmic scale while S remains in linear scale, the SN curve will become approximately a linear line. Hence this scheme is employed in this thesis to exhibit strength degradation of shear-critical beams with number of cycles.

Type-two beams have been analyzed by DUCOM-COM3 under fatigue loading of maximum amplitude; 90%, 85%, 80% and 75% of their monotonic capacity. As mentioned in the previous section, the specimens exhibited faster strength and stiffness degradation in low-cycle fatigue ranges. However for the 75% maximum amplitude simulation, the specimen

displayed a higher fatigue life confirming with SN curves developed by previous researches. (Okamura and Ueda[10], Hsu[8])

Figure 5.56 shows progress of mid-span deflection with number of cycles for beams with shear reinforcement (Type-two beams). Since a force based approach was employed for fatigue analysis, the increase of mid-span deflection is used as an indicator for damage progress and ultimate failure.

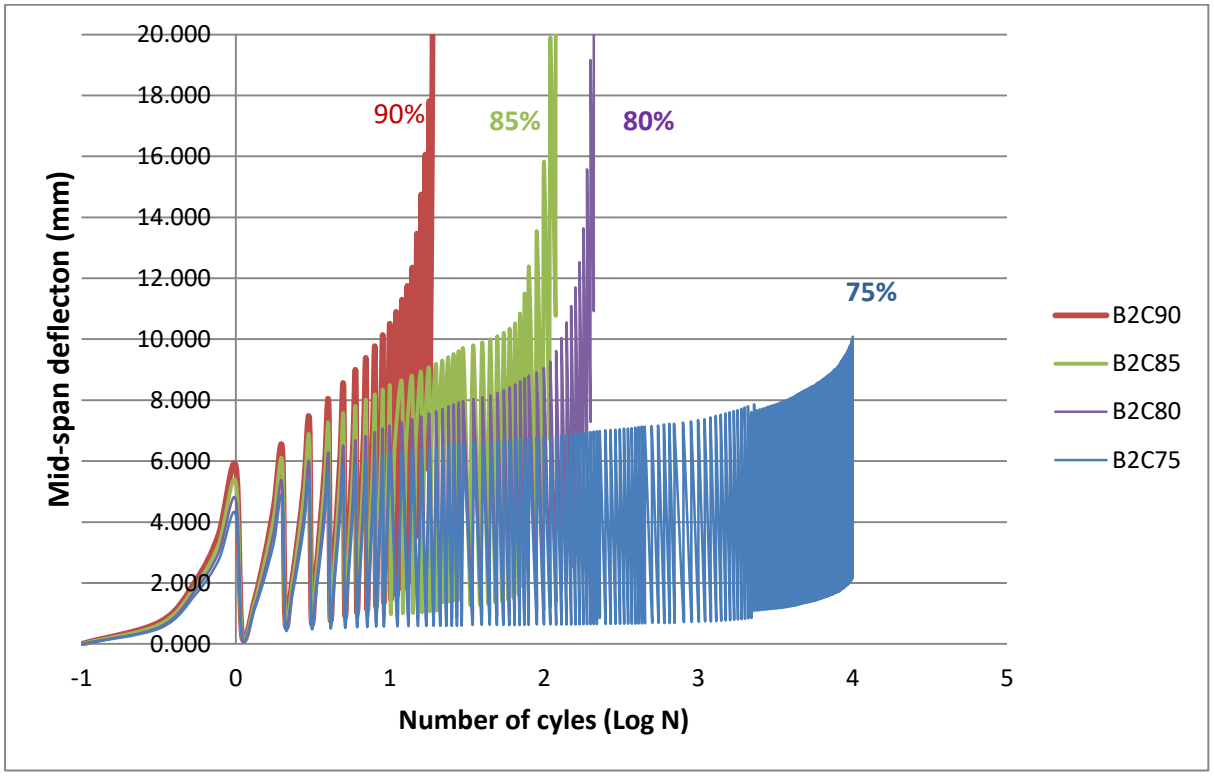

Figure 5.56 : relationship between Mid-span deflection and number of cycles

Based on analytical simulation of Type-two beams, S-N curve has been developed to clearly display shear strength degradation of shear-critical beams with number of cycles. The S-N curve displayed on Figure 5.57 is calculated based on equation (5.1) derived by linear regression from analytical simulation outputs. The computed S-N curve coincides with other S-N curves developed by other researchers mentioned earlier. [8], [10]

$$\frac{V_{\max}}{V_{cu}} = 1 - 0.0638 \log N \qquad (5.1)$$

Where,

V_{max} - Maximum amplitude of shear force

V_{cu} - shear capacity of the specimen computed from static loading test

N – Number of cycles of repeated loading

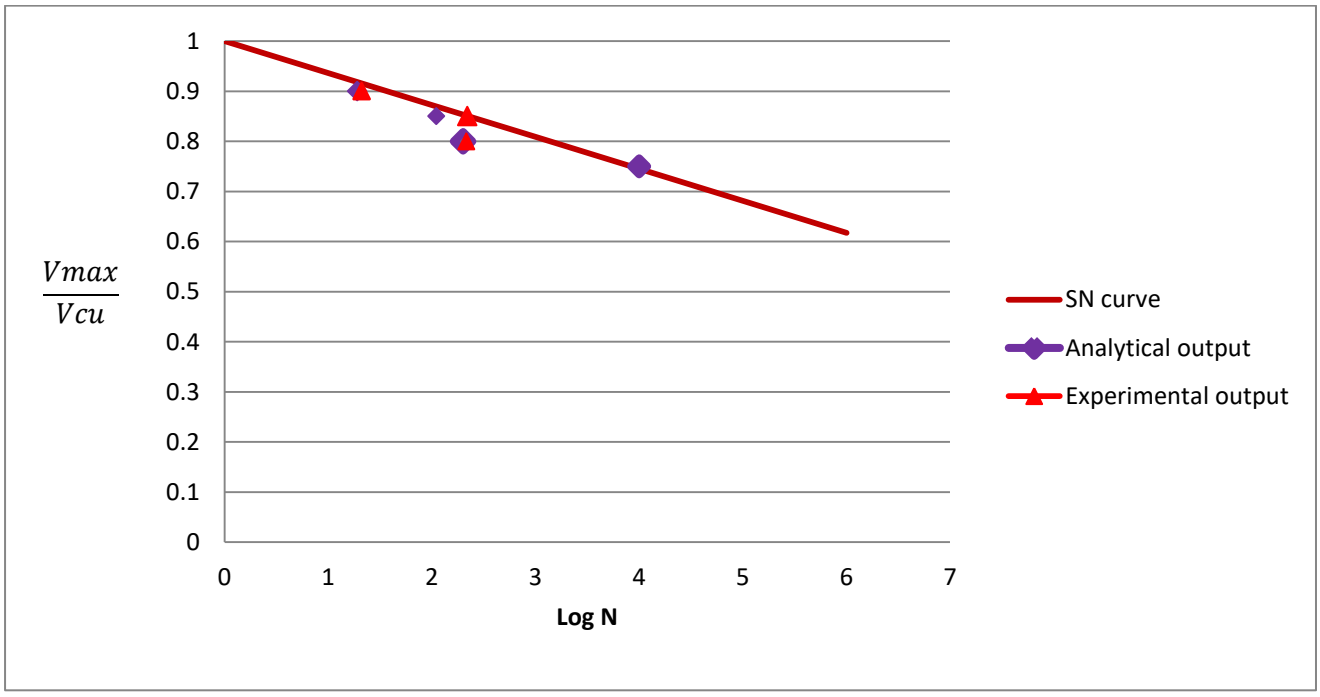

Figure 5.57 : S-N diagram for Type-two beam

The analytical and experimental results obtained are displayed in purple and red respectively on the figure above.

6 CONCLUSION AND RECCOMENDATION

6.1 Conclusion

In this thesis, the shear behavior of Reinforced Concrete beams failing in shear under one-side cyclic loading has been observed. Six experimental beams were tested under constant amplitude fatigue loading until failure. Moreover, analytical investigation was also conducted using FEA software comprising a strain path and time-dependent fatigue constitutive model. Load deflection diagrams, crack patterns, web-reinforcement strain measurements and deformed shapes were assessed to obtain a comprehensive view of cyclic shear behavior of shear-critical beams. Based on experimental and analytical investigation outputs the following conclusions have been put forth:

- In assessing shear strength of RC beams, beams with transverse reinforcement ratio 0.13%, nearing the minimum requirement (0.12%), exhibited a higher capacity under monotonic loading by 51.93% and higher fatigue life. Therefore, provision of shear reinforcement greatly enhances the shear capacity of Reinforced concrete beams and also improves their performance under fatigue loading.

- For members with shear reinforcement, the load deflection response measured under monotonic loading provided an excellent envelope for load deflection response under fixed amplitude fatigue loading.

- Strain measurements on shear reinforcement exhibited progressive increase in strain with every cycle. This shows cyclic material softening of both the concrete and the stirrups.

- One-side cyclic loading of shear-critical slender beams causes shear strength degradation with respect to their expected monotonic capacity. Previously, it has been assumed that shear strength degradation won't occur if longitudinal reinforcement doesn't yield. The outputs of this experimental research suggest otherwise; even with more rapid degradation under low-cycle fatigue for shear-critical beams.

- It is possible that fatigue loading might have a favorable effect on RC beams by altering diagonal crack path and enhancing the shear capacity of the beams. A beam subjected to certain number of cycles of loading, less than its fatigue life, can exhibit a higher strength than its expected monotonic capacity. This alteration in diagonal

crack path is not random, but the result of the state of stress of a beam under repeated loading.

- S-N curve for shear-critical Reinforced Concrete beams is developed along with an equation to calculate fatigue shear strength of shear-critical beams. It is observed that this equation is in close agreement with S-N curves proposed by different researchers for beams without shear reinforcement and plain concrete.

6.2 Recommendation

The aim of this research has been to investigate the shear behavior of Reinforced concrete beams failing in shear under one-side cyclic loading. Better insight has been obtained on the topic with novel observations on diagonal shear crack path. In light of the experimental and analytical results and lack of research database on fatigue behavior of shear-critical beams, areas for further investigation are recommended.

- Due to limitation in resource and laboratory equipment, only low-cycle fatigue analysis could be conducted. Hence, high-cycle fatigue analysis of Reinforced concrete shear-critical beams should be conducted to obtain a more comprehensive overview and develop SN curve.

- Recent researches suggest non-proportional fatigue loading accelerates crack growth and strength degradation. Moreover practically occurring cyclic loads such as seismic motion and traffic loading are highly variable and inconsistent. Thus non-proportional variable amplitude fatigue analysis of beams failing in shear is an important area of study.

- The current research can be undertaken by varying shear reinforcement ratio, concrete strength, loading rate and minimum stress (f_{min}) for a more comprehensive understanding.

- The proposed idea that diagonal crack path alteration has influenced shear capacity of RC beams merits further investigation to verify the hypothesis.

REFERENCE

[1] ACI committee 318, Building code requirements for structural concrete (ACI 318-08) and commentary. 2008.

[2] European Committee for Standardization (C.E.N.), Eurocode 2: Design of Concrete Structures: Part 1-1: General Rules and Rules for Buildings, no. En 1992-1-1. 2004, p. 225.

[3] E. B. C. Standards, ES EN2 Design of Concrete Structures (EBCS EN 1992-1-1:2015). Addis Ababa, Ethiopia: Ministry of Urban Development & Construction, 2015.

[4] J. K. WIGHT and J. G. MacGREGOR, Reinforced concrete: mechanics and design, 6th ed., vol. 27, no. 6. New Jersey, USA: Pearson Education, INC, 2012.

[5] T. T. C. Hsu and Y. L. Mo, Unified Theory of Concrete Structures. Chichester, UK: John Wiley and Sons, Ltd., 2010.

[6] A. H. NILSON, D. DARWIN, and C. W. DOLAN, DESIGN of CONCRETE STRUCTURES, Thirteenth. New York, US: The McGaw-Hall Companies, 2004.

[7] T. Paulay, "SHEAR STRENGTH REQUIREMENTS," Bull. NEW Zeal. Natl. Soc. Earthq. Eng., vol. 10, no. 2, pp. 80–84, 1977.

[8] T. T. C. Hsu, "Fatigue of Plain Concrete," ACI J. Proc., vol. 78, no. 4, pp. 292–304, 1981.

[9] H. OKAMURA, S. A. FARGHALY, and T. UEDA, "BEHAVIOURS OF REINFORCED CONCRETE BEAMS FAILING IN SHEAR UNDER FATIGUE LOADING," proceeings JSCE, no. 308, p. 14, 1981.

[10] T. Ueda and H. Okamura, "Behavior in Shear of Reinforced Concrete Beams Under Fatigue Loading.," Trans. Japan Soc. Civ. Eng., vol. 15, no. 2, 1982.

[11] M. B. PÈREZ and S. J. PANTAZZOPOULOU, "A STUDY OF THE MECHANICAL RESPONSE OF REINFORCED CONCRETE TO CYCLIC SHEAR REVERSALS," Elev. World Confeerence Earthq. Eng., vol. Paper No., 1996.

[12] F. J. Vecchio, "Analysis of shear-critical Reinforced Concrete Beams," ACI Struct. J., no. 97, pp. 102–110, 2000.

[13] H. G. Park, E. J. Yu, and K. K. Choi, “Shear-strength degradation model for RC columns subjected to cyclic loading,” Eng. Struct., vol. 34, pp. 187–197, 2012.

[14] R. C. Fenwick and A. Fong, “THE BEHAVIOUR OF REI NFORCED CONCRETE BEAMS UNDER CYCLIC LOADING,” Bull. NEW Zeal. Natl. Soc. Earthq. Eng., vol. 12, no. 3, pp. 158–167, 1979.

[15] B. G. Ang, M. J. N. Priestley, and T. Paulay, “Seismic Shear Strength of Circular Reinforced Concrete Columns,” ACI Struct. J., no. 86, pp. 45–59, 1989.

[16] F. J. Vecchio and M. P. Collins, “The modified compression-field theory for reinforced concrete elements subjected to shear,” ACI Journal Proceedings, vol. 83, no. 2. pp. 219–231, 1986.

[17] N. J. Stevens, S. M. Uzumeri, and M. P. Collins, “Reinforced Concrete Subjected Reversed Cyclic Shear - Experiments and Constitutive Model,” ACI Struct. J., vol. 88, no. February, pp. 135–146, 1991.

[18] Y. L. Wong, T. Paulay, and M. J. N. Priestley, “Response of circular reinforced concrete columns to multi-directional seismic attack,” ACI Struct. J., vol. 90, no. 2, pp. 180–191, 1993.

[19] M. J. N. Priestley, R. Verma, and Y. Xiao, “Seismic Shear Strength of Reinforced Concrete Columns,” Journal of Structural Engineering, ASCE, vol. 120. pp. 2310–2329, 1994.

[20] D. E. Biskinis, G. K. Roupakias, and M. N. Fardis, “Degradation of shear strength of reinforced concrete members with inelastic cyclic displacements,” ACI Struct. J., vol. 101, no. 6, pp. 773–783, 2004.

[21] B. I. Mihaylov, E. C. Bentz, and M. R. Collins, “Behavior of large deep beams subjected to monotonic and reversed cyclic shear,” ACI Struct. J., vol. 107, no. 6, pp. 726–734, 2010.

[22] G. Arslan and Z. Polat, “Contribution of Concrete To Shear Strength of Rc Beams Failing in Shear,” J. Civ. Eng. Manag., vol. 19, no. 3, pp. 400–408, 2013.

[23] D. M. Ruggiero, E. C. Bentz, G. M. Calvi, and M. P. Collins, “Shear response under reversed cyclic loading,” ACI Struct. J., vol. 113, no. 6, pp. 1313–1324, 2016.

[24] ACI committee 211, Standard Practice for Selecting Proportions for Normal , Heavyweight , and Mass Concrete (ACI 211 . 1-91). American concrete Institute, 2002.

[25] ASTM Standards C 496 - 96, Standard Test Method for Splitting Tensile Strength of Cylindrical Concrete, vol. 04.02. 1996, pp. 1–4.

[26] ASTM Standards C 42/ C42M - 99, "Standard Test Method for Obtaining and Testing Drilled Cores and Sawed Beams of Concrete," vol. 4, pp. 100–103, 1999.

[27] ACI committee 214, "Guide for Obtaining Cores and Interpreting Compressive Strength Results (ACI 214.4R-10)," Am. Concr. Inst., pp. 1–16, 2010.

[28] H. Maekawa, k., Pimanmas, A. Okamura, Nonlinear Mechanics of Reinforced Concrete. London: Spon Press, 2003.

[29] K. Maekawa, K. Toongoenthong, E. Gebreyouhannes, and T. Kishi, "Direct path-integral scheme for fatigue simulation of reinforced concrete in shear," J. Adv. Concr. Technol., vol. 4, no. Compendex, pp. 159–177, 2006.

[30] E. Gebreyouhannes, N. Chijiwa, C. Fujiyama, and K. Maekawa, "Shear Fatigue Simulation of RC Beams Subjected to Fixed Pulsating and Moving Loads," vol. 6, no. 1, pp. 215–226, 2008.

ANNEX A

Material tests on component of concrete

Material tests were performed on the component of concrete according to ASTM standards. The results in this section were used as input for the mix design.

Silt Content :					
sample 1 :		sample 2 :		sample 3 :	
A (silt content)=	15 ml	A (silt content)=	15ml	A (silt content)=	10 ml
B (sand) =	305 ml	B (sand) =	300 ml	B (sand) =	340 ml
Silt content =	4.92 %	Silt content =	5 %	Silt content =	2.94 **%**

Sieve Analysis

For coarse aggregate

Sieve size (mm)	Weight of Sieve (gm)	Weight of Sieve and Retained (gm)	Weight Retained (gm)	Percentage retained (%)	Cumulative Coarser (%)	Cumulative Passing (%)
37.5	1083	1083	0	0.000	0.000	100.000
25	1164	1354	190	9.548	9.548	90.452
19	1390	1894	504	25.327	34.874	65.126
12.5	1158	2141	983	49.397	84.271	15.729
9.5	1162	1420	258	12.965	97.236	2.764
4.75	1265	1319	54	2.714	99.950	0.050
Pan	735	736	1	0.050		
Total			1990			

For fine aggregate

Sieve size(mm)	Weight of Sieve (gm)	Weight of Sieve and Retained (gm)	Weight Retained (gm)	Percentage retained (%)	Cumulative Coarser (%)	Cumulative Passing (%)
9.5	445	445	0	0.000	0.000	100.000
4.75	431	435	4	0.798	0.798	99.202
2.36	387	423	36	7.186	7.984	92.016
1.18	354	482	128	25.549	33.533	66.467
600 µm	327	487	160	31.936	65.469	34.531
300 µm	302	417	115	22.954	88.423	11.577
150 µm	270	313	43	8.583	97.01	2.994
Pan	254	269	15	2.994		
Total			501			
			Fineness Moduli =	2.932135729		

Moisture content

For Coarse aggregate			***For fine aggregate***		
A =	2000		A =	500	
B =	1961		B =	444	
Moisture content	1.989	%	Moisture content	12.613	%

Unit weight of coarse aggregate:

Dry rodded density = 1570.03 Kg/m^3

Specific gravity and absorption

For Coarse aggregate			
A (oven dry) =	4947 g	Bulk specific gravity =	2.75
B (SSD) =	5023 g	Bulk specific gravity (SSD) =	2.79
C (water immersed) =	3222.5 g	Apparent specific gravity =	2.87
		Absorption Capacity =	1.54 %

For fine aggregate			
A (oven dry) =	496 g	Bulk specific gravity =	2.49
B (flask + water) =	1313 g	Bulk specific gravity (SSD) =	2.51
C (water immersed) =	1614 g	Apparent specific gravity =	2.54
		Absorption Capacity =	0.81 %

ANNEX B

MATERIAL PROPERTY

B1. Concrete strength data on test day

- **Specimen B1M**

Cubic compressive strength on test day (101 days)							
specimen	mass (kg)	density	Fcu		Variance	**12.49849**	
1	7.705	2282.962963	44.11		SD =	**3.53532**	
2	7.685	2277.037037	46.19		COV=	**8.274917**	%
3	7.841	2323.259259	37.87		Fck (EC2) =	33.57708	MPa
Mean	**7.74367**	**2294.419753**	**42.723**		Ecm (EC2)=	33.71542	GPa

Split tensile strength of concrete (101 days)					Variance	**0.002**	
specimen	Max Force (P)	σt (tensile stress)	Fctk (EC2)		SD =	**0.040107**	
1	153.9	2.177239621	1.959516		COV=	**2.005731**	%
2	160.2	2.26636639	2.03973				
Mean	**119.833**	**2.221803006**	**2.000**				

The third cylinder for split tensile test exhibited a lower strength and did not comply with appropriate failure criteria of ASTM; so it was neglected from the analysis and report.

- **Specimen B1C90**

Cubic compressive strength on the day of testing (99 days)							
specimen	Mass (Kg)	density (Kg/m^3)	Fcu (MPa)		Variance =	50.665	
1	7.786	2306.96	45.05		SD =	**7.117944**	
2	7.637	2262.81	40.36		COV=	**16.29524**	%
3	7.567	2242.07	39.6				
4	7.95	2355.56	47.69				
5	7.765	2300.74	46.97				
6	7.822	2317.63	26.89				
7	7.879	2334.52	44.54				
8	7.842	2323.56	48.86				
9	7.939	2352.30	53.17				
Mean	**7.798556**	**2310.68**	**43.681**				

Splitting tensile strength of concrete (99 days)					Variance =	0.011	
specimen	Load (KN)	σt (tensile stress)	Fctk (EC2)		SD =	**0.104**	
1	204	2.886	2.597		COV=	**4.057**	%
2	191.2	2.705	2.434		Fctk (EC2)	2.573	
3	211	2.985	2.687				
Mean	**202.0667**	**2.859**	**2.573**				

- **Specimen B2M**

Cubic compressive strength on the day of testing (63 days)							
specimen	Mass (Kg)	density (Kg/m3)	Fcu (MPa)		Variance =	**3.341**	
1	7.896	2339.556	40.090		SD =	**1.828**	
2	7.947	2354.667	41.500		COV=	**4.551**	%
3	7.847	2325.037	39.410		F'C =	31.980	MPa
4	7.894	2338.963	39.010		Ecm =	33.396	GPa
5	8.070	2391.111	37.660				
6	7.978	2363.852	43.340				
Mean	**7.939**	**2352.198**	**40.168**				

Split tensile strength of concrete on the 64th day					Variance =	**0.001**	
specimen	Max Force (P)	σt (tensile stress)	Fctk (EC2)		SD =	**0.027**	
1	error!	error!	error!		COV=	**1.113**	%
2	190.800	2.699	2.429		Fctm (EC2)=	2.403	MPa
3	186.600	2.640	2.376		Fctk (EC2)=	1.68	MPa
Mean	**188.700**	**2.670**	**2.403**				

The data for the first cylinder sample was not recorded due to machine malfunction.

- **Specimen B2C90**

Cubic compressive strength on the day of testing (64 days)							
specimen	Mass (Kg)	Density (Kg/m3)	Fcu (MPa)		Variance =	11.2433	
1	7.953	2356.444	36.4		SD =	**3.353**	
2	7.883	2335.704	45.05		COV=	**8.229**	%
3	7.877	2333.926	39.28		F'C =	32.343	
4	7.83	2320	45.31		Ecm =	33.469	GPa
5	7.943	2353.481	38.12				
6	7.899	2340.444	40.33				
Mean	**7.8975**	**2340**	**40.748**				

Splitting tensile strength of concrete on day 64					Variance =	**0.062**	
specimen	Load (KN)	σt (tensile stress)	Fctk (EC2)		SD =	**0.249885**	
1	171.8	2.430	2.187		COV=	**13.48241**	%
2	124.6	1.762	1.586		Fctm (EC2)	1.853	
3	140.3	1.984	1.786		Fctk (EC2)	1.297	
Mean	**145.5667**	**2.059**	**1.853**				

- **B2C85**

Cubic compressive strength on the day of testing (63 days)							
specimen	Mass (Kg)	density (Kg/m3)	Fcu (MPa)		Variance =	**0.629**	
1	7.794	2309.333	40.71		SD =	**0.793**	
2	7.73	2290.370	41.05		COV=	**1.911**	%
3	7.958	2357.926	40.7		F'C =	32.813	MPa
4	7.875	2333.333	42.33		Ecm =	33.563	GPa
5	7.892	2338.370	42.77				
6	7.818	2316.444	41.44				
Mean	**7.8445**	**2324.296**	**41.500**				

Splitting tensile strength of concrete on day 63					Variance =	**0.028**	
specimen	Load (KN)	σt (tensile stress)	Fctk (EC2)		SD =	**0.166491**	
1	164.3	2.324	2.091933		COV=	**8.79367**	%
2	149.5	2.115	1.903493		Fctk (EC2)	1.893307	MPa
3	132.3	1.872	1.684496				
Mean	**148.7**	**2.104**	**1.893**				

- **B2C80**

Cubic compressive strength on the day of testing (94 days)							
specimen	Mass (Kg)	density (Kg/m3)	Fcu (MPa)		Variance =	**12.458**	
1	7.827	2319.111111	41.13		SD =	**3.529**	
2	7.779	2304.888889	43.8		COV=	**8.257**	%
3	7.741	2293.62963	43.95				
4	7.752	2296.888889	39.7		ρmean =	2287.038	
5	7.887	2336.888889	40.9				
6	7.845	2324.444444	49.06				
7	7.672	2273.185185	42.6				
8	7.605	2253.333333	46.91				
9	7.834	2321.185185	36.66				
Mean	**7.771333**	**2302.617284**	**42.746**				

Splitting tensile strength of concrete on day 94						Variance =	**0.014**	
specimen	Mass (Kg)	Load (KN)	σt (tensile stress)	Fctk (EC2)		SD =	**0.120**	
1	12.117	154.5	2.186	1.967		COV=	**6.541**	%
2	12.014	146.3	2.069	1.862		Fctk (EC2)	1.836	
3	11.995	131.7	1.863	1.676				
Mean	**12.042**	**144.167**	**2.039**	**1.836**				

B2. Tension tests on Reinforcement

Average test results for tension test on reinforcements used in beam specimens.

Specimen	d1	d2	Average diameter	Average Yield stress (MPa)	Average Fracture stress (MPa)	ultimate Strain (‰)
φ 6	5.49	6.51	6.00	574.64	651.13	91.67
φ 8	7.46	8.74	8.10	539.53	613.98	100
φ 10	9.61	11.16	10.39	486.40	563.14	55
φ 20	18.80	20.82	19.81	603.47	696.26	175

B3. Core taking and testing

B2C80									
sample	maximum nominal size of aggregate	Date of coring	Mass (g)	Length	Average Diameter	L/D	date of testing	F_{core}	Density (Kg/m3)
1	25	12/18/2017	5984	225	112.5	2.00	1/3/2018	20.86	2675.56
2	25	12/18/2017	5953	225	113	1.99	1/3/2018	25.90	2638.19
3	25	12/19/2017	5726	225	112	2.01	1/3/2018	21.46	2583.11
Mean	**25**			**225**	**112.5**	**2.00**		**22.74**	**2632.29**

B2C85									
sample	maximum nominal size of aggregate	Date of coring	Mass (g)	Length	Average diameter	L/D	Date of testing	Fcore (MPa)	Density (Kg/m3)
1	25	12/19/2017	5650	223	111	2.009	1/3/2018	29.57	2618.23
2	25	12/19/2017	5676	225	112	2.008	1/3/2018	18.35	2560.554
Mean	**25**			**224**	**111.5**	**2.008**		**23.96**	**2589.392**

For specimen B2C85, since such a large variation in compressive strength was observed between the test samples and sample 2 did not confirm to failure profiles acceptable for report, results from sample 2 were neglected.

Estimation of equivalent in-place strength of the concrete samples according to ACI and British standards were computed and reported as follows.

Equivalent in-place strength according to ACI 214.4R-10								
Specimen	F_{core} (MPa)	L/d	diameter	$F_{l/d}$	f_{dia}	f_{mc}	f_d	F'c (MPa)
B2C80	22.74	2.000	112.5	1.000001	0.995	0.96	1.06	23.02
B2C85	29.57	2.009	111	1.093572	0.9956	0.96	1.06	32.76

Estimated in situ cube strength according to British standards				
Specimen	F_{core} (MPa)	λ	D	Fcu (Mpa)
B2C80	22.74	2.000	2.5	28.42
B2C85	29.57	2.009	2.5	37.00

The outputs from ACI were finally utilized because core taking and testing was performed according to ASTM which is in close correlation to ACI. The cylindrical strength of B2C80 was observed to be much lower and its low life cycle could be attributed to such decrease in concrete strength. However, ACI clearly stipulates results obtained from coring are hardly conclusive and should not be directly compared with representative samples outputs.